國立臺灣大學工學院土木工程學系

碩士論文

Department of Civil Engineering
College of Engineering
National Taiwan University

Master's Thesis

臺灣山岳隧道受震脆弱性曲線之建立

The Establishment of Fragility Curves for Mountain Tunnels in Taiwan under Seismic Events

辛奕呈

Yi-Cheng Xin

指導教授：郭安妮 博士

Advisor: Annie On-Lei Kwok, Ph.D.

中華民國 114 年 7 月

July, 2025

doi:10.6342/NTU202503897

國立臺灣大學碩士學位論文
口試委員會審定書
NATIONAL TAIWAN UNIVERSITY
MASTER'S THESIS ACCEPTANCE CERTIFICATE

臺灣山岳隧道受震脆弱性曲線之建立

The Establishment of Fragility Curves for Mountain Tunnels in Taiwan under Seismic Events

本論文係 辛奕呈 (R12521127) 在國立臺灣大學土木工程學系大地工程組
完成之碩士學位論文，於民國114年7月21日承下列考試委員審查通過及口試及格，特此證明。

The undersigned, appointed by the Department of Civil Engineering (Geotechnical engineering) Engineering on 21 July,2025 have examined a Master's Thesis entitled above presented by (Yi-Cheng Xin) (R12521127) candidate and hereby certify that it is worthy of acceptance.

口試委員 Oral examination committee:

郭安妮 (指導教授 Advisor)	郭安妮
邱俊翔	邱俊翔
邱雅筑	邱雅筑

系主管 Director： 葛宇甯 葛宇甯

doi:10.6342/NTU202503897

誌謝

進入國立臺灣大學的這兩年間，是我學術與人格成長最深刻的歷程。研究所的訓練不僅提升了我在專業領域的知識，更培養了我獨立思考與自主學習的能力。透過論文的撰寫與研究歷程，我學會如何閱讀大量文獻、分析前人研究成果，並善用網路資源作為工具，尋找解決問題的方法與參考資料。這段期間的學習不僅讓我累積了知識與技能，也讓我更加明白持續學習與主動探索在研究中所扮演的重要角色。感謝臺大提供的優質學習環境，讓我在這段時間中得以不斷磨練、成長。

接著很感謝郭安妮教授特別感謝指導教授郭安妮教授在研究過程中的耐心指導與專業建議，無論是在論文的方向規劃，還是細節的調整修正，郭老師總是能給予我明確而深入的回饋。我也想感謝大地組的同學們，你們在課業、研究給予我許多幫助，也常常舉行很多郊遊行程豐富我的碩士生活，這邊特別提一下謝謝李宥安同學使我的酒量得到巨大的提升，雖然還是幾杯就倒了。再來是郭門的兩位優等生，有你們在讓我的研究生活多了好多分歡笑，從參加風力發電平台競賽開始到最後的口試，我只想說有你們真好。在我碩士的後半年謝謝張詒茹的督促及陪伴是我在這段求學旅程中最重要的後盾，也讓我更堅定地走完這段不易的過程。

最後，最深的感謝獻給我的家人。謝謝你們一直以來的無條件支持與鼓勵，沒有你們我真的辦不到。我愛你們。

doi:10.6342/NTU202503897

摘要

台灣的山岳隧道工程在設計階段時，通常僅會依據工程沿線所預估會遭遇的地質狀態進行支撐種類的設計，有關於地震對隧道的影響則不一定會加以考慮。也因為隧道或維生管線等線型構造與傳統的建築物形式大相逕庭，特別是台灣的地質狀態相對年輕且複雜，導致山岳隧道沿線的地層變化經常相當劇烈。近年更因為隧道結構逐漸老化或是圍岩風化等原因，地震對於隧道的影響有可能加劇。

本研究利用 FLAC 2D 軟體進行山岳隧道受震反應的數值模擬，以嘉寶隧道周圍岩體的地質與材料性質作為分析參數，建立貼近現場條件的模型。模擬過程考量覆土深度、剪力波速等重要影響因子，並施加具有特定回歸期之設計地震，以全面評估隧道於地震作用下之動態行為。最終，從分析輸出的隧道襯砌彎矩結果中提取損傷指標，據此繪製脆弱性曲線，以量化並評估山岳隧道在各種地震強度條件下之損傷潛勢與耐震性能。

關鍵字：脆弱性曲線、山岳隧道、地盤反應分析、隧道數值模擬、襯砌強度設計

doi:10.6342/NTU202503897

Abstract

In Taiwan, mountain tunnels are typically designed based solely on anticipated geological conditions encountered along the tunnel alignment, and seismic impacts on tunnels are often overlooked at the design stage. Unlike conventional buildings, long tube-like structures such as tunnels or lifelines differ significantly in their structural behavior. Particularly, Taiwan's relatively young and complex geological settings cause abrupt variations in geological conditions along tunnel routes. Furthermore, due to progressive structural aging and surrounding rock weathering, tunnels may become increasingly vulnerable to seismic risks.

This study employs FLAC 2D software to numerically simulate the seismic response of mountain tunnels. Lining properties and geotechnical properties from the rock mass surrounding the Jiabao Tunnel were incorporated into the numerical model, ensuring realistic and representative conditions. Critical influencing factors, including overburden depth and shear wave velocity, were considered. On the other hand, seismic input motions with different ground motion attributes were used to comprehensively evaluate the dynamic tunnel response. Finally, the bending moment results of the tunnel linings served as damage indicators, facilitating the development of fragility curves to quantify and evaluate the seismic vulnerability and resilience of mountain tunnels under various seismic intensity scenarios.

Keywords: Fragility curves, Mountain tunnels, Site response analysis, Tunnel numerical simulation, Lining strength design

doi:10.6342/NTU202503897

TABLE OF CONTENTS

doi:10.6342/NTU202503897

doi:10.6342/NTU202503897

doi:10.6342/NTU202503897

LIST OF FIGURES

doi:10.6342/NTU202503897

doi:10.6342/NTU202503897

doi:10.6342/NTU202503897

LIST OF TABLES

doi:10.6342/NTU202503897

Chapter 1 Introduction

1.1 Research Background and Objectives

Taiwan is situated along the seismically active Pacific Ring of Fire and is frequently subjected to strong ground motions. Among various infrastructure systems, mountain tunnels are especially vulnerable due to their complex geological settings and burial conditions. The 1999 Chi-Chi earthquake demonstrated this vulnerability, causing not only widespread surface destruction but also significant damage to several tunnel structures. These observations underscore the urgent need for seismic design provisions and fragility assessment tools tailored for Taiwan's tunnel systems.

While three-dimensional dynamic time-history analyses offer the highest accuracy in evaluating seismic responses of underground structures, their application requires detailed input on geological conditions, tunnel geometry, and material properties. Consequently, they are computationally intensive and impractical for large-scale or regional assessments. As an alternative, fragility curve–based vulnerability analysis provides a more feasible solution. By combining simplified numerical simulations with empirical observations from past earthquake damage cases in Taiwan and abroad, it becomes possible to develop an efficient seismic risk assessment framework for mountain tunnels.

Fragility curves describe the conditional probability of a structure reaching or exceeding a certain level of damage under a given seismic intensity measure (e.g., PGA or PGV). However, existing fragility models for tunnel structures often rely on expert judgment or empirical estimation, and rarely account for structural and material variability inherent in different tunnel configurations or geological conditions.

doi:10.6342/NTU202503897

This study aims to develop fragility curves that are specifically applicable to Taiwan's mountainous tunnels. Using the Jiabao Tunnel as a representative case, this research employs two-dimensional numerical simulations based on the finite difference method to explore tunnel performance under varying seismic demands. The simulations incorporate parameters such as overburden depth and shear wave velocity to evaluate their influence on tunnel response. Through a damage index defined by the ratio of bending moment demand to structural capacity, fragility curves are constructed to quantify the probability of different damage states occurring, thus providing a scientific basis for seismic design, post-earthquake inspection, and emergency response planning.

1.2 Research Process and Steps

The main research workflow of this study is presented in Figure 1.1, and the following outlines the essential tasks undertaken throughout the research process.

(1) Literature Review and Data Collection

Initially, this research systematically compiles and classifies existing academic literature, research reports, and analytical studies related to seismic performance and damage assessment of tunnels. Particular attention is paid to reviewing methods for assessing tunnel damage post-earthquake and approaches for constructing seismic fragility curves. Through this literature review, key factors influencing tunnel vulnerability and effective numerical modeling techniques are identified.

(2) Numerical Modeling and Verification of Tunnel Seismic Response

A numerical analysis framework based on the finite difference method is developed to perform dynamic time-history analyses of rock tunnels. This numerical model specifically addresses tunnel responses under seismic loading, considering plane strain conditions, seismic-induced lining deformations, and corresponding response spectra.

doi:10.6342/NTU202503897

The verification procedure consists of two main components:

a. Analytical vs. Numerical Solutions under Dynamic Conditions:

Numerical results are compared to established analytical solutions to ensure accuracy and reliability of the numerical modeling approach.

b. Free-Field Response Validation:

The numerical model under free-field conditions (without tunnels) is validated against response spectra generated using the DEEPSOIL software to confirm the correctness of boundary and material property assumptions.

(3) Development of Tunnel Fragility Curves

Following successful validation of the numerical modeling approach, the study investigates the impact of various influential factors on tunnel seismic response. By selecting suitable damage indicators representative of tunnel performance, fragility curves are systematically constructed. These curves facilitate comparative discussions regarding the seismic vulnerability of tunnels subjected to different geological, structural, and seismic conditions.

doi:10.6342/NTU202503897

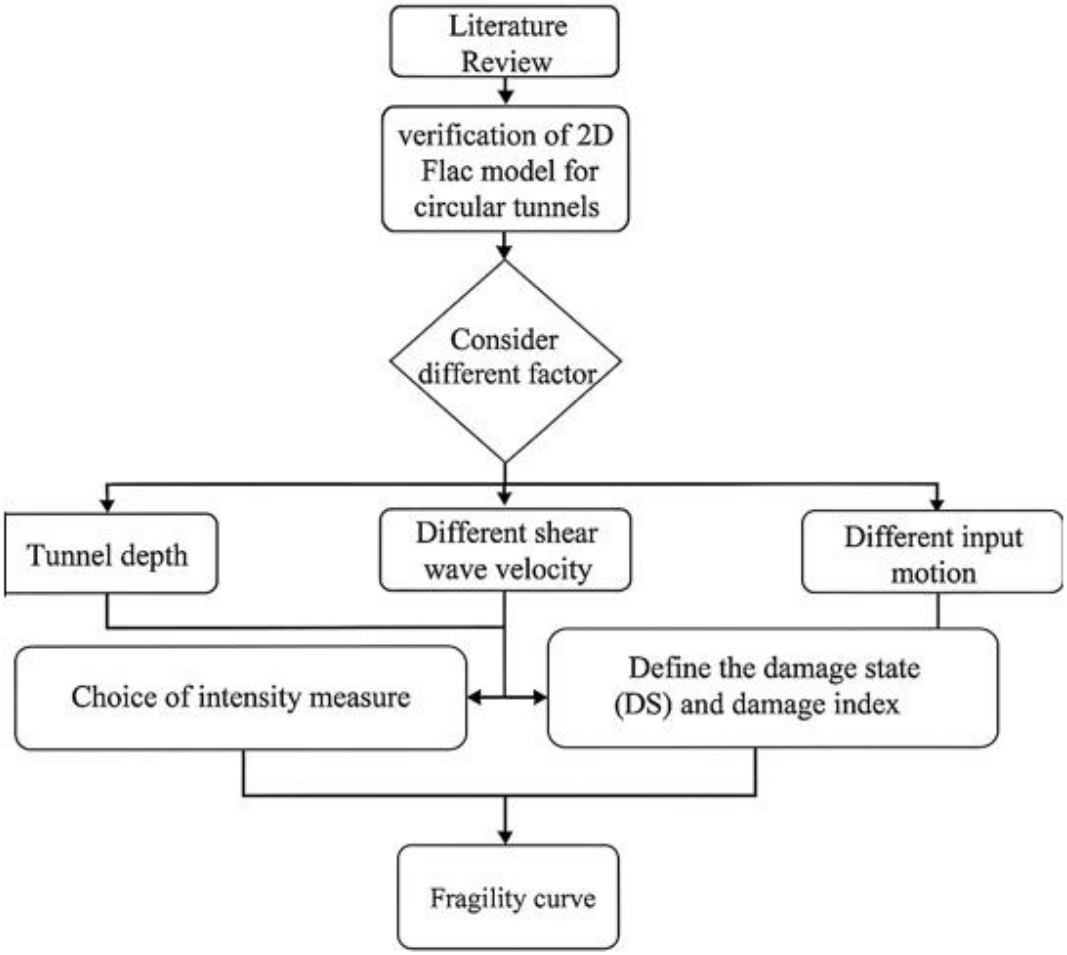

Figure 1.1 Research process diagram

1.3 Organization of this Thesis

This thesis is structured into five chapters. Chapter 1 introduces the research motivation and objectives. Chapter 2 reviews past case studies on the seismic performance of tunnels, discussing common damage patterns and the key factors influencing seismic tunnel damage. Chapter 3 presents the validation process of the numerical models used in this study. Chapter 4 focuses on the results of numerical simulations and the development of fragility curves. Finally, Chapter 5 summarizes the key findings and provides suggestions for future research directions.

doi:10.6342/NTU202503897

Chapter 2 Literature review

Underground facilities such as tunnels and subway systems play a vital role in modern infrastructure, facilitating transportation, utility provision, and storage needs in urbanized societies. Traditionally, it has been observed that underground structures tend to exhibit better resilience against seismic activities compared to above-ground facilities. This improved seismic performance is largely attributed to their confinement within geological formations, which reduces the inertial forces that typically affect surface structures during seismic events. Nonetheless, recent seismic events have challenged this assumption, as several significant earthquakes have caused notable damage to underground structures, highlighting vulnerabilities previously underestimated or neglected during the design phase.

2.1 Earthquake-induced damage in mountain tunnels: The Chi-Chi Earthquake Case Study

The Chi-Chi Earthquake, which occurred on September 21, 1999, is a landmark seismic event that significantly impacted Taiwan, causing catastrophic damage across multiple infrastructures. Historically, underground structures such as mountain tunnels were often assumed to possess inherent seismic resilience, predominantly due to their embedded nature and the surrounding geological confinement that presumably attenuates seismic energy. However, the devastating consequences observed in the aftermath of the Chi-Chi Earthquake challenged these traditional assumptions and prompted extensive investigations into the seismic vulnerability of tunnel structures. A comprehensive assessment conducted by Wang et al. (2001) offers critical insights into the nature and extent of damage incurred by mountain tunnels during this seismic event, highlighting

doi:10.6342/NTU202503897

key factors influencing tunnel stability under seismic conditions. Figure 2.1 indicates the locations of the investigated tunnels and the intensity of the earthquake on the ground surface.

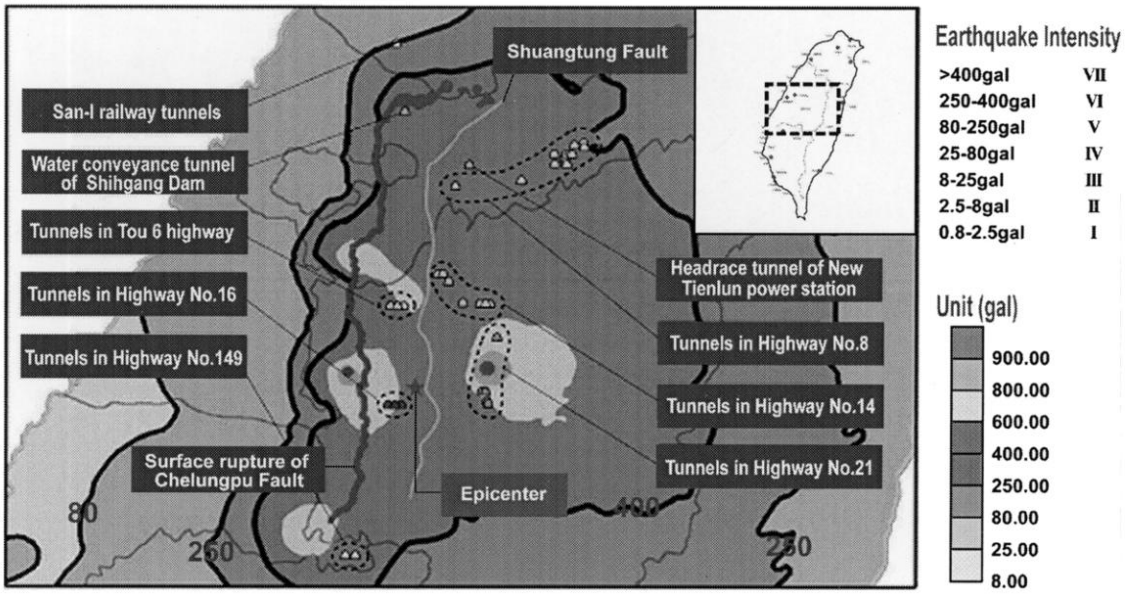

Figure 2.1 The location of tunnels investigated and the earthquake intensity on ground surface. (Wang et al., 2001)

2.1.1 Cases of tunnel damage due to earthquakes

According to Wang et al. (2001), a total of 57 mountain tunnels located in central Taiwan were investigated systematically post-earthquake. Contrary to previous assumptions of inherent seismic robustness, it was found that 49 out of these 57 tunnels exhibited varying degrees of damage. This extensive damage inventory underscores the importance of revising existing seismic design practices for tunnels, especially in seismic-prone regions. Figure 2.2,the most common damage is lining cracking, followed by tunnel entrance slope collapse and lining peeling.

doi:10.6342/NTU202503897

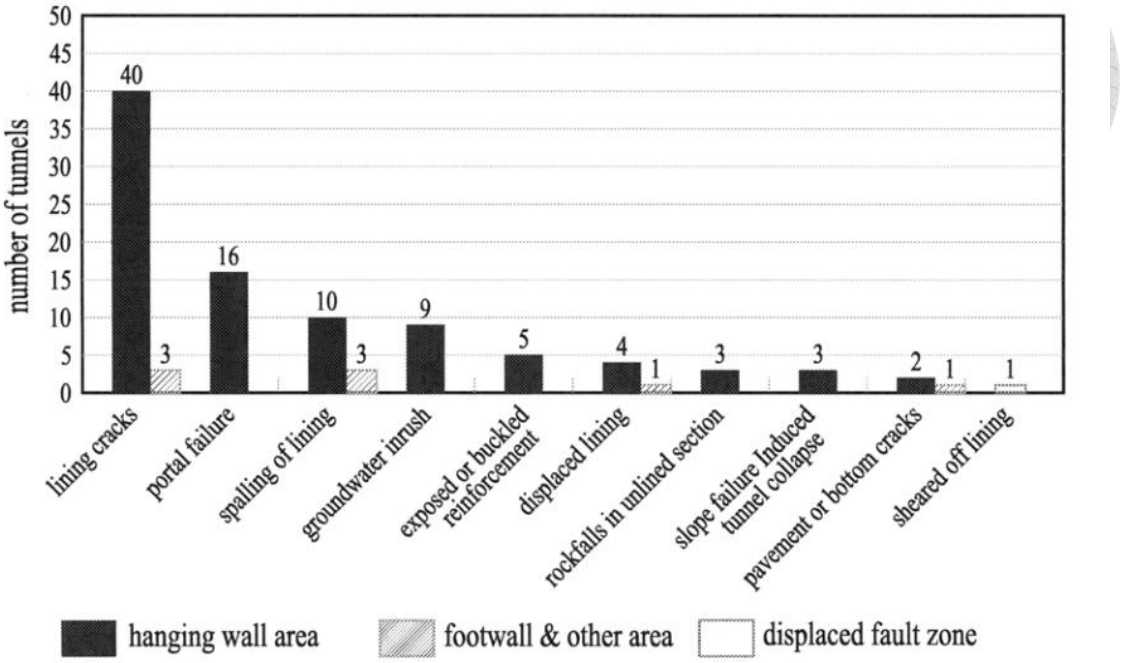

Figure 2.2 Statistics of tunnel damage (Wang et al., 2001)

Slope instability emerged as another critical contributor to tunnel collapse and damage, particularly for tunnels located near portal sections or in shallow overburden areas. A prominent example reported by Wang et al. involved the Chingshue Tunnel on Highway No.149A, which collapsed due to massive slope failures triggered by the seismic event.as shown in Figure 2.3.Photographic documentation from before and after the earthquake clearly shows dramatic slope-induced collapse near tunnel entrances, demonstrating how surface topographical conditions significantly amplify seismic vulnerability in underground infrastructure.

doi:10.6342/NTU202503897

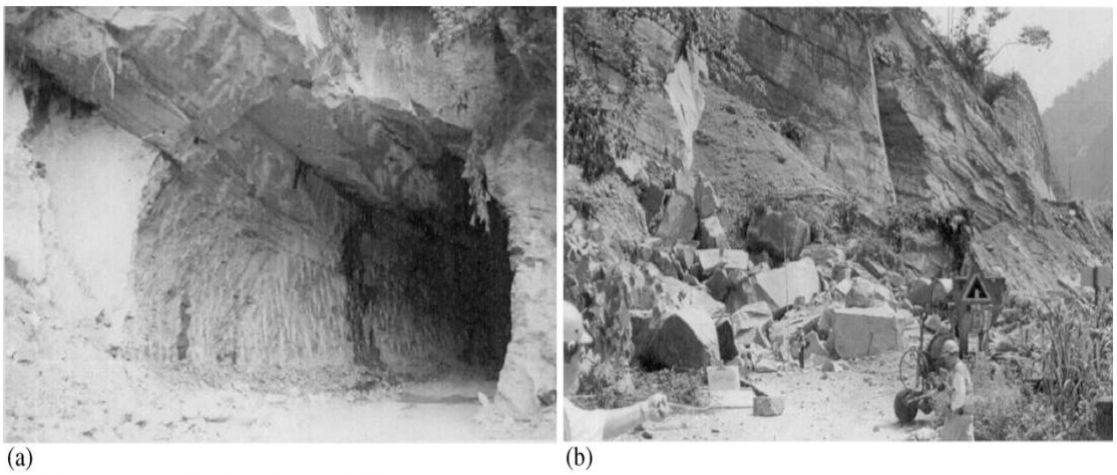

Figure 2.3 Damage pattern slope failure induced tunnel collapse. (a) photo of Chi-Shue Tunnel before Chi-Chi Earthquake; (b) photo of Chi-Shue Tunnel after Chi-Chi Earthquake. (Wang et al., 2001)

In addition to fault rupture and slope instability, structural and lining failures constituted major damage patterns observed across many tunnels. These failures were extensively classified by Wang et al. (2001) into various categories, including longitudinal cracks, transverse cracks, inclined cracks, extended cross cracks, pavement or bottom cracks, and wall deformation, as shown in Figure 2.4.

doi:10.6342/NTU202503897

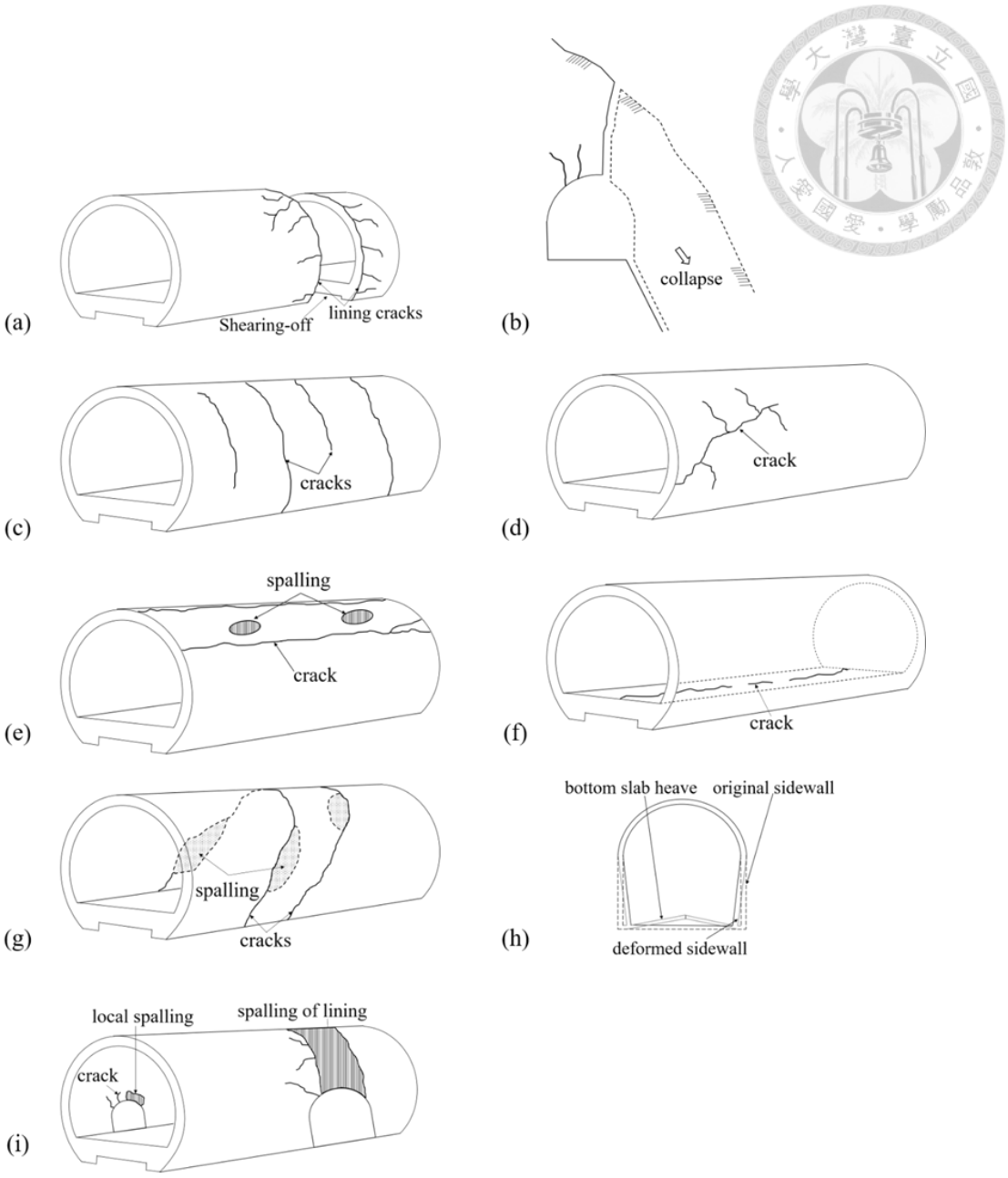

Figure 2.4 Illustration of seismic damage patterns in rock tunnels (Wang et al., 2001).

Wang et al. (2001) concluded their extensive survey by stressing the critical importance of integrating comprehensive seismic hazard analyses, including fault displacement assessments and slope stability evaluations, into the design and planning phases for mountain tunnels.

doi:10.6342/NTU202503897

2.2 Tunnel damage mechanism

Based on a synthesis of existing literature and documented cases of tunnel damage during earthquakes, the mechanisms responsible for seismic damage to mountain tunnels can generally be categorized into three types:

1. Ground Shaking Effects

The seismic loads experienced by a tunnel vary significantly depending on its spatial location relative to nearby active faults, the epicenter (or hypocenter), and the ground surface or adjacent slopes. As seismic waves propagate through the ground, their energy attenuates due to geometric spreading and material damping effects. Consequently, tunnels located closer to fault rupture zones or the seismic source are subjected to higher levels of ground motion.

Post-earthquake surveys in both domestic and international contexts have indicated that tunnels rarely suffer damage when the peak ground acceleration (PGA) is below 0.19g. In contrast, severe tunnel damage is frequently observed when the PGA exceeds 0.25g. Asakura (2008) statistically analyzed cases of tunnel damage in Japan from the 1923 Kanto Earthquake to the 2004 Niigata Earthquake and found that for earthquakes with a moment magnitude (Mw) of 8, tunnels within 20–30 km of the epicenter may experience significant damage. For events of Mw 7, damage may occur within a 10 km radius, as shown in Figure 2.5.

Although there exists a general correlation between PGA and tunnel damage, exceptions are not uncommon. These are often attributed to wave reflection and refraction phenomena occurring at interfaces between soft and hard soil layers or at the ground surface, particularly near slopes. The greater the difference in wave propagation characteristics between materials, the more energy is released at the boundary. Tunnels

doi:10.6342/NTU202503897

near the ground surface or adjacent to inclined slopes are thus exposed to amplified seismic forces.

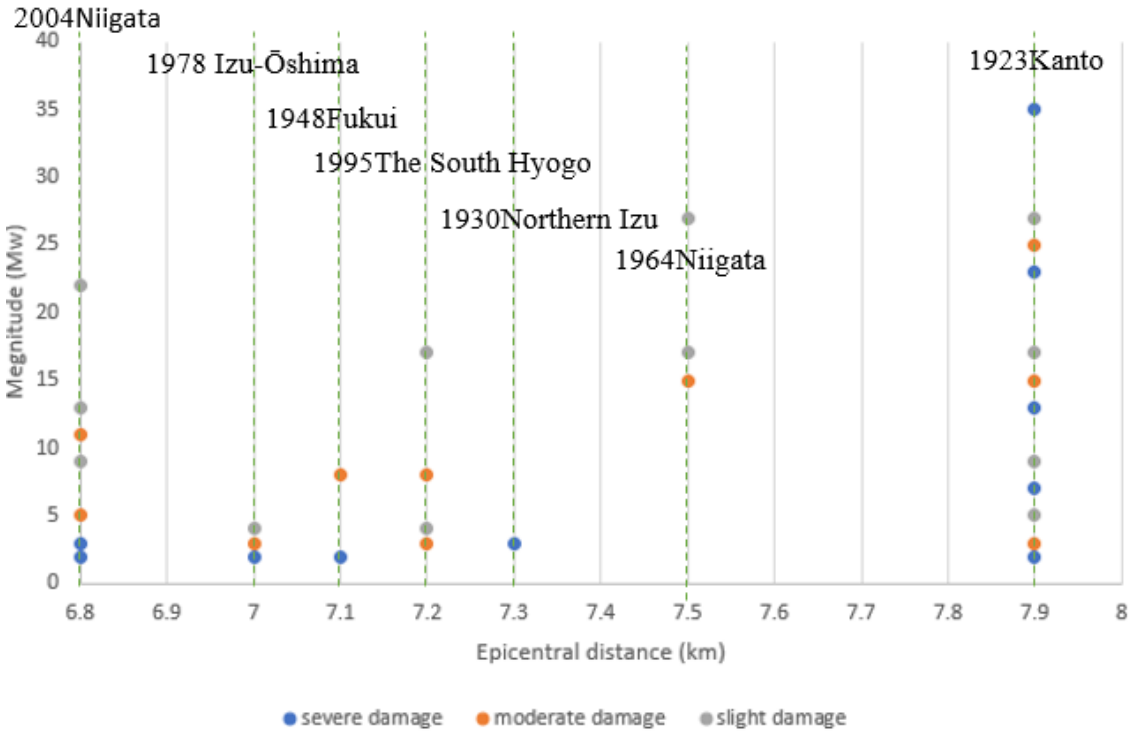

Figure 2.5 Relationship between earthquake magnitude and distance from earthquake source and tunnel damage (Redraw from Asakura et al., 2008)

2. Intersection with Fault Rupture Zones

When tunnels intersect active faults or experience displacement triggered by seismic faulting, the resulting intense shear forces exceed the structural resistance of man-made tunnel linings. These interactions invariably lead to structural displacement and damage. The extent and severity of damage are influenced by the type of fault and the amount of relative displacement. Table 1 provides a summary of domestic and international cases where fault-induced offset resulted in tunnel damage. Such mechanisms represent one of the most destructive seismic hazards for underground structures.

doi:10.6342/NTU202503897

Table 1 Cases of tunnel damage caused by fault movement at home and abroad (Chen 2011)

Tunnel	Earthquake	Mw	Fault	Type	Offset amplitude (m)
Urban Kern Country railway tunnel(USA)	1952 Kern Country earthquake	7.5	White Wolf fault	Reverse	1.3
Wrights tunnel (USA)	1906 San Francisco earthquake	7.7	San Andreas fault	Strike-slip	1.7 to 1.8
Tanna tunnel (Japan)	1930 Kita-Izu earthquake	7.3	Tanna fault		2.4
Inataro tunnel (Japan)	1978 Izu-Oshima-Kinkai earthquake	7.0			70 cm (H); 20 cm (V)
MATJHABENG mine (South Africa)	1999 unknown earthquake	4.6	Dagbreek fault	Normal dip-slip	21 cm or 44 cm (V)
Shih-Gan dam Water Conveyance tunnel (Taiwan)	1999 Chi–Chi earthquake	7.3	Chelungpu fault	Thrust	9.06 m (H); 9.80 m (V)

3. Ground Failure Surrounding the Tunnel

Damage caused by ground failure surrounding the tunnel typically includes collapse of the tunnel crown, deformation of the tunnel portal, or local collapse of the lining, particularly near the entrance zones,as shown in Figure 2.6. These types of failures are prevalent in mountain tunnels, as entrances are often situated adjacent to steep, unstable slopes. Even if the tunnel body does not intersect the landslide slip surface directly, seismically induced slope instability may alter the surrounding stress field, resulting in secondary damage to the tunnel structure.

Unlike direct ground shaking failure, this mechanism arises from an imbalance between the induced seismic ground response and the structural capacity of the tunnel support system, leading to soil-structure interaction effects that are difficult to predict without detailed geotechnical modeling.

doi:10.6342/NTU202503897

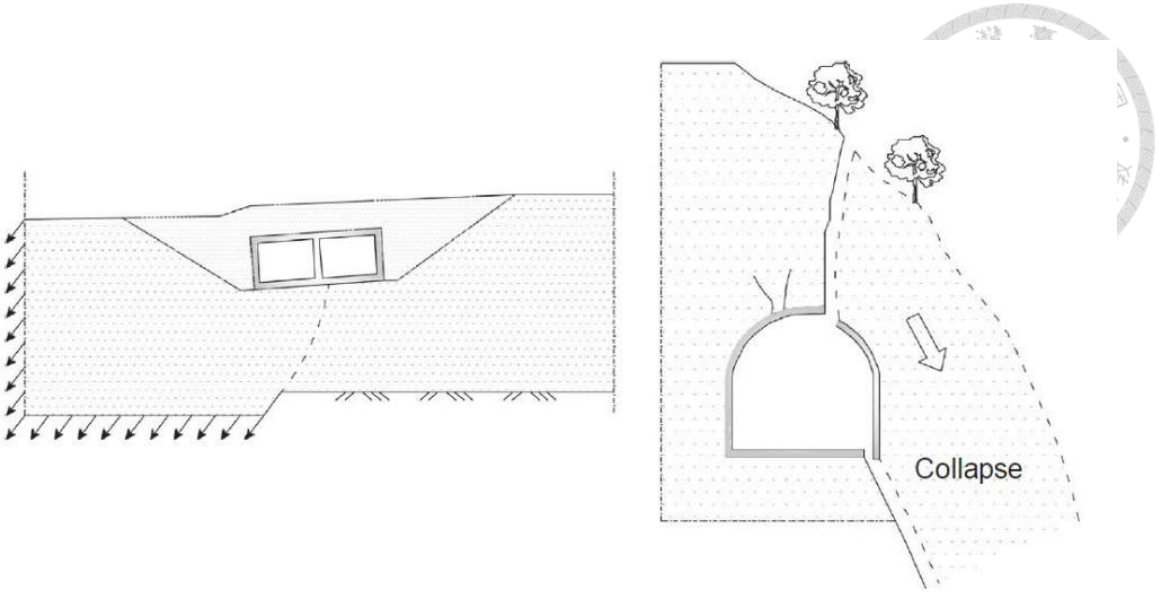

Figure 2.6 Illustration of common tunnel damage due to ground failure (Tsinidis et al., 2020)

2.3 Seismic response and earthquake resistance analysis of rock tunnels

2.3.1 Seismic Response of Tunnels

During an earthquake, seismic energy propagates in the form of stress waves that interact with underground structures. In the case of tunnels, the type and angle of incidence of these waves significantly influence their seismic response. Most current understanding of tunnel damage mechanisms is derived from qualitative assessments of historical earthquake case studies involving tunnel failures.

When subjected to seismic waves, tunnels may experience a variety of deformation modes, such as longitudinal extension or compression along the tunnel axis, cross-sectional compression, axial bending induced by shear (S) or Rayleigh (R) waves, ovaling deformation of circular cross-sections, and racking deformation in rectangular or box-

doi:10.6342/NTU202503897

shaped tunnels.

Figure 2.7(a) illustrates longitudinal deformation resulting from P-waves propagating parallel to the tunnel axis; (b) shows cross-sectional compression due to P-waves propagating perpendicular to the tunnel. Figure 2.7(c) and (d) represent axial bending caused by S- and R-waves traveling parallel to the tunnel axis. Figure 2.7 (e) demonstrates ovaling deformation caused by S-waves propagating perpendicular to the tunnel axis. Lastly, (f) depicts racking deformation in box-type tunnels induced by lateral S-wave excitation.

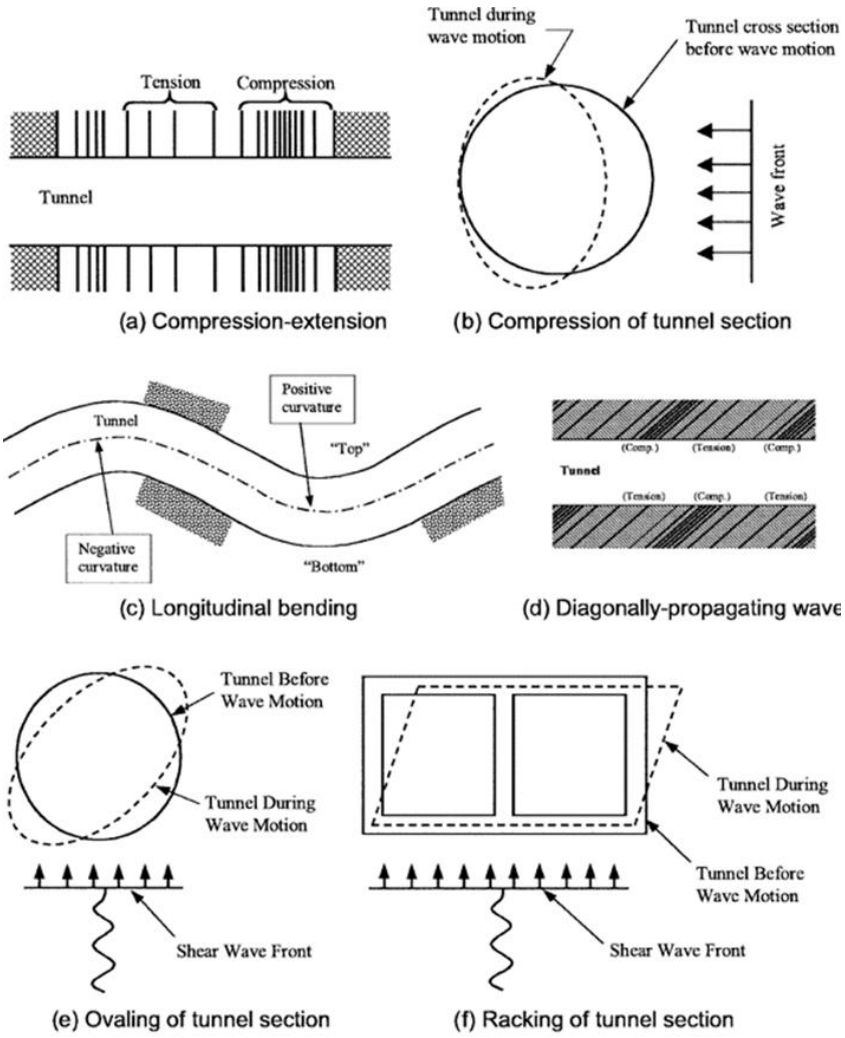

Figure 2.7 Tunnel deformation behavior under seismic wave action (Owen & Scholl,

doi:10.6342/NTU202503897

1981)

2.3.2 Seismic Analysis of Tunnels

With the advancement of wave propagation theory, the seismic behavior of circular cavities embedded in infinite, homogeneous, linear-elastic media has garnered significant attention since the 1960s. In one of the earliest studies, Pao (1962) investigated the phenomenon of stress concentration around a circular cavity subjected to incident P-waves in an infinite elastic plate. Subsequently, Mow and Mente (1963) derived analytical solutions for the stress and strain distributions around unlined circular cavities under plane strain conditions when subjected to harmonic S-wave excitation.

In the context of tunnel seismic analysis, a commonly adopted theoretical framework is the Free Field Deformation Approach. This method assumes that when the stiffness of the underground structure is comparable to that of the surrounding soil, the structure deforms synchronously with the free-field ground motion. Under this assumption, the stiffness of the tunnel is neglected, and the seismic forces are considered equivalent to those necessary to impose the same deformation on the structure as experienced by the surrounding soil. This simplified perspective has been widely utilized in traditional tunnel seismic design methodologies.

To further quantify such free-field deformation, Newmark (1968) and Kuesel (1969) proposed a simplified analytical technique for evaluating ground deformation under harmonic wave excitation at various incidence angles relative to the tunnel axis (Figure 2.8). Building on this foundational work, St. John and Zahrah (1987) developed a more comprehensive model that accounts for longitudinal and transverse strains and curvatures induced in homogeneous, isotropic, elastic soil media by incident P-, S-, and R-waves.

doi:10.6342/NTU202503897

Their approach involves projecting the ground deformations onto the tunnel axis to estimate deformation characteristics along the tunnel alignment, with key results summarized in Table 2.

Wang (1993) extended the theoretical understanding of tunnel deformation by analyzing the ovaling response of circular tunnel sections under S-wave excitation perpendicular to the tunnel axis. He proposed that this scenario could be modeled as a two-dimensional plane strain problem, and further distinguished two cases based on the relative stiffness of the tunnel lining and the surrounding ground.

In the first case (Figure 2.9(a)), where the lining stiffness is significantly lower than that of the surrounding medium, the ground is assumed to behave as if no excavation exists. The maximum radial strain at the excavation boundary correlates directly with the free-field shear strain, as expressed in Equation (2.1).

$$\frac{\Delta D}{D} = \pm 2\Upsilon_{\max}(1-\nu_m) \qquad (2.1)$$

In the second case (Figure 2.9(b)), where the lining and the ground have similar stiffness, the influence of the circular cavity must be explicitly considered. Here, the resulting maximum radial strain depends not only on the free-field shear strain but also on the Poisson's ratio of the surrounding soil, as represented in Equation (2.2).

$$\frac{\Delta D}{D} = \pm 2\Upsilon_{\max}(1-\nu_m) \qquad (2.2)$$

doi:10.6342/NTU202503897

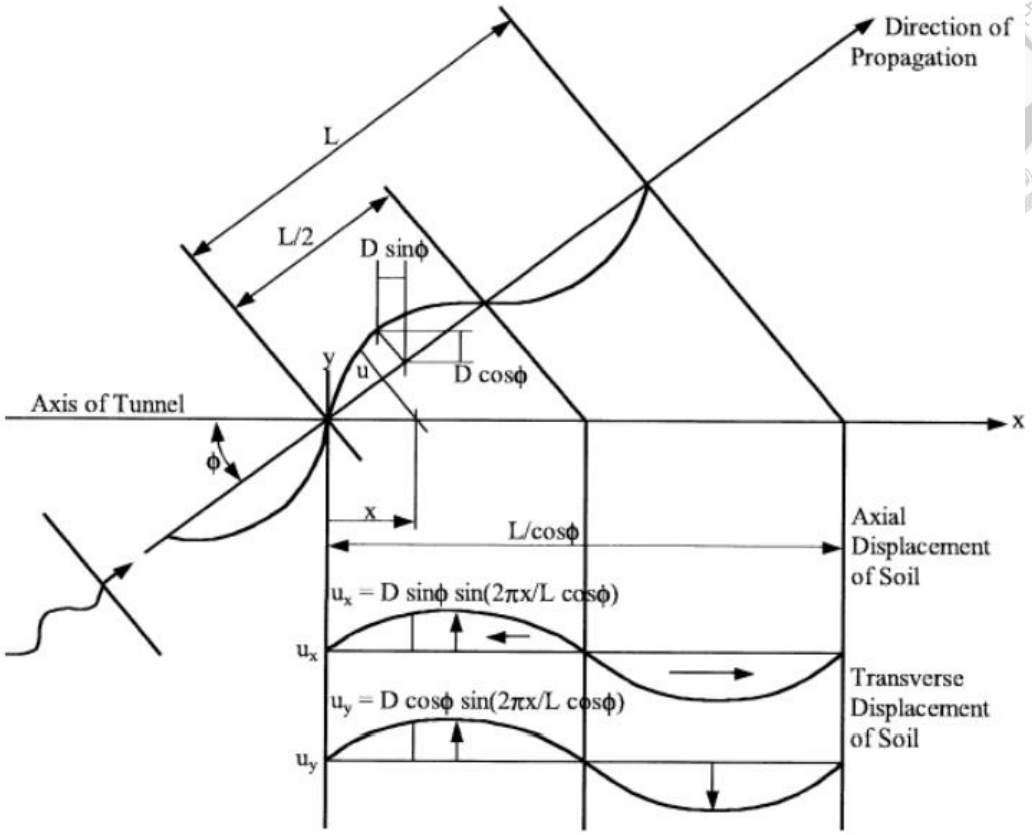

Figure 2.8 Simple harmonic wave and tunnel (after Wang, 1993)

Table 2 Strain and curvature due to body and surface waves (after St. John and Zahrah, 1987)

doi:10.6342/NTU202503897

Wave Type		Longitudinal strain	Normal strain	Shear strain	Curvature
P-Wave		$\epsilon_l = \frac{V_p}{c_p}\cos^2\phi$ $\epsilon_{lm} = \frac{V_p}{c_p}$ for $\phi = 0°$	$\epsilon_n = \frac{V_p}{c_p}\sin^2\phi$ $\epsilon_{nm} = \frac{V_p}{c_p}$ for $\phi = 90°$	$\gamma = \frac{V_p}{c_p}\sin\phi\cos\phi$ $\gamma_m = \frac{V_p}{2c_p}$ for $\phi = 45°$	$\frac{1}{\rho} = \frac{a_p}{c_p^2}\sin\phi\cos^2\phi$ $\frac{1}{\rho_m} = 0.385\frac{a_p}{c_p^2}$ for $\phi = 35°16'$
S-Wave		$\epsilon_l = \frac{V_s}{c_s}\sin\phi\cos\phi$ $\epsilon_{lm} = \frac{V_s}{2c_s}$ for $\phi = 45°$	$\epsilon_n = \frac{V_s}{c_s}\sin\phi\cos\phi$ $\epsilon_{nm} = \frac{V_s}{2c_s}$ for $\phi = 45°$	$\gamma = \frac{V_s}{c_s}\cos^2\phi$ $\gamma_m = \frac{V_s}{c_s}$ for $\phi = 0°$	$K = \frac{a_s}{c_s^2}\cos^3\phi$ $K_m = \frac{a_s}{c_s^2}$ for $\phi = 0°$
Rayleigh wave	Compressional component	$\epsilon_l = \frac{V_{RP}}{c_R}\cos^2\phi$ $\epsilon_{lm} = \frac{V_{RP}}{c_R}$ for $\phi = 0°$	$\epsilon_n = \frac{V_{RP}}{c_R}\sin^2\phi$ $\epsilon_{nm} = \frac{V_{RP}}{c_R}$ for $\phi = 90°$	$\gamma = \frac{V_{RP}}{c_R}\sin\phi\cos\phi$ $\gamma_m = \frac{V_{RP}}{2c_R}$ for $\phi = 45°$	$K = \frac{a_{RP}}{c_R^2}\sin\phi\cos^2\phi$ $K_m = 0.385\frac{a_{RP}}{c_R^2}$ for $\phi = 35°16'$
	Shear component		$\epsilon_n = \frac{V_{RS}}{c_R}\sin\phi$ $\epsilon_{nm} = \frac{V_{RS}}{c_R}$ for $\phi = 90°$	$\gamma = \frac{V_{RS}}{c_R}\cos\phi$ $\gamma_m = \frac{V_{RS}}{c_R}$ for $\phi = 0°$	$K = \frac{a_{RS}}{c_R^2}\cos^2\phi$ $K_m = \frac{a_{RS}}{c_R^2}$ for $\phi = 0°$

doi:10.6342/NTU202503897

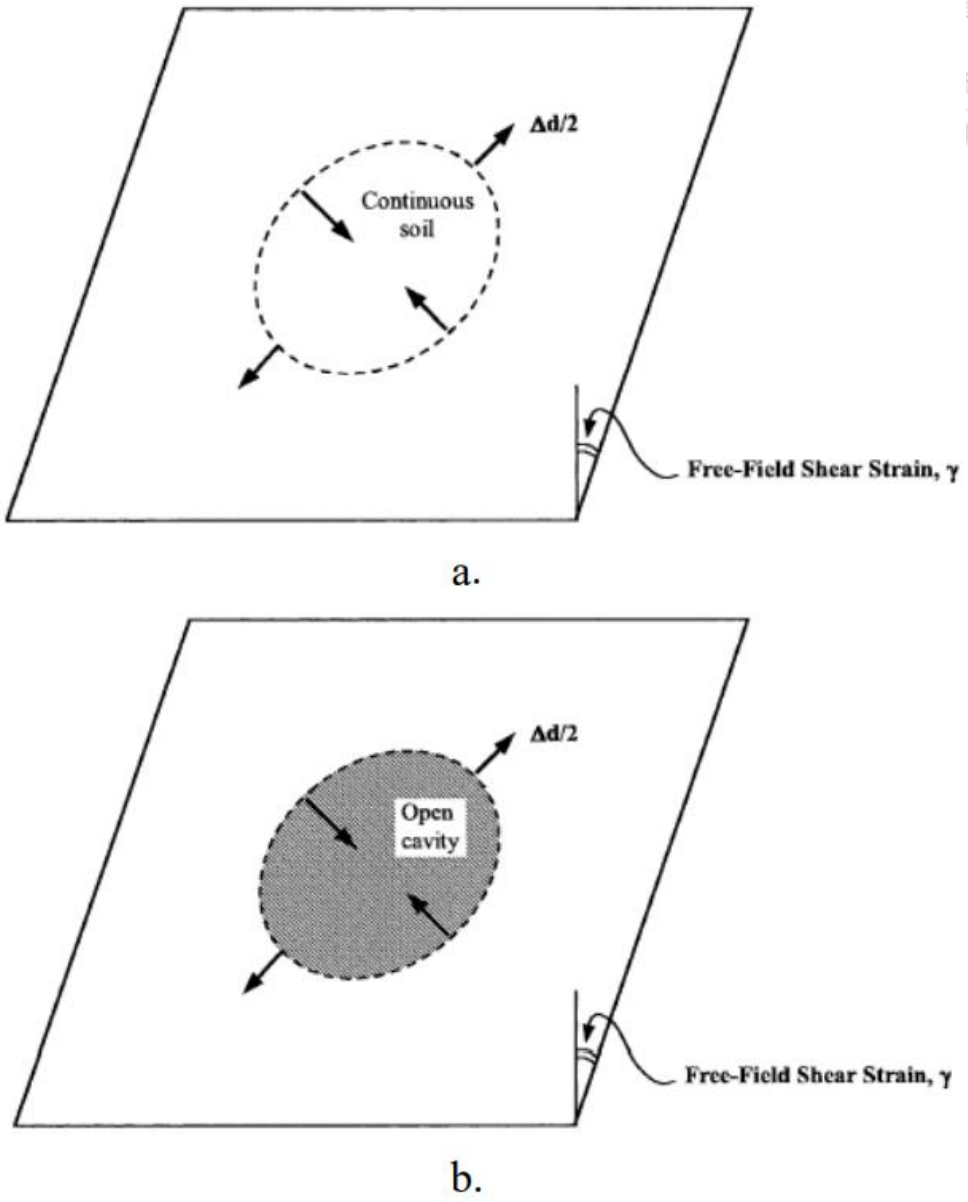

Figure 2.9 Free-field shear distortion of perforated and non-perforated ground, circular shape (after Wang, 1993).

2.4 Fragility Curves

To date, no comprehensive seismic fragility studies have been conducted in Taiwan specifically targeting tunnels, particularly mountain tunnels. Internationally, although several studies have attempted to quantify tunnel seismic fragility, their methodologies

doi:10.6342/NTU202503897

are typically based on statistical analysis of documented tunnel damage cases. However, these datasets are often limited in scope and detail due to incomplete post-earthquake investigations and the scarcity of well-documented cases. Over the past two decades, there has been a notable lack of new studies that provide a holistic evaluation of tunnel fragility under seismic loading. Most existing research considers only one or two influencing factors—such as tunnel depth or cross-sectional shape—thus limiting the applicability of their findings.

Given Taiwan's complex topography, a substantial portion of its transportation and water conveyance infrastructure relies on tunnels. As many of these tunnels are aging and approaching the end of their service lives, there is a pressing need for an effective framework to assess their vulnerability to various hazards, including seismic loading, before initiating large-scale replacement projects. Therefore, this study emphasizes the necessity of systematically identifying and quantifying the most critical parameters influencing seismic damage to tunnels. It further aims to develop corresponding fragility and resilience curves that can support risk-informed decision-making and infrastructure management.

2.4.1 Related Studies in Taiwan and Abroad

Fragility analysis has been widely applied across various infrastructure sectors, including buildings (Yeh and Chou, 2018), bridges (Billah and Alam, 2014; Stefanidou and Kappos, 2017), lifelines (Fragiadakis and Christodoulou, 2014), and nuclear power plants (Kennedy and Ravindra, 1984). As noted by Yucemen (2013), it is one of the most commonly used approaches for evaluating seismic vulnerability. However, research related to tunnels and underground structures remains limited, particularly for mountain tunnels, which are common in Taiwan. The primary challenge lies in the scarcity of

doi:10.6342/NTU202503897

complete damage records and the limited number of well-documented case histories. These limitations render traditional empirical or expert judgment methods difficult to apply and hinder the development of representative analytical results.

The earliest systematic studies of seismic fragility for rock tunnels were conducted in the United States. Notable examples include the ATC-13 guidelines published by the Applied Technology Council (ATC, 1985), the seismic guidelines issued by the American Lifelines Alliance (ALA, 2001), and the HAZUS risk assessment module developed by the Federal Emergency Management Agency (FEMA, 2022). While the original HAZUS version was released in 1997 and has since been updated to include risks from hurricanes, floods, and tsunamis, the tunnel fragility curves remain largely based on early estimates. In essence, the purpose of fragility analysis is to generate a set of curves that quantify the probability of reaching various damage states given a specific level of seismic intensity. For tunnels, these fragility curves represent the likelihood of different damage states occurring due to earthquake shaking.

Fragility methodologies can generally be classified into four categories based on data sources and analytical techniques (Rossetto, 2003): (1) expert judgment-based, (2) empirical, (3) analytical, and (4) hybrid. The respective strengths and limitations of each method are summarized in Table 3. Expert judgment approaches were particularly common before the 1980s, when reliable damage records were limited. These methods rely on expert classification of seismic intensity and damage severity (Pitilakis et al., 2008). The ATC-13 guidelines (ATC, 1985), for example, employed this approach to develop Damage Probability Matrices (DPMs) and fragility curves.

As seismic damage records became more comprehensive and techniques for measuring ground motion intensity improved, empirical methods gradually replaced

doi:10.6342/NTU202503897

expert judgment. These methods statistically correlate observed damage with seismic parameters. In the tunnel domain, however, such data remain sparse compared to buildings, resulting in only a few empirical fragility models, such as those developed by ALA (2001), FEMA HAZUS (2022), and Corigliano et al. (2007).

Analytical methods emerged with advancements in computational modeling and simulation techniques. In tunnel fragility studies, analytical approaches can be further categorized into studies on soil/urban tunnels (e.g., Argyroudis and Pitilakis, 2012; Argyroudis et al., 2014; Osmi et al., 2016; Argyroudis et al., 2017; Hu et al., 2020; Huang, 2022; Huang et al., 2022) and those focusing on rock/mountain tunnels (e.g., Le et al., 2014; Osmi et al., 2015; Qiu et al., 2018; Andreotti and Lai, 2019; Moayedifar et al., 2019; Sun et al., 2020; Zi et al., 2021; Sarkar and Pareek, 2021). Notably, most of these studies have emerged within the past decade, particularly after 2010.

Hybrid methods, which combine historical data, numerical simulations, and experimental results, offer a more comprehensive approach to fragility assessment. However, their application in tunnel research remains relatively rare.

doi:10.6342/NTU202503897

Table 3 Advantages and disadvantages of four vulnerability analysis methods (after Billah and Alam, 2014)

Method	Advantages	Disadvantages
Expert based	Easy to implement and straightforward Allows inclusion of all relevant factors	Highly subjective Strongly dependent on the knowledge and experience of the experts Limited accuracy
Empirical	Reflects actual vulnerability Presents a realistic picture	Lack of sufficient data Inconsistencies in damage observations
Analytical	Less biased All types of uncertainties can be considered	Computationally expensive Time-consuming
Hybrid	Incorporates post-earthquake data May reduce computational effort	Requires multiple data sources due to combining experimental and analytical methods High inconsistency in demand modeling

2.4.2 Definition and Probabilistic Formulation of Fragility Curves

Fragility curves are commonly employed in seismic risk assessment to describe the probability that a structure will reach or exceed a certain level of damage in response to a given seismic intensity. Since observed damage data are typically discrete in nature, fragility curves serve as a mathematical framework to transform these discrete damage states into a continuous probability function. Specifically, they quantify the conditional probability of exceeding a particular damage state DS_i given a seismic intensity measure (IM), such as peak ground acceleration (PGA) or spectral acceleration (Sa).

While PGA and Sa are widely adopted in fragility studies, several researchers have pointed out that peak ground velocity (PGV) often exhibits a stronger correlation with damage in underground structures, particularly tunnel linings (e.g., Corigliano et al., 2007). PGV is considered to better capture the effects of low-frequency ground motion components that significantly influence the deformation of flexible tunnel supports.

doi:10.6342/NTU202503897

Therefore, this study incorporates PGA, PGV, and Sa as intensity measures to investigate their respective impacts on the resulting fragility curves, aiming to evaluate which parameter provides the most reliable correlation with tunnel damage.

A lognormal distribution is typically assumed for fragility curves due to its simplicity and analytical convenience, enabling a probabilistic description using only two parameters: the median seismic intensity IM_{DS_i} at which a specific damage state is expected to occur, and the total logarithmic standard deviation β_{tot,DS_i} that captures the associated uncertainty. Under this assumption, all sources of uncertainty—stemming from structural capacity, seismic demand, and damage state thresholds—are incorporated into the dispersion term β_{tot,DS_i}.(Kennedy et al., 1980).

The conditional probability of exceeding a given damage state DS_i can be expressed using the standard cumulative distribution function Φ of the normal distribution, as follows (NIBS, 2004; Argyroudis and Pitilakis, 2012; Qiu et al., 2018):

$$P\left[DS \geq DSi \middle| IM \right] = \phi\left(\frac{\ln IM - \ln IM_{DSi}}{\beta_{tot,DSi}} \right) \quad (2.3)$$

This formulation enables the construction of fragility curves using numerical simulation, empirical observation, or hybrid methodologies, and is widely adopted in performance-based seismic assessments. For tunnel structures, where damage data are limited, such models provide a practical means to relate structural response to seismic demand in a probabilistic context.

The generation of fragility curves based on Equation (1) requires the specification of two primary parameters: the median seismic intensity IM_{DS_i} for each damage state, and the total lognormal standard deviation β_{tot,DS_i} .To obtain these values, the methodology developed by S.A. Argyroudis and K.D. Pitilakis (2012) is adopted, in

doi:10.6342/NTU202503897

which coupled numerical simulations are used to construct a damage-intensity relationship. In this approach, the Damage Index (DI) is plotted against a selected seismic intensity measure—such as peak ground acceleration (PGA)—to capture the evolution of structural response under increasing seismic demand, as shown in Figure 2.10. From this plot, the median threshold intensity IM_{DS_i} corresponding to each defined damage state (as described in Table 4) can be determined.

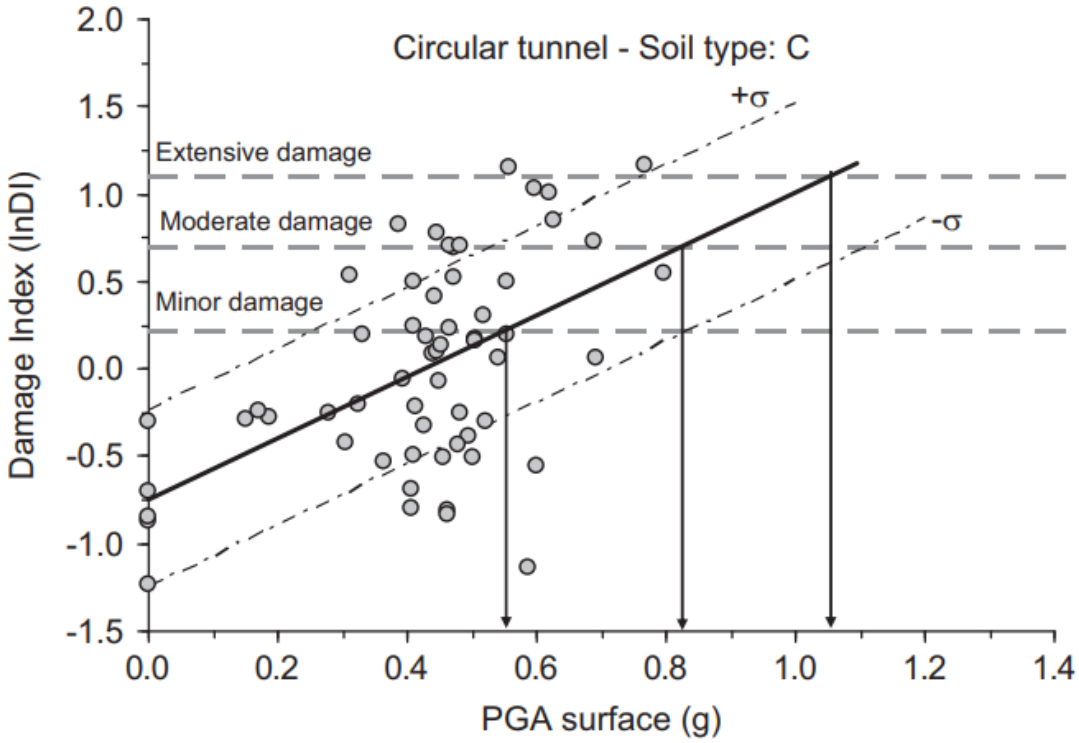

Figure 2.10 Examples of the evolution of damages with PGA at the ground surface for circular tunnel cross-sections. Estimation of the median threshold values of PGA for each damage state.(Argyroudis and Pitilakis, 2012)

The total uncertainty β_{tot,DS_i} is then computed by combining two independent components using the Square Root of the Sum of the Squares (SRSS) approach, as shown in equationasda:

$$\beta_{tot,DSi} = \sqrt{\beta_C^2 + \beta_D^2 + \beta_{DSi}^2} \quad (2.4)$$

doi:10.6342/NTU202503897

In this expression, β_C represents the variability related to the tunnel capacity and β_D represents the uncertainty of the seismic demand, while β_{DSi} reflects the uncertainty in defining the damage state thresholds.

Andreotti and Lai (2019) derived β_{DSi} subjectively by referencing external literature. This approach introduces an element of expert judgment, thereby reducing the dependence on simulation-based outcomes and resulting in what is referred to as hybrid fragility curves. Given the analytical nature of this study and the absence of sufficient empirical damage data, the primary analysis presented herein excludes the influence of β_{DSi}, and the fragility functions are initially derived solely from the variability inherent in numerical modeling results.

Nevertheless, in order to evaluate the effect of including uncertainty associated with damage state threshold estimation, this study further investigates the differences between two fragility curve formulations: one incorporating only β_{DSi}, and another considering the total lognormal standard deviation β_{tot,DS_i}, which combines uncertainties from three distinct sources—seismic demand (β_D), structural capacity (β_C), and damage state thresholds (β_{DSi}). According to Huang et al. (2017), typical values for underground structures are β_C =0.3 and β_{DSi} =0.4.

By comparing the fragility curves derived from these two scenarios—(1) using only β_D, and (2) incorporating all three components—the study aims to quantify how the inclusion of capacity and demand variability affects the resulting probability of damage. This analysis helps clarify the role of uncertainty modeling in the generation of fragility curves and provides insights into the reliability and conservatism of different modeling assumptions.

doi:10.6342/NTU202503897

2.4.3 Post-earthquake tunnel damage assessment methods

In the process of conducting seismic fragility analysis for tunnels, several key elements require further clarification. For instance, FEMA-351 (FEMA, 2000) classifies damage states (DS) for general buildings into four levels: Slight, Moderate, Extensive, and Complete. More recently, with the shift toward performance-based seismic design, structural performance levels have been redefined as Operational, Immediate Occupancy, Life Safety, and Collapse Prevention (ASCE, 2013). These performance levels are often quantified using the Incremental Dynamic Analysis (IDA) procedure, initially proposed by Bertero (1977) and formalized by Vamvatsikos and Cornell (2004), to relate the structural response to specific damage states.

However, in the field of tunnel engineering, no systematic methodology currently exists to quantify damage states or performance levels based on site-relevant damage indicators. Most existing studies—primarily based on expert judgment or empirical approaches (e.g., ATC, 1985; ALA, 2001; Corigliano et al., 2007; HAZUS, 2022)—define tunnel damage levels using observable phenomena, particularly the presence and severity of cracks in tunnel linings, as shown in Table 4.

For example, Corigliano et al. (2007) based their damage classification on the "Post-earthquake Rapid Assessment and Emergency Retrofit Techniques for Tunnel Structures" report published by the Public Construction Commission of Taiwan (Huang et al., 1999). This classification was further integrated with damage state definitions from the American Lifelines Alliance's water pipeline fragility guidelines (ALA, 2001) and Japan's Railway Technical Research Institute (RTRI, 2001) design specifications for railway tunnels. In addition to qualitative descriptions, these standards generally adopt a crack width of 3 mm and a crack length of 5 meters as the threshold between slight and

doi:10.6342/NTU202503897

moderate damage levels.

Table 4 Seismic Damage Classification Criteria for Tunnels (after Corigliano et al., 2007)

Damage level		Damage description	Functionality
None	A	No visible signs of damage observed during inspection.	Immediate interruption of operations is not strictly required
Slight	A	Minor visible damage, such as small cracks in the concrete lining, slight joint separations, partial obstruction at openings, or minor deformations. Typically, cracks are less than 3 mm wide and shorter than 5 meters.	
Moderate	B	Noticeable structural damage including partial wall or roof collapse, failure or detachment of tunnel lining, concrete spalling, exposed rebar, significant cracking, pavement damage, and deformation of walls or surrounding rock.	Interruption of operation only for 2 or 3 days
Severe	C	Portal failure, slope instability induce tunnel collapse, shared off lining, pavement uplift, rising of the invert, tunnel being flooded or where a tunnel shows damage on ventilation or lighting system	Interruption of its serviceability for a long period of time

Osmi et al. (2015), W. Qiu et al. (2018), and H. Zi et al. (2021) defined the damage index (DI) as the ratio of the bending moment acting on the tunnel lining (M) to its design capacity (M_{Rd}). This formulation is compatible with displacement-based analysis under the equal displacement assumption, which allows moment-based criteria to represent deformation-based performance.

The tunnel structure is idealized as an elastic beam subject to deformations imposed by seismic waves traveling perpendicular to the tunnel axis. The actual bending moment (M) incorporates both static and seismic loading, while the moment capacity (M_{Rd}) is determined based on the structural geometry and material properties, accounting for the

doi:10.6342/NTU202503897

combined effects of axial force (N) and bending moment (M).

Drawing from previous case histories and engineering judgment, four discrete damage states are established: minor, moderate, extensive, and complete damage. These levels primarily reflect the condition of the tunnel lining. While the numerical thresholds for DI remain tentative, the adopted limits offer a reasonable basis for estimating tunnel damage severity. A summary of the classification is provided in Table 5.

Table 5 Definition of damages states for tunnel lining

Damage state(dsi)	Range of damage index (DI)	Central value of damage index
ds0. None	$M/M_{Rd} \leqq 1.0$	-
ds1. Minor/slight	$1.0 < M/M_{Rd} \leqq 1.5$	1.25
ds2. Moderate	$1.5 < M/M_{Rd} \leqq 2.5$	2.00
ds3. Extensive	$2.5 < M/M_{Rd} \leqq 3.5$	3.00
ds4. Collapse	$M/M_{Rd} > 3.5$	-

This study references the use of the ratio between the actual bending moment experienced by the tunnel lining and its moment capacity to assess tunnel damage.One key advantage of this index is its direct correlation to structural mechanics principles. Tunnels are often modeled as continuous elastic beams subjected to deformation due to seismic ground motion, particularly when seismic waves propagate perpendicularly to the tunnel axis. In such cases, the dominant failure mode is flexural, making the bending moment a natural and interpretable damage parameter.

Compared to purely observational indices, such as crack width or displacement, the

doi:10.6342/NTU202503897

moment-based definition allows for a unified and quantitative interpretation of damage states across different tunnel geometries and soil-structure interaction conditions. It bridges numerical simulation with performance-based evaluation, enabling engineers to not only simulate damage patterns but also assess the proximity of structural demand to failure thresholds based on material strength and section geometry. Furthermore, unlike relative displacement indices, which may be sensitive to measurement techniques and boundary conditions, the bending moment ratio can be consistently extracted from coupled static–dynamic analyses.

Moreover, this method facilitates compatibility with standard design frameworks such as Eurocode and ACI, which define structural limits in terms of ultimate moment and axial capacities. By integrating static and seismic load effects, the DI reflects both the dynamic response and the cumulative demand imposed on the structure.

In summary, the adoption of M/M_{Rd} as a damage index offers a well-grounded, physically meaningful, and analytically tractable approach to fragility modeling for tunnels. It effectively captures both structural demand and capacity in a single normalized parameter, and has been successfully applied in numerous studies (e.g., Osmi et al., 2015; Qiu et al., 2018; Zi et al., 2021) to generate robust fragility curves for underground infrastructure.

doi:10.6342/NTU202503897

Chapter 3 Methodology

3.1 FLAC Dynamic Analysis

This research develops an analytical framework through numerical simulations that integrate both static and dynamic analyses using the finite difference method. Specifically, the approach involves static tunnel stress analysis under plane strain conditions, which is compared against dynamic time history responses derived from seismic input. This chapter outlines the assumptions, boundary conditions, and parameter settings adopted in building the analytical model, along with the methods used to verify its accuracy and validity.

FLAC 2D was selected as the primary analysis tool for its strong capabilities in handling complex geotechnical problems. Based on the finite difference method, FLAC is particularly suitable for simulating nonlinear material behavior, large deformations, and time-dependent processes such as seismic loading. These features are especially relevant in mountain tunnel applications, where the interaction between tunnel linings and surrounding rock masses is highly nonlinear and often subject to instability. Furthermore, FLAC allows for flexible mesh zoning and the incorporation of user-defined constitutive models, enabling detailed control over simulation parameters. Compared to finite element–based software, FLAC also offers greater computational efficiency when analyzing a large number of simulation cases, making it ideal for parametric studies such as those required in fragility curve generation.

doi:10.6342/NTU202503897

3.1.1 Governing Equations in FLAC Dynamic Analysis

In solving dynamic problems within a specific domain, FLAC 2D employs the principles of the explicit finite difference method to compute the governing equations of motion. The general form of the dynamic equilibrium equation is expressed as:

$$m\frac{d^2\dot{u}}{d^2t} = F \tag{3.1}$$

where m represents the material density, u is the displacement vector, and F denotes the external force applied to the system.

Further elaborated, the motion equation in component form becomes:

$$\rho\frac{d^2u_i}{d^2t} = \frac{\partial\sigma_{ij}}{\partial x_j} + \rho g_i \tag{3.2}$$

In this expression, ρ is the mass density, t is time, x_j is the spatial coordinate component, g_i is the component of gravitational acceleration (representing body forces), and σ_{ij} refers to the components of the stress tensor.

This formulation allows FLAC 2D to simulate the propagation of seismic waves and the resulting dynamic response in geotechnical systems with time-dependent behavior and nonlinear characteristics.

3.1.2 Selection of dynamic boundaries

(a) Free-Field boundaries:

Seismic excitation is typically introduced as upward-propagating plane waves through the underlying soil or rock. To simulate realistic wave behavior, the lateral boundaries of the model must account for the free-field motion that would occur if the structure were not present.

In some simplified cases, basic lateral boundary conditions may be adequate. For

doi:10.6342/NTU202503897

instance, if the seismic input consists solely of a shear wave applied along a horizontal boundary (e.g., boundary AC in Figure 3.1), then vertical constraints applied to side boundaries AB and CD may suffice—provided that these boundaries are placed far enough away to minimize wave reflections and approximate free-field behavior. In materials with high damping, this condition can be achieved with relatively small model widths (Seed et al., 1975). However, in cases with low material damping, a much larger model domain would be required, which may be computationally inefficient or impracticl.

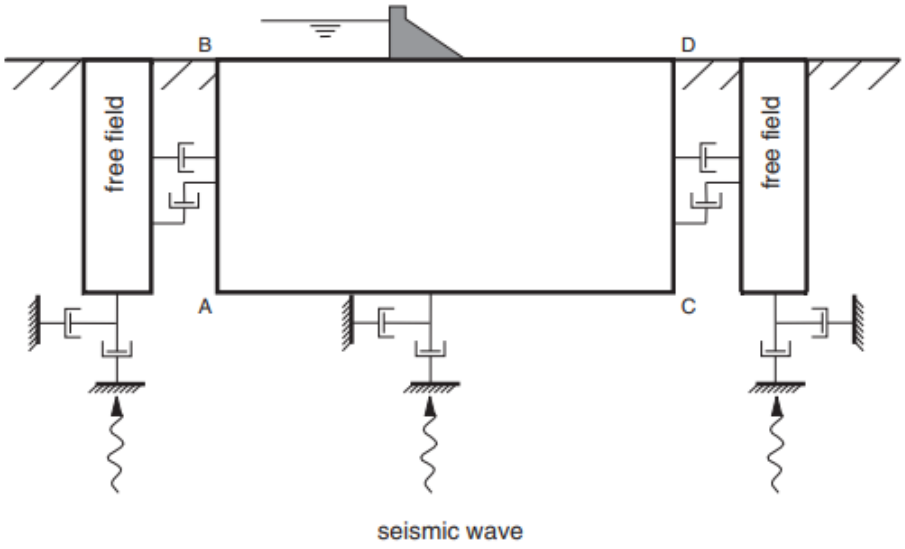

Figure 3.1 Model for seismic analysis of surface structures and free-field mesh

To overcome this limitation, an alternative method involves actively imposing free-field conditions along the model boundaries to preserve non-reflective behavior—that is, to allow outward-propagating waves to be absorbed rather than reflected.

In FLAC, this method is realized by performing a one-dimensional free-field simulation concurrently with the main model analysis. The lateral boundaries of the main grid are connected to the free-field columns using viscous dashpots, mimicking a quiet boundary condition. The unbalanced forces computed from the free-field grid are then imposed on the corresponding boundaries of the main grid. The governing relationships

doi:10.6342/NTU202503897

for these interactions are given in Equations (1.19) and (1.20) for the left-hand side, and similar equations apply to the right-hand boundary.

$$F_x = -[\rho C_p(\upsilon_x^m - \upsilon_x^{ff}) - \sigma_{xx}^{ff}]\Delta S_y \quad (3.3)$$

$$F_y = -[\rho C_s(\upsilon_y^m - \upsilon_y^{ff}) - \sigma_{xy}^{ff}]\Delta S_y \quad (3.4)$$

Where ρ = density of material along vertical model boundary;

C_p = p-wave speed at left-hand boundary;

C_s = s-wave speed at left-hand boundary;

ΔS_y = mean vertical zone size at boundary gridpoint;

υ_x^m = x-velocity of gridpoint in main grid at left boundary;

υ_y^m = y-velocity of gridpoint in main grid at left boundary;

υ_x^{ff} = x-velocity of gridpoint in left free field;

υ_y^{ff} = y-velocity of gridpoint in left free field;

σ_{xx}^{ff} = mean horizontal free-field stress at gridpoint; and

σ_{xy}^{ff} = mean free-field shear stress at gridpoint.

(b) Quiet boundaries:

In geomechanical modeling, the materials involved are often best represented as extending infinitely beyond the area of interest, especially at the scale of typical engineering analyses. For example, deep underground excavations are usually treated as being embedded within an infinite domain, whereas surface or near-surface structures are modeled atop a semi-infinite half-space. However, numerical simulations must work within a finite computational domain, and this necessitates the application of artificial boundary conditions at the model edges.

doi:10.6342/NTU202503897

In static analyses, these artificial boundaries—often modeled as fixed or elastic—can be positioned sufficiently far from the area of interest to minimize their influence, especially when using boundary element methods. In dynamic simulations, however, traditional boundary conditions pose a significant challenge: they tend to reflect outward-propagating waves back into the model domain, which violates the physical requirement for energy to radiate freely out of the system. One solution is to enlarge the model domain such that material damping naturally attenuates the reflected waves. However, this approach significantly increases computational demands.

A more efficient alternative is the use of absorbing or quiet boundaries, which are specifically designed to allow outgoing seismic energy to exit the model with minimal reflection. In FLAC, this is achieved through the implementation of the viscous boundary formulation developed by Lysmer and Kuhlemeyer (1969). This technique employs dashpots placed at model boundaries in both the normal and shear directions to absorb incident wave energy. The method is particularly effective for absorbing body waves that strike the boundary at angles greater than 30°, and is widely used in dynamic geotechnical simulations to improve boundary realism while maintaining computational efficiency.

(c) Flexible base

In dynamic soil-structure interaction (SSI) analyses, the assumption regarding the base boundary condition plays a critical role in influencing the accuracy of the simulated seismic response. A flexible base model, in contrast to a rigid base, allows for the representation of ground compliance and energy dissipation mechanisms at the interface between the structure and the underlying soil or rock. This approach is particularly important when modeling underground structures such as tunnels, where the interaction with the surrounding medium is a key factor in the propagation of seismic waves and the

doi:10.6342/NTU202503897

resulting deformation patterns.

The flexible base concept recognizes that the underlying soil or rock is not infinitely stiff, and thus can deform in response to dynamic loading. By incorporating deformable boundary conditions—often implemented through compliant springs, dashpots, or coupled free-field elements—the model can more realistically simulate both the transmission and reflection of seismic waves at the base. This not only reduces artificial wave reflections that would occur with a perfectly rigid base, but also better captures the impedance contrast and wave amplification effects associated with site-specific stratigraphy and material properties.

In FLAC 2D, flexible base modeling is often realized through quiet (absorbing) boundaries or free-field boundaries that impose velocity or stress constraints consistent with one-dimensional site response (Figure 3.2). These methods enable energy to radiate out of the model domain, approximating semi-infinite conditions and thus improving the fidelity of the analysis in representing real seismic behavior. Consequently, flexible base modeling is essential in seismic analyses where accurate representation of boundary wave propagation and soil-structure interaction is required, particularly for systems with large extents, significant depth variation, or nonlinear soil behavior.

doi:10.6342/NTU202503897

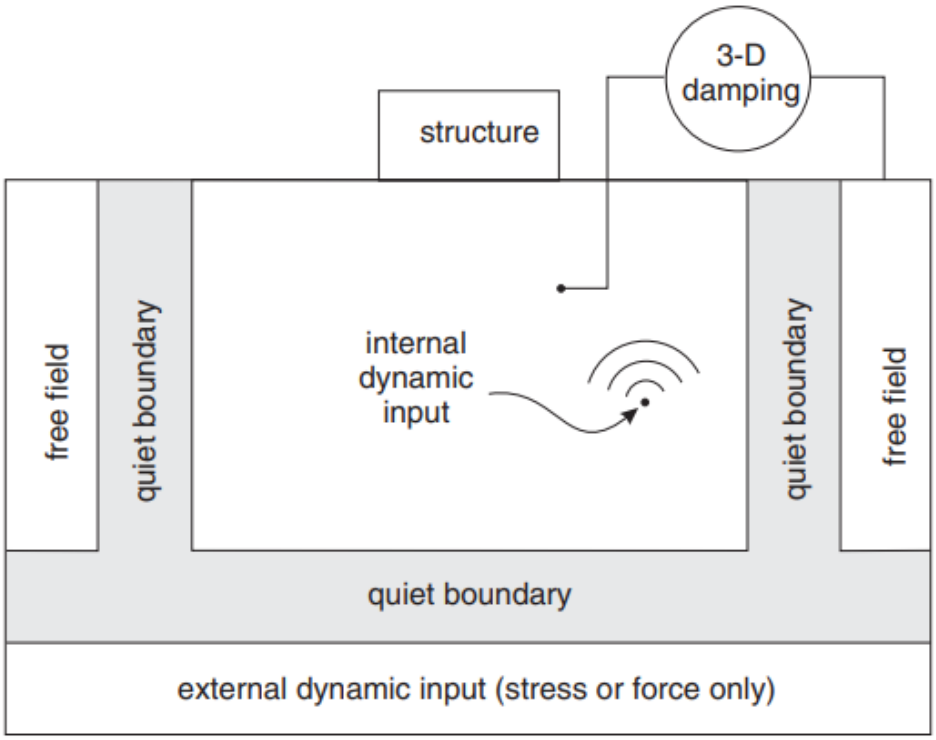

Figure 3.2 Flexible base

3.1.3 Element size

The size of the elements used in a numerical model directly influences the number of grid points and, consequently, the overall computational cost of dynamic simulations. According to the guidelines proposed by Kuhlemeyer and Lysmer (1973), to ensure accurate simulation of wave propagation, the element dimension should not exceed one-eighth to one-tenth of the shortest wavelength associated with the highest frequency component of the input motion. Adhering to this principle, the present study adopted an element size smaller than one-tenth of the minimum incident wavelength. The numerical mesh was constructed using four-node quadrilateral elements, allowing for reliable wave transmission while maintaining computational efficiency.

3.1.4 Damping Considerations in Dynamic Analysis.

a. Rayleigh damping

doi:10.6342/NTU202503897

Rayleigh damping, commonly applied in the dynamic analysis of structures and elastic continua, is a method for attenuating the natural vibration modes of a system. Also referred to as viscous damping, it introduces energy dissipation proportional to both mass and stiffness. The damping matrix in this model is expressed as a linear combination of the mass and stiffness matrices:

$$C = \alpha M + \beta K \tag{3.5}$$

Here, α and β represent the mass-proportional and stiffness-proportional damping coefficients, respectively. The damping ratio for a particular vibration mode ξ_i is related to its angular frequency ω_i by:

$$2\xi_i\omega_i = \alpha + \beta\omega_i^2 \tag{3.6}$$

As illustrated in Figure 3.3, the critical damping ratio varies with angular frequency. At lower frequencies, damping is dominated by the mass-proportional term, while at higher frequencies, the stiffness-proportional component prevails. The overall damping curve reaches its minimum at a characteristic frequency, which is defined as:

$$\alpha = \xi_{\min}\omega_{\min} \tag{3.7}$$

$$\beta = \xi_{\min} / \omega_{\min} \tag{3.8}$$

This center frequency represents the point at which the total damping is least. In most practical applications, the parameters α and β are calibrated to match desired damping ratios at two selected frequencies. Solving the system of equations derived from these two damping-frequency pairs yields the required coefficients.

Due to the complexity of directly computing the damping matrix for real-world systems, empirical methods are often adopted. In such cases, damping ratios are estimated based on engineering judgment, material properties, and prior experience with similar structures. This empirical calibration ensures that the applied damping realistically

doi:10.6342/NTU202503897

captures energy dissipation without overcomplicating the numerical model.

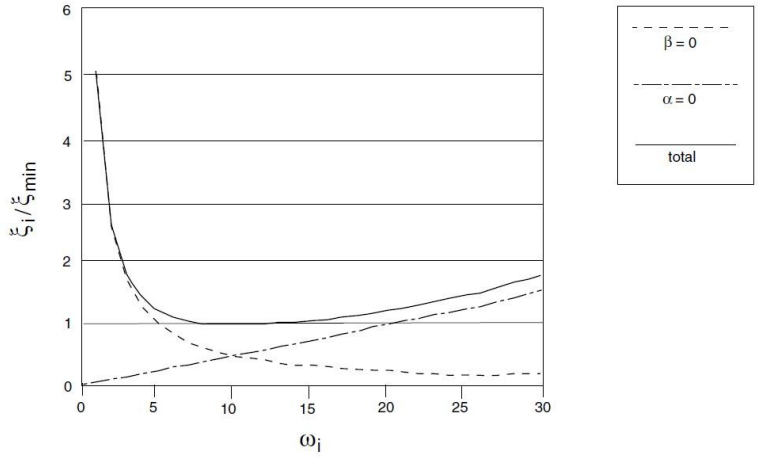

Figure 3.3 Variation of normalized critical damping ratio with angular frequency (Itasca, 2011. FLAC Version 7.0)

b. Hysteretic damping

In FLAC, nonlinear soil behavior is simulated through the reduction of shear stiffness based on predefined degradation relationships. These relationships describe how the secant shear modulus M_s varies with cyclic shear strain amplitude γ, and are expressed as:

$$\bar{\tau} = M_s \gamma \tag{3.9}$$

where $\bar{\tau}$, is the normalized shear stress given by τ/Go.

Given the degradation curve $M_s(\gamma)$, the tangent shear modulus M_t can be calculated as the derivative of the stress–strain curve, defined as:

$$\mathrm{M}_t = \frac{d\bar{\tau}}{d\gamma} = M_s(\gamma) + \gamma \frac{dM_s(\gamma)}{d\gamma} \tag{3.10}$$

During dynamic simulations, FLAC replaces the initial shear modulus G_0 with an incremental shear modulus defined as G= $G_0 \cdot \mathrm{M}_t$, updating it at every time step in the explicit time integration scheme. This modulus reduction mechanism introduces material

doi:10.6342/NTU202503897

nonlinearity and allows energy dissipation to be realistically captured.

FLAC provides built-in fitting tools, one of which is the sigmoid function "Sig3", described by the following equation:

$$M_s = \frac{a}{1+\exp\left[-(L-x_0)/b\right]} \quad (3.11)$$

where L = log10(γ), and a, b, x_0 are fitting parameters that control the shape of the degradation curve.

This modeling framework enables the simulation of strain-dependent stiffness degradation and associated hysteretic damping, making it particularly effective for nonlinear dynamic analyses of soil–structure interaction problems.

3.2 Model Validation

3.2.1 Model material and element test

In this study, the numerical model was developed using FLAC 2D to simulate the seismic behavior of rock masses, incorporating both static linear elastic and dynamic nonlinear analyses. The model dimensions were chosen to ensure adequate boundary spacing to minimize wave reflections, as detailed in Table 6. Material parameters were adopted based on the quartz mica schist properties surrounding the Jiabao Tunnel, following the input data established by Su (2021) (see Table 7). Since three burial depths were considered in the simulations, the dynamic characteristics were referenced from Anbazhagan et al. (2017) for depths ranging from 75 to 300 meters. Accordingly, two distinct shear modulus reduction curves were developed to reflect depth-dependent nonlinear behavior (Figure 3.4).

Although the deepest tunnel model considered in this study reaches 400 meters, the modulus reduction curve for the 150-300 meters depth range was still adopted for the

doi:10.6342/NTU202503897

deepest layer. This decision is justified by the fact that the 150-300 meters curve already reflects the stiffness behavior of moderately deep rock masses, and no significant deviations are expected beyond 300m based on the available attenuation trends. Therefore, the use of the 150-300 meters curve provides a conservative and reasonable approximation for representing nonlinear soil behavior at depths greater than 300 meters.

To better capture nonlinear soil behavior, the "Sig3" model was adopted to fit the shear modulus degradation curves. The results of this matching process are presented in Figure 3.5 and Figure 3.6.Table 8 and is Table 9 are the parameters of fitting G/G_{max} curve in different depth in Flac. Because the nonlinear stiffness degradation curves inherently incorporate material damping characteristics, supplementary numerical simple shear tests were conducted using a single-zone FLAC model to derive the corresponding damping ratio curves.

It was observed that the hysteretic damping response predicted by FLAC tends to be higher than that observed in laboratory tests, even when the stiffness degradation curves are well-matched (Cundall 2006)**.** This overestimation has been previously discussed in the literature and is likely attributed to the nonstationary characteristics of soil response under dynamic loading conditions. In other words, while the matched degradation functions accurately represent stiffness reduction, the associated energy dissipation behavior—i.e., damping—may be exaggerated due to the idealized assumptions embedded in the hysteretic formulation used in FLAC

The analysis further incorporated ground motion records from the KiK-net downhole array database, selecting profiles with both surface and corresponding bedrock motions. Site response analyses were carried out under equivalent-linear and total-stress nonlinear conditions using varying shear modulus and damping curves. The resulting surface

doi:10.6342/NTU202503897

response spectra were compared against the observed response spectra at each site to evaluate which modulus reduction curve best matched the empirical data.

During the initial gravity equilibrium phase, both the rock mass and the tunnel lining were modeled as homogeneous, isotropic, and linearly elastic materials. Model accuracy was validated by comparison with theoretical solutions. The subsequent dynamic analysis was conducted in two stages: first, assuming the rock mass to be linearly elastic to validate boundary conditions and wave propagation behavior using DEEPSOIL; and second, by introducing nonlinear behavior in the rock mass to examine the influence of material nonlinearity on seismic response.

Table 6 Model dimensions.

Model Size		Encrypted Radiation Grid Size		Tunnel Dimensions	
Depth	Width	Depth	Width	Diameter	Thickness
200m	200m	80m	80m	6m	0.3m

Table 7 Numerical model material parameter

Name	Unit Weight (kg/m^3)	Elastic Modulus (Pa)	Poisson's ratio	P-wave velocity (m/s)	S-wave velocity (m/s)
Rock Mass	2779	1.21E+09	0.25	722	417
Concrete Lining	2400	2.13E+10	0.2	-	-

doi:10.6342/NTU202503897

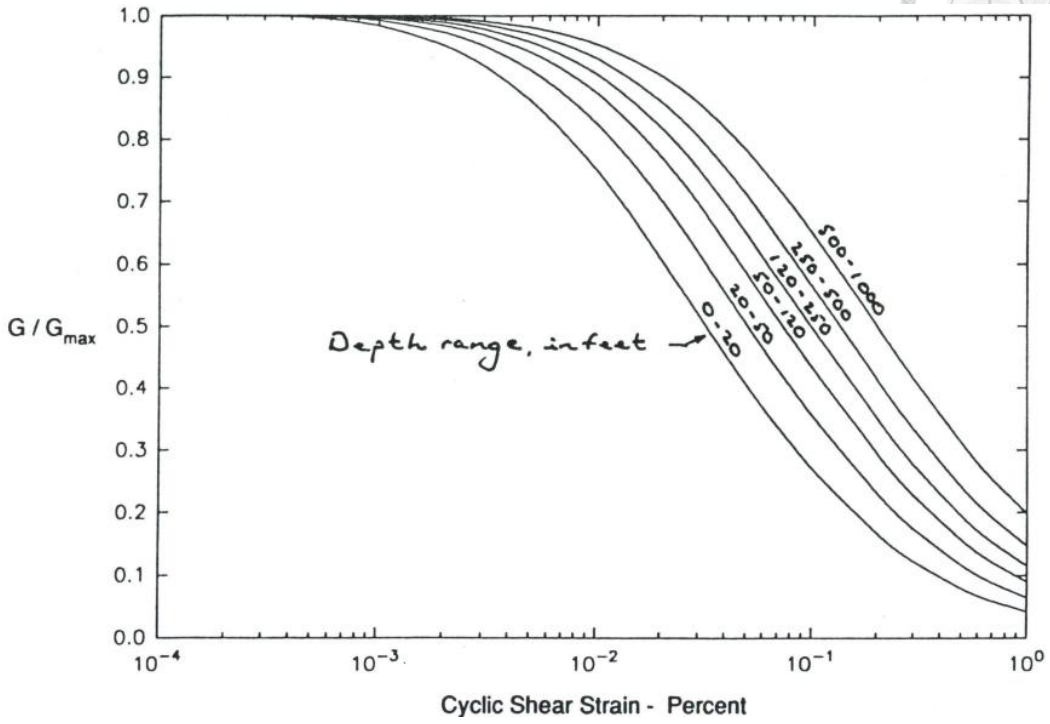

a. Shear modulus reduction curve

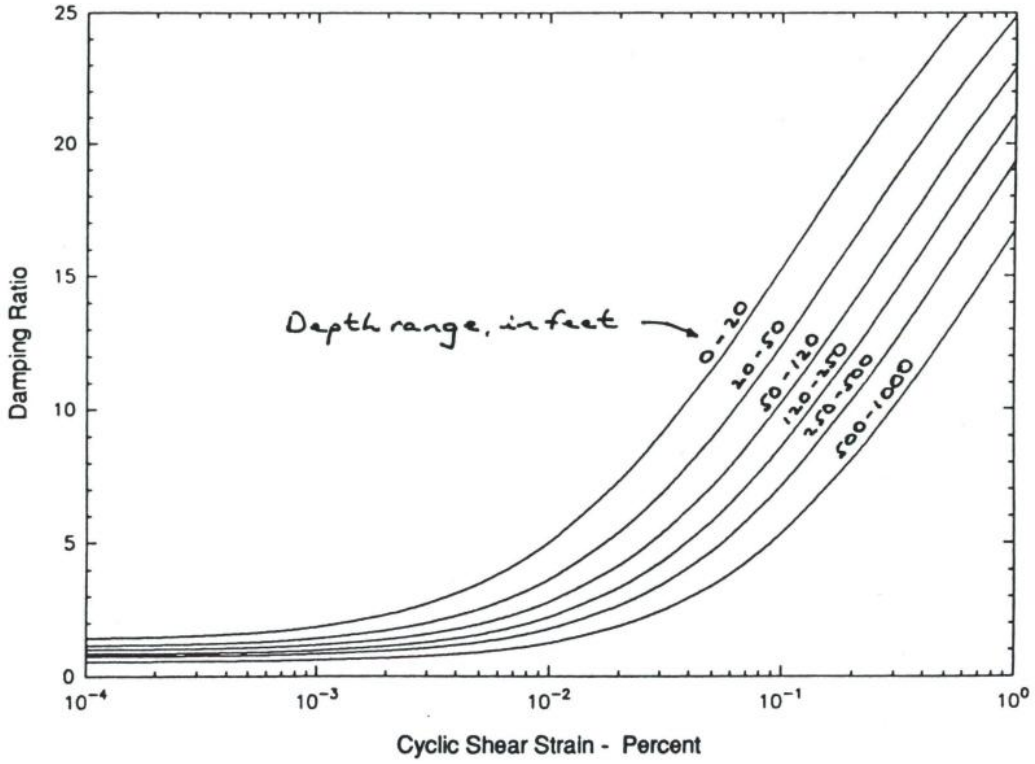

b. Damping curve

doi:10.6342/NTU202503897

Figure 3.4 Variation of shear modulus (epri,1993)

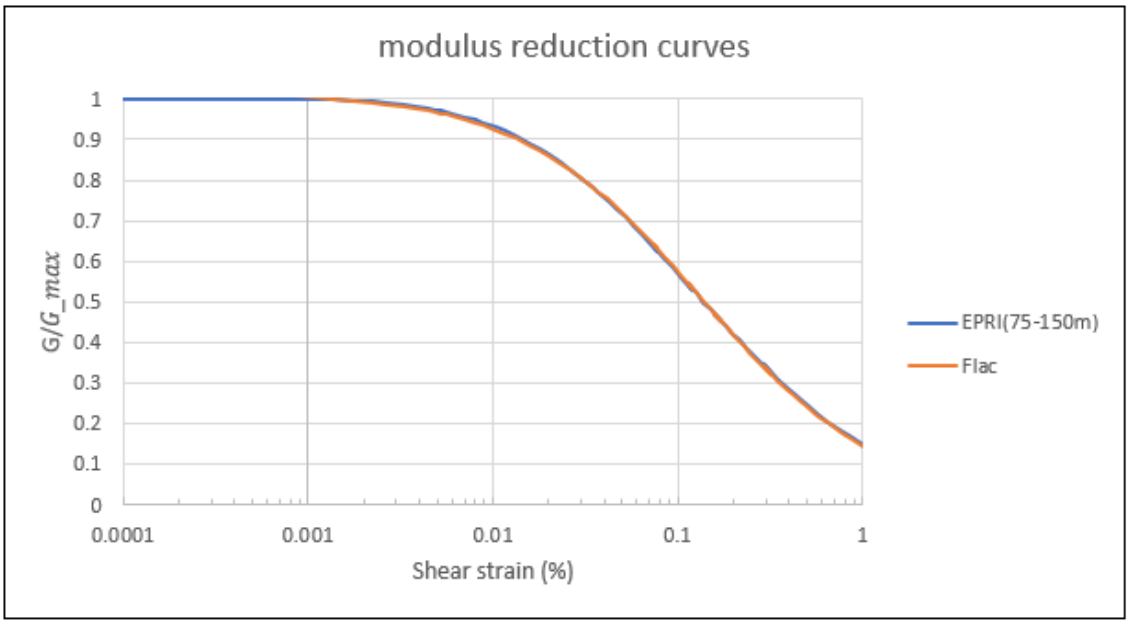

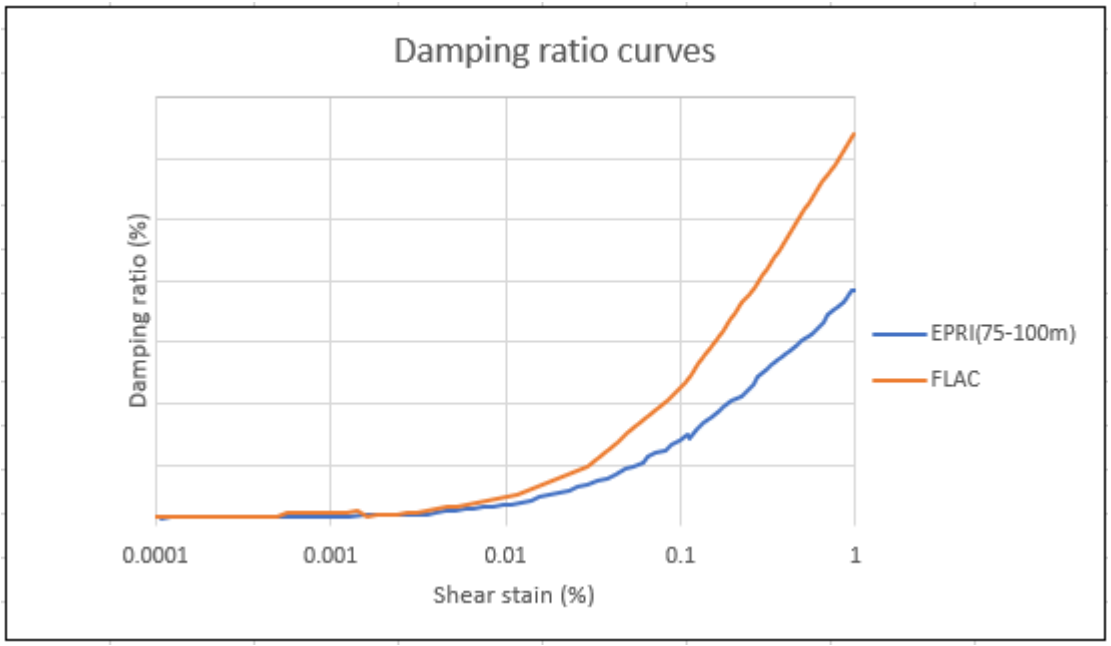

Figure 3.5 The comparison of modulus reduction and damping ratio curves between Flac and EPRI (75-150m)

doi:10.6342/NTU202503897

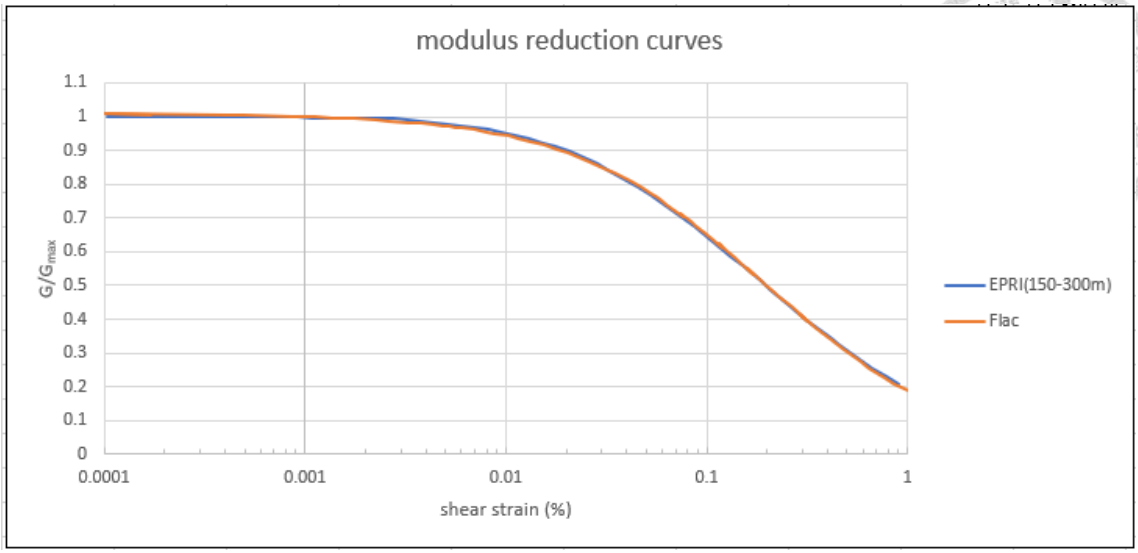

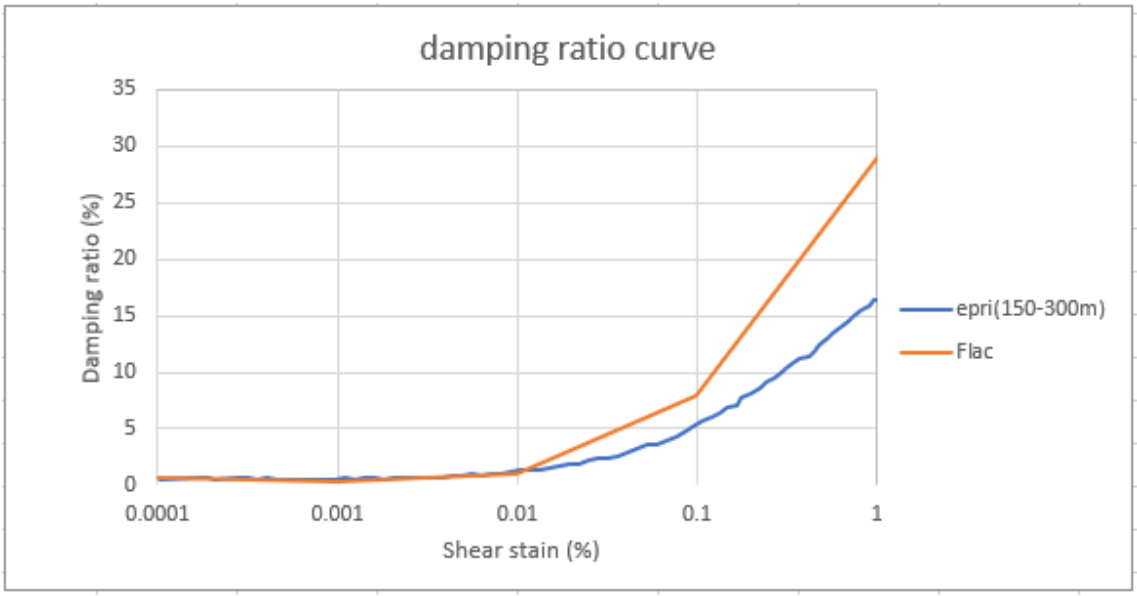

Figure 3.6 The comparison of modulus reduction and damping ratio curves between Flac and EPRI (150-300m)

Table 8 Parameters of fitting G/G_{max} curve (75-150m)

Sig3 model parameters of hysteretic damping			Rayleigh damping	
a^*	b^*	x_0^*	f_{min}^*	ξ_{min}^*
1.00	-0.4877	-0.873	0.01059	2.809

doi:10.6342/NTU202503897

Table 9 Parameters of fitting G/G_{max} curve (150-300m)

Sig3 model parameters of hysteretic damping			Rayleigh damping	
a^*	b^*	x_0^*	f_{min}^*	ξ_{min}^*
1.00	-0.4819	-0.7113	0.01059	1.405

3.2.2 Validation of theoretical rock-lining interaction

This study specifically chooses the analytical solution proposed by Park et al. (2009), known as the PTTO no-slip solution, for validation purposes. The primary motivation is its comprehensive and rigorous theoretical formulation, clearly distinguishing between the extreme boundary conditions of no-slip and full-slip interfaces. Park et al.'s work offers explicit mathematical derivations for lining–rock interface interactions, explicitly addressing and resolving discrepancies among previous analytical solutions. Furthermore, the reference extensively investigates the sensitivity of lining responses to interface slip coefficients and deformation ratios, which significantly enhances its value for verifying numerical models. Selecting this analytical solution as a validation benchmark ensures robust verification of the accuracy and reliability of the numerical modeling approach adopted in this research. By doing so, the subsequent analyses, particularly those regarding the seismic responses of tunnel linings, can accurately reflect actual physical behaviors. Consequently, the reliability and credibility of the study's outcomes are greatly improved, laying a solid theoretical foundation for engineering applications and practical decision-making related to the seismic assessment of tunnel structures.

I. Problem Definition and Assumptions

Consider a deeply embedded circular tunnel with radius R. Under seismic shear-

doi:10.6342/NTU202503897

wave-induced deformation (ovaling), the tunnel lining experiences ovaling deformation. Such deformation can be modeled as equivalent static shear loading, derived from the free-field shear strain, as illustrated in Figure 3.7:

The maximum shear strain in the free-field is:

$$\gamma_c = \frac{u(-R,t_c) - u(R,t_c)}{2R} \tag{3.12}$$

The equivalent static shear stress applied to the tunnel is:

$$\tau = \frac{E_s \gamma_c}{2(1+\nu_s)} \tag{3.13}$$

$$\tau = \frac{E_s \gamma_c}{2(1+\nu_s)} \tag{3.14}$$

Where:

E_s : Young's modulus of the rock

ν_s : Poisson's ratio of the rock

$u(y,t)$: Free-field displacement as a function of depth y and time t.

doi:10.6342/NTU202503897

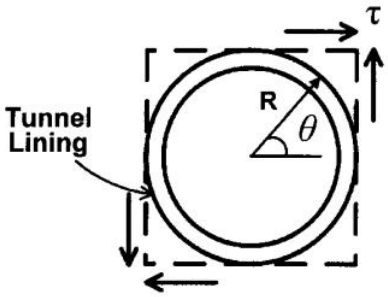

Fig. 1. A circular tunnel.

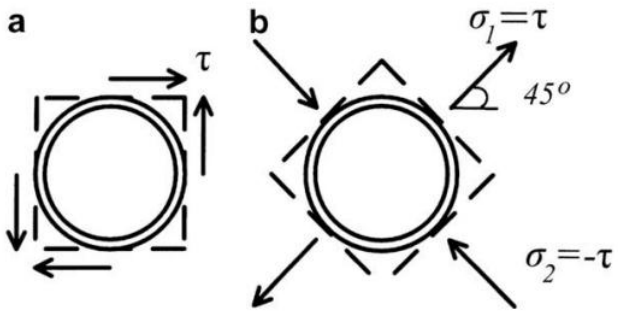

Figure 3.7 Seismic shear loading and equivalent static loading.

II. Problem Decomposition and Mathematical Modeling

For analytical convenience, the problem is decomposed into three sub-problems (see Fig. 3):

a. Cylindrical cavity subjected only to external loading.

b. Circular lining subjected only to interface stresses.

c. Cylindrical cavity in rock subjected only to interface stresses.

Stress-displacement relationships are separately established for each sub-problem, then combined through compatibility and equilibrium conditions.

doi:10.6342/NTU202503897

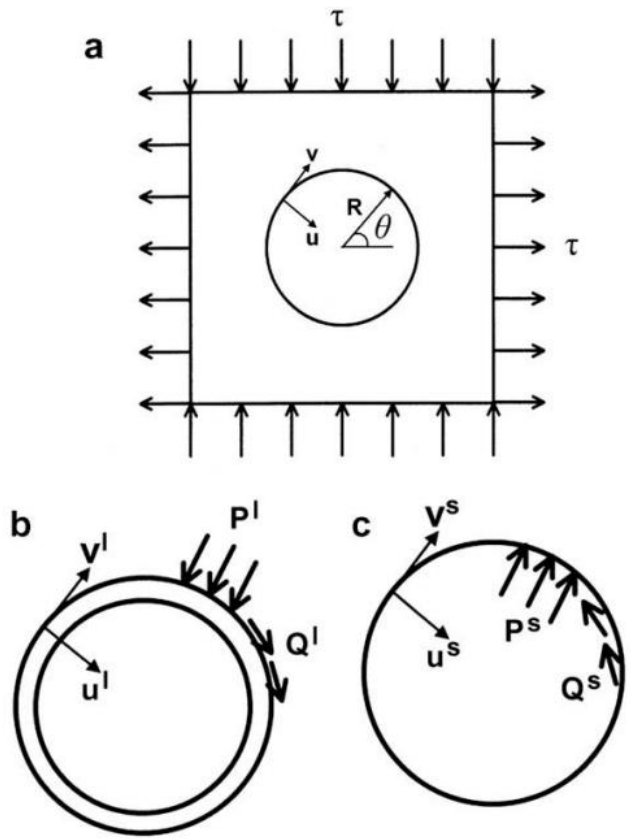

Figure 3.8 Separation of equivalent static loading

III. Derivation of Displacement–Stress Relationships:

The displacement–stress relations for cases (a), (b), and (c):

For a cylindrical cavity under external loads (Fig. 3a):

$$\begin{bmatrix} u \\ v \end{bmatrix} = \begin{bmatrix} u_d \cos(2\theta + \frac{\pi}{4}) \\ v_d \sin(2\theta + \frac{\pi}{4}) \end{bmatrix} \quad (3.15)$$

Where, $u_d = 2(1-\nu_s)R\gamma_c$, $v_d = -u_d$

For the lining (Fig. 3b):

The lining displacement-interface stress relation is:

$$\begin{bmatrix} u_l \\ v_l \end{bmatrix} = I_l \begin{bmatrix} P_l \\ Q_l \end{bmatrix} \quad (3.16)$$

doi:10.6342/NTU202503897

with I_l as the lining's influence matrix depending on lining elasticity.

For the rock cavity (Fig. 3c):

Rock displacement–stress relation:

$$\begin{bmatrix} u_s \\ v_s \end{bmatrix} = I_s \begin{bmatrix} P_s \\ Q_s \end{bmatrix} \tag{3.17}$$

IV. Boundary and Interface Conditions

For the PTTO no-slip condition (perfectly bonded interface), the boundary conditions are:

Force equilibrium:

$P_s + P_l = 0$, $Q_s + Q_l = 0$

Displacement compatibility (no-slip):

$u_d = u_l - u_s$, $v_d = v_l - v_s$

doi:10.6342/NTU202503897

V. Derivation of Interface Forces

Integrating displacement and equilibrium conditions leads to expressions for interface forces:

$$\begin{bmatrix} P_l \\ Q_l \end{bmatrix} = \frac{(1-v_s)E_s\gamma_c}{(1+v_s)\Delta''} \begin{bmatrix} -2F+3C(1-2v_s)+4+D\dfrac{12E_s}{R(1+v_s)} \\ -4F-4 \end{bmatrix} \quad (3.18)$$

Where

$$\Delta'' = CF(1-2v_s)+F(3-2v_s)+C(2.5-8v_s+6v_s^2)+6-8v_s+2D\frac{(2F+5-6v_s)E_s}{R(1+v_s)} \quad (3.19)$$

$$C(\text{compressibility ratio}) = \frac{E_s(1-v_l^2)R}{E_lA_l(1+v_s)(1-2v_s)} \quad (3.20)$$

$$F(\text{flexibility ratio}) = \frac{Es(1-v_l^2)R^3}{3E_lI_l(1+v_s)} \quad (3.21)$$

VI. Analytical Solution for Lining Moment

$$M_{ptto} = \frac{R^2}{3}\left(-P_l+\frac{Q_l}{2}\right)\cos\left(2\theta+\frac{\pi}{4}\right) \quad (3.22)$$

By substituting interface forces, the no-slip analytical solution for lining moment becomes:

$$M_{PTTO(N-S)} = -\frac{(1-v_s)E_s\gamma_cR^2}{(1+v_s)\Delta''}\left[(1-2v_s)C+2\right]\cos 2(\theta+\frac{\pi}{4}) \quad (3.23)$$

VII. By comparing with Flac

To validate the numerical modeling results obtained from FLAC simulations, the moment distribution along the circular tunnel lining was compared with the analytical solution proposed by Park et al. (2009), which revisits the seismic-induced ovaling behavior of tunnel linings under no-slip

doi:10.6342/NTU202503897

interface conditions.

To obtain the shear strain value, I used DEEPSOIL software to analyze the same parameters as the FLAC and loaded the same input motion. I extracted the maximum shear strain at 100 meters (the center of the tunnel) and used it as the source of the analytical seismic load.

As shown in Figure 3.9 (a), the numerical results exhibit a sinusoidal variation in bending moment with angular position, reaching maxima and minima at θ = 45°, 135°, 225°, and 315°, consistent with the theoretical prediction of ovaling deformation under shear wave incidence. The numerical peak moments closely match the amplitude and phase of the analytical solution, especially in the vicinity of $\theta = 45°$ and $\theta = 225°$, where tensile and compressive moments dominate.

Figure 3.9 (b) illustrates the maximum bending moment experienced at each tunnel lining segment throughout the earthquake simulation. For each angular position, the peak absolute bending moment value was extracted from the time history, providing a clear representation of the spatial distribution of seismic demand around the tunnel perimeter.

This agreement confirms that the FLAC model accurately captures the seismic-induced ovaling mechanism and that the rock-lining interface was appropriately represented as a no-slip boundary in the numerical scheme. Minor discrepancies observed at intermediate angles may be attributed to mesh discretization or damping formulation in the numerical model but remain within acceptable engineering tolerance.

doi:10.6342/NTU202503897

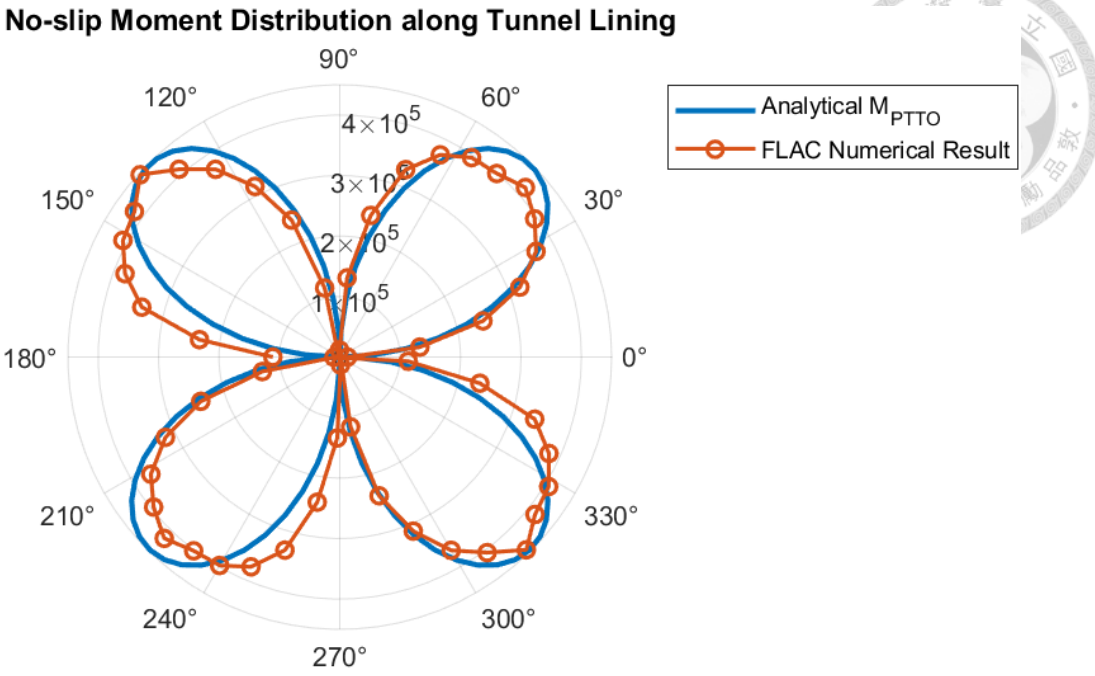

(a)

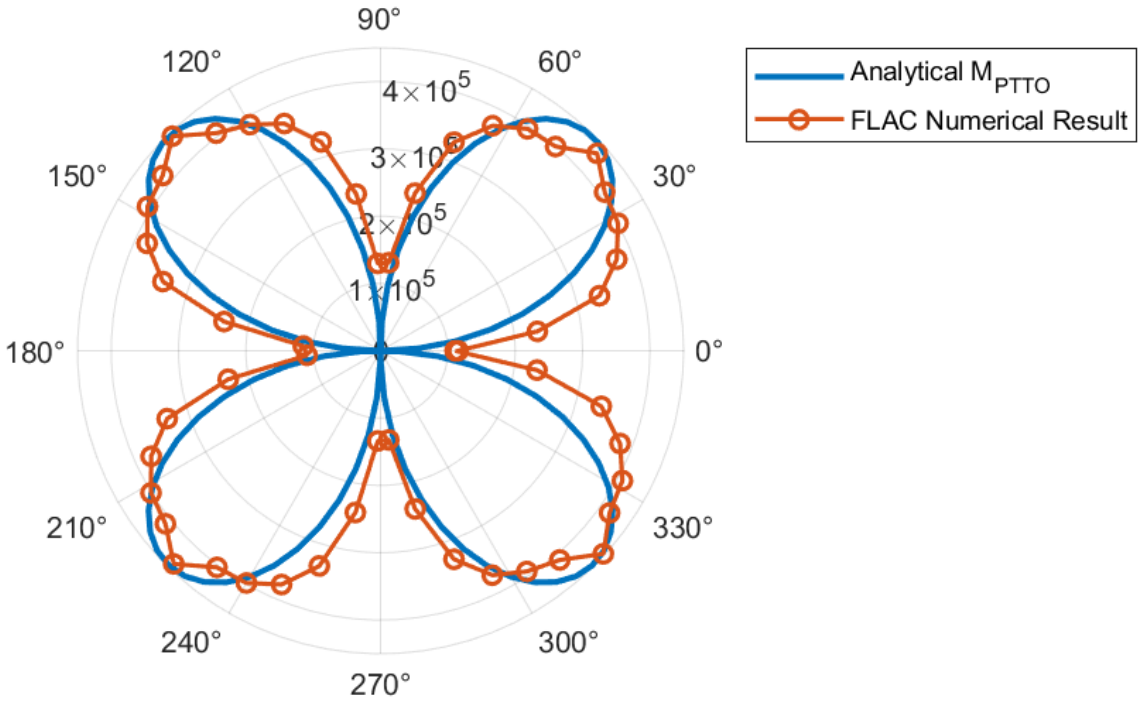

(b)

Figure 3.9 Rock-Lining Interaction Validation

doi:10.6342/NTU202503897

3.2.3 Validation of wave propagation

(a) Linear Elastic Rock Models:

To validate the accuracy of boundary conditions and wave propagation behavior in the numerical model, the dynamic analysis was initially conducted under the assumption that the rock mass behaves as a linear elastic material. A two-dimensional model measuring 200 meters in both width and height was constructed in FLAC 2D to represent the rock mass domain. To focus exclusively on wave propagation characteristics without introducing material nonlinearity, only Rayleigh damping was applied during this stage of the simulation.

This linear model configuration enabled direct comparison of simulated ground motion with results from a one-dimensional equivalent site response analysis performed using DEEPSOIL, a widely accepted software for seismic site response evaluation. In this phase, vertically propagating shear waves were input at the base of the FLAC model, and the resulting ground surface acceleration time histories were recorded. The agreement between the FLAC and DEEPSOIL outputs served as a verification of the model's ability to replicate the expected free-field dynamic behavior under elastic conditions.To perform the comparison, the surface acceleration time history obtained from FLAC was post-processed to generate a 5%-damped acceleration response spectrum, using the same frequency range and damping ratio settings as those used in DEEPSOIL.Special care was taken to apply the same input motion, material properties, and layering profile in both software platforms to ensure consistency in modeling assumptions.

Figure 3.10 illustrates the comparison between the response spectra obtained from FLAC and DEEPSOIL at the different depth. The spectral shapes exhibit high consistency in the predominant period and amplitude of peak spectral acceleration, particularly within

doi:10.6342/NTU202503897

the period range of 0.1 to 1.0 seconds, which is critical for the structural response of underground facilities. Minor deviations at longer periods can be attributed to numerical dispersion inherent in finite difference discretization and differences in boundary condition implementations between the two programs.

The good agreement between the FLAC-generated and DEEPSOIL-calculated response spectra confirms the validity of the boundary conditions applied in the FLAC model, including the use of free-field boundaries and absorbing dashpots. It also suggests that the input motion is correctly transmitted through the domain and that the numerical mesh resolution is sufficient to capture key wave propagation characteristics without introducing significant numerical artifacts. This validation step establishes a reliable baseline for subsequent nonlinear dynamic simulations and damage evaluations under more complex material models.

doi:10.6342/NTU202503897

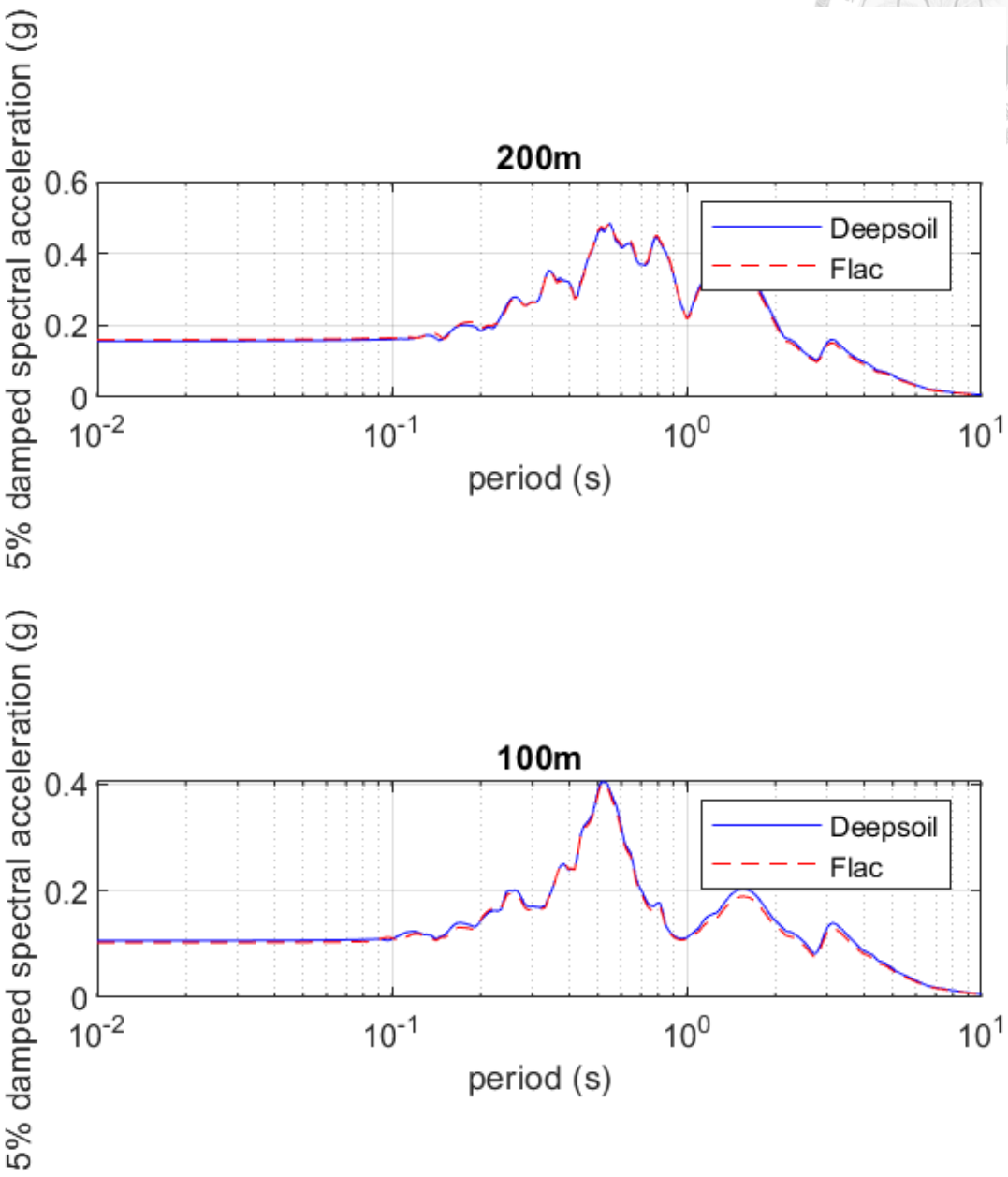

Figure 3.10 Comparison of response spectra with DEEPSOIL at different depth (linear model)

`

doi:10.6342/NTU202503897

(b) Nonlinear elastic mode

To verify the accuracy of the nonlinear model implemented in FLAC, the simulated surface acceleration response spectrum was compared with the total-stress nonlinear analysis results obtained from DEEPSOIL, referred to as the TD model. As shown in Figure 3.6, both spectra correspond to the Chi-Chi earthquake input and are plotted with 5% damping.

The comparison reveals a high degree of consistency between the FLAC and TD results across a wide range of periods. In particular, the spectral acceleration curves exhibit similar trends in peak locations and amplitudes between 0.1 and 1.5 seconds, which corresponds to the predominant range for rock-structure interaction. Slight discrepancies are observed in the short-period range (< 0.2 s), where the FLAC results slightly underestimate the amplitude compared to DEEPSOIL. This variation may be attributed to differences in the implementation of damping and the time integration schemes used by the two programs.

Overall, the good agreement between the two simulations confirms that the nonlinear material model and boundary conditions in FLAC can adequately reproduce site-specific seismic response characteristics. This verification step provides confidence in the reliability of subsequent simulations involving complex tunnel–ground interaction under seismic loading.

doi:10.6342/NTU202503897

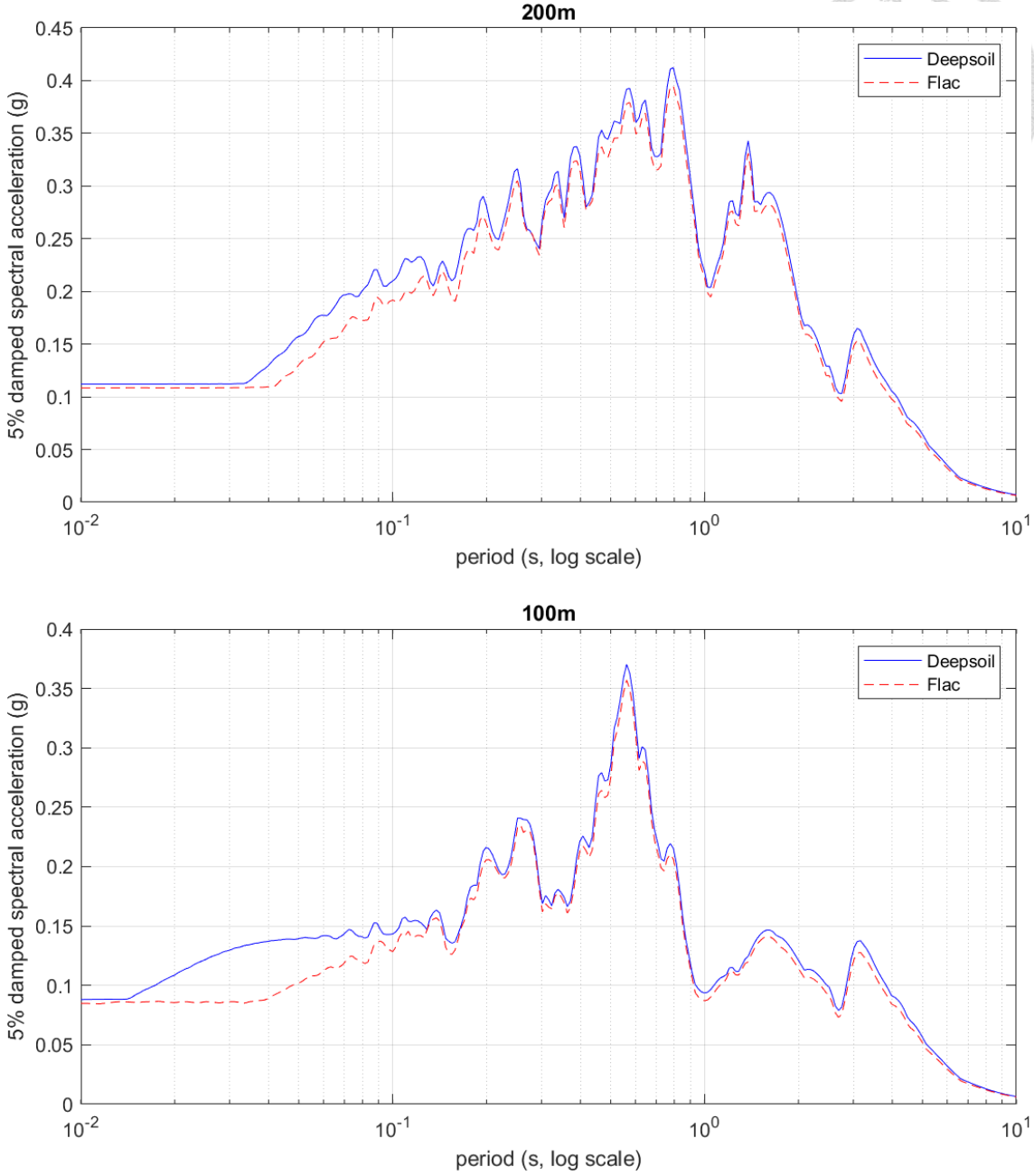

Figure 3.11 Comparison of response spectra with DEEPSOIL at different depth (Nonlinear model)

3.3 Earthquakes and Stations

In this study, two ground motion records were selected as seismic input motions for the FLAC 2D nonlinear site response and tunnel fragility analyses: the 1999 Chi-Chi earthquake (Taiwan) and the 1985 Nahanni earthquake (Canada). These two events were

doi:10.6342/NTU202503897

obtained from the DEEPSOIL ground motion library and were chosen based on their distinct spectral characteristics. Figure 3.12 and Figure 3.13 show the acceleration time histories from DEEPSOIL. Figure 3.14 shows the surface response spectra obtained using the DEEPSOIL station.

The primary purpose of selecting these two earthquake records is to investigate the influence of ground motion frequency content—specifically, long-period versus short-period dominant motions—on the seismic fragility behavior of underground structures. The Chi-Chi earthquake is known for its relatively rich low-frequency content, resulting in long-period ground motions due to its large magnitude and rupture characteristics. In contrast, the Nahanni earthquake features strong high-frequency components, leading to a ground motion profile dominated by short-period energy. By comparing the fragility curves generated under these two different input motions, this study can also evaluate how the frequency content of seismic waves affects overall damage probability.

doi:10.6342/NTU202503897

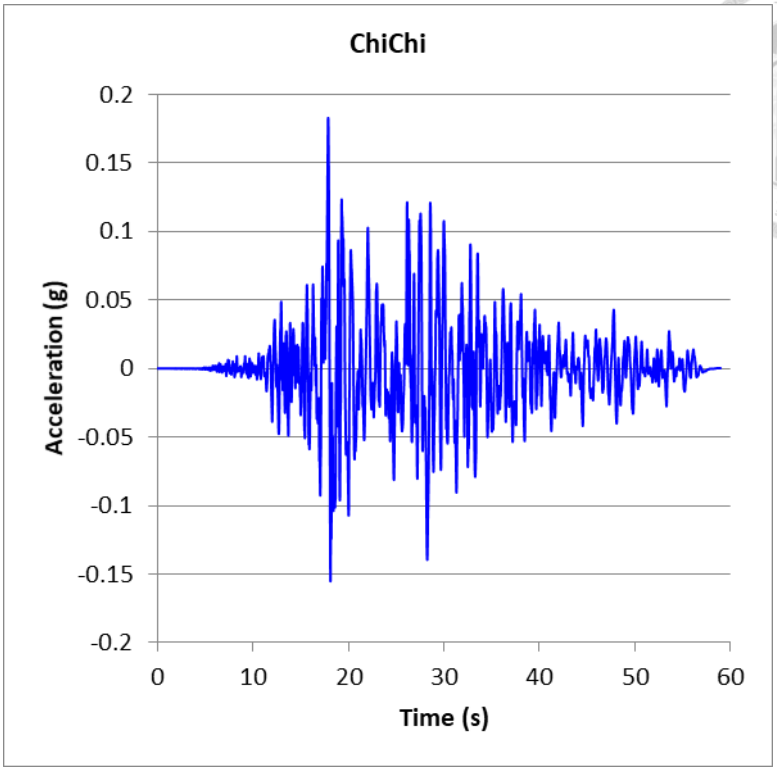

Figure 3.12 Acceleration time history of the ChiChi earthquake (DEEPSOIL)

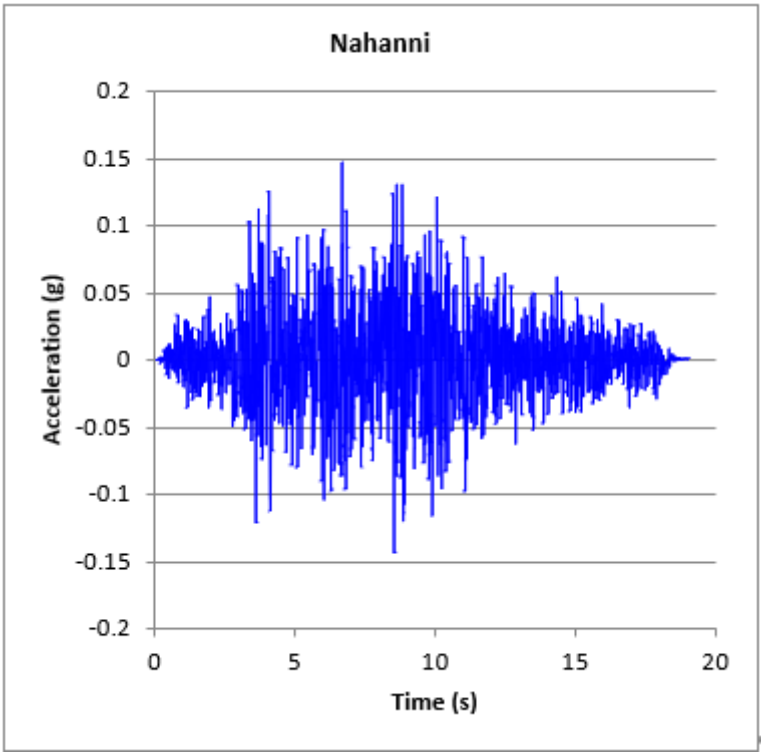

Figure 3.13 Acceleration time history of the Nahanni earthquake (DEEPSOIL)

doi:10.6342/NTU202503897

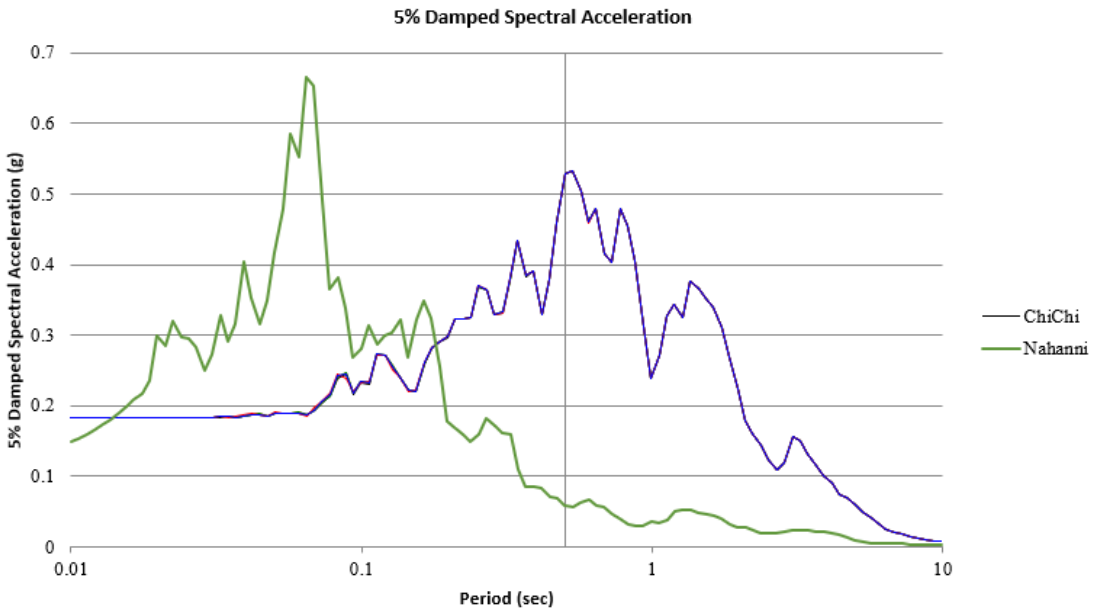

Figure 3.14 Response spectrum of the earthquake used for cyclic softening calculations (DEEPSOIL)

3.3.1 Return Period Design Earthquakes for Chi-Chi and Nahanni Events

In order to evaluate the seismic performance of underground structures under different hazard levels, this study adopts ground motions corresponding to earthquakes with return periods of 475 years and 2500 years.

The selection of these return periods is based on probabilistic seismic hazard analysis (PSHA), which estimates the probability that a specific level of ground motion will be exceeded at a given site within a specified time frame. A return period of 475 years corresponds to a 10% probability of exceedance within 50 years, while a 2500-year return period corresponds to a 2% exceedance probability over the same duration. These hazard levels are widely used in performance-based design to ensure that both operational functionality and structural integrity are maintained under varying seismic demands.

doi:10.6342/NTU202503897

To construct the design ground motions, the original earthquake time histories were scaled to match the target design response spectra derived for the corresponding return periods. The scaling was performed by matching the spectral acceleration values at short-period (SDS) and 1-second-period (SD1) demands, following the procedure outlined in national seismic design provisions. This allows the ground motions to retain their frequency content while adjusting their intensity to reflect the appropriate hazard level.

Figure 3.15 illustrates a simplified representation of seismic design parameters commonly used in earthquake engineering to characterize ground motion intensity and structural demand. The graph displays the relationship between spectral acceleration (S_a), spectral velocity (Sv), and spectral displacement (S_d) across varying structural vibration periods (T), forming the basis of the design response spectrum.

In the figure, two key periods—T = 0.3 sec and T = 1.0 sec—are selected as representative points for simplified design. The acceleration at T = 0.3 sec corresponds to a constant spectral acceleration plateau (S_a), which reflects short-period demand typical of stiff or low-rise structures. At T = 1.0 sec, the curve intersects the constant spectral velocity region, from which the velocity-related intensity measure (S_v) can be derived. The figure also presents conversion relationships between diff-erent intensity measures based on the structural period, such as:

$$S_v = \frac{T}{2\pi} S_a \tag{3.24}$$

$$S_d = \frac{T^2}{4\pi^2} S_a \tag{3.25}$$

These formulas allow engineers to convert spectral acceleration into spectral displacement or velocity, depending on the dominant response period of the structure.

doi:10.6342/NTU202503897

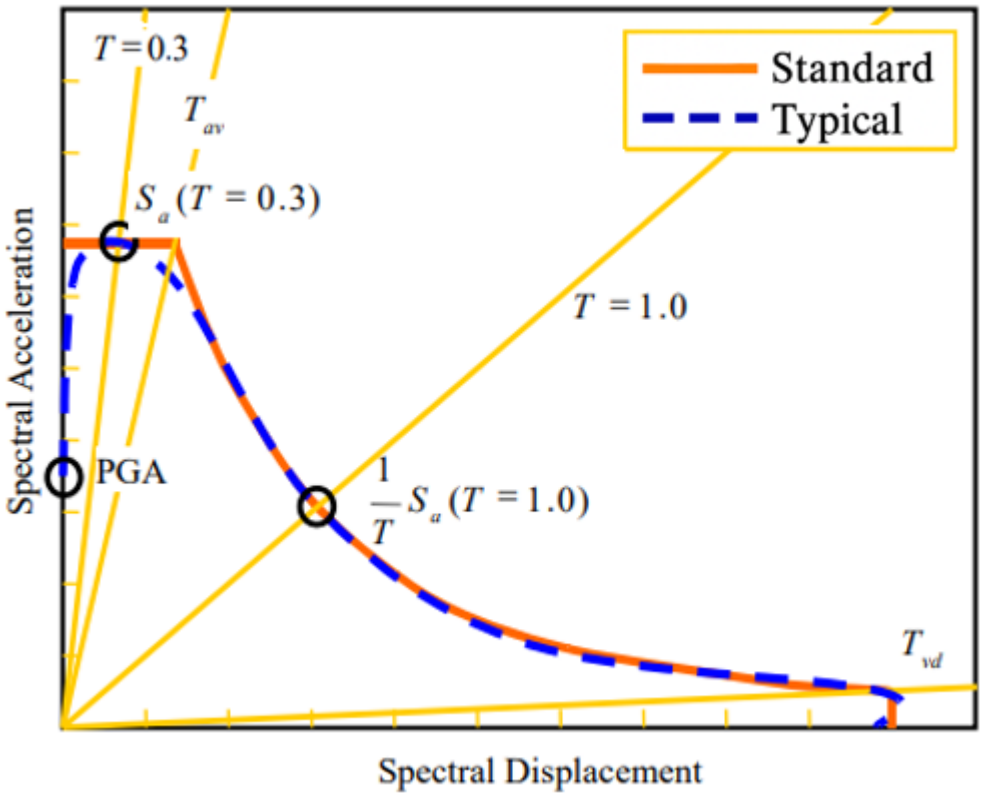

Figure 3.15 Schematic diagram of design response spectrum

In this study, the seismic design response spectra corresponding to five representative regions were obtained from You (2024). Among these, [TTN020 Chishang, Taitung] was selected as the standard site for ground motion scaling. Based on the target seismic intensities associated with return periods of 475 years and 2500 years, the two ground motion records introduced in Section 3.3 were amplitude-scaled accordingly. Figure 3.16 shows the design response spectra from five representative regions, and Figure 3.17 presents the scaled spectra converted to the design-level ground motions.

doi:10.6342/NTU202503897

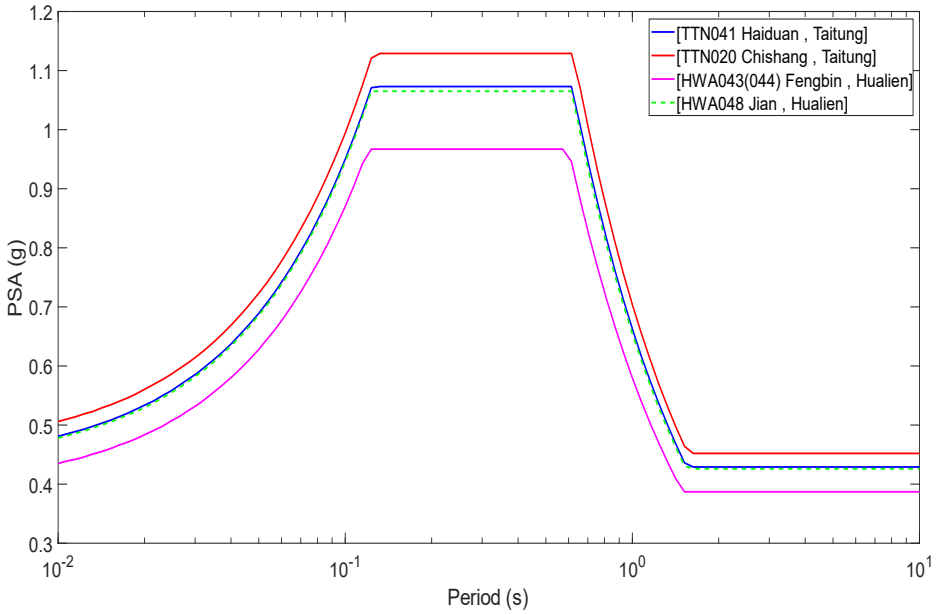

(a) 475-year return period of design response spectrum

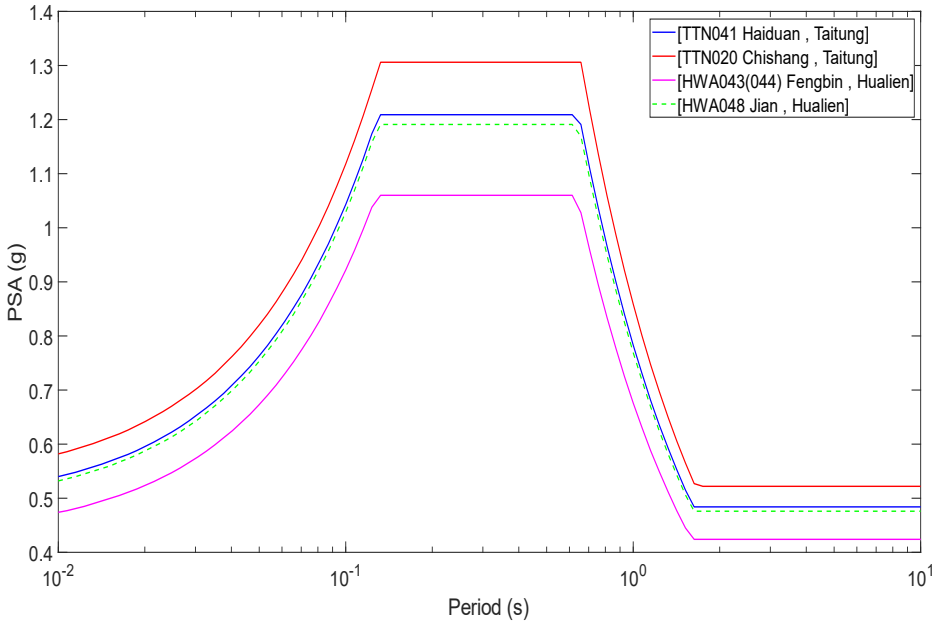

(b) 2500-year return period of design response spectrum

Figure 3.16 The seismic design response spectra for different regions (after You 2024)

doi:10.6342/NTU202503897

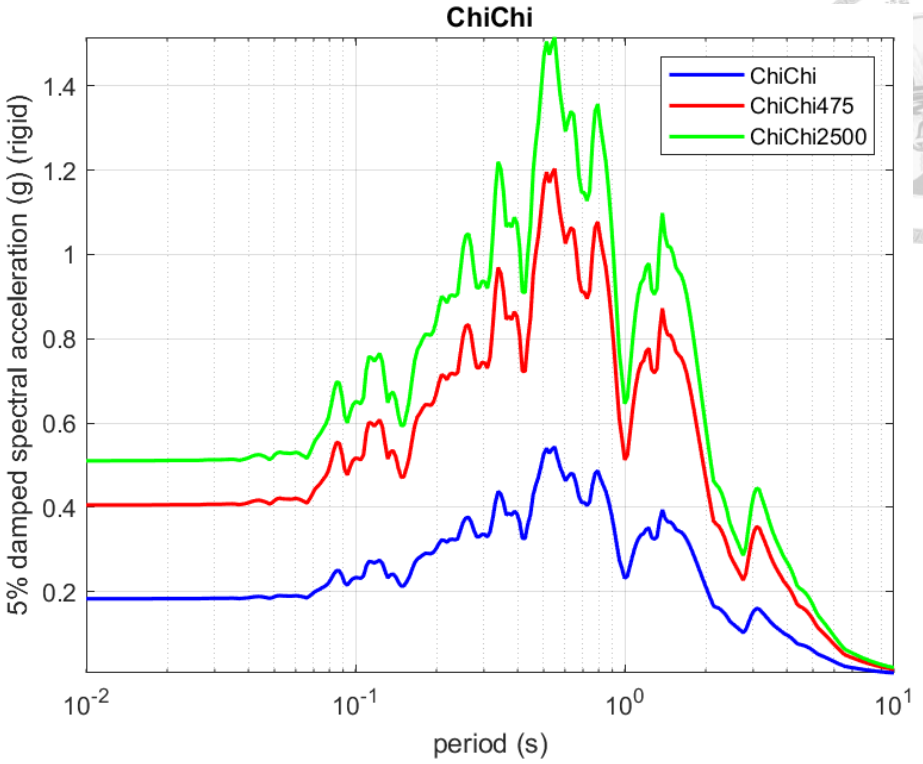

(a) return period of design response spectrum of ChiChi earthquake

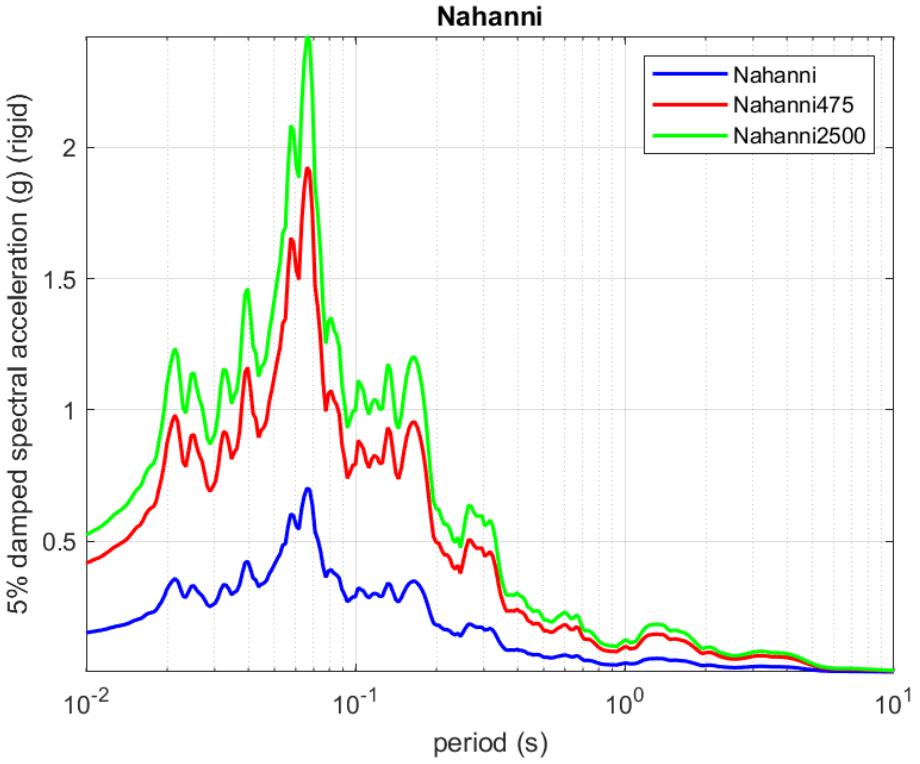

(b) return period of design response spectrum of Nahanni earthquake

Figure 3.17 Response spectrum results of return period of design earthquakes

doi:10.6342/NTU202503897

Chapter 4 Numerical Simulation of Tunnel Response under Seismic Loading

Building upon the numerical analysis framework developed in Chapter 3, this chapter further explores the influence of overburden depth, shear wave velocity, and different seismic intensity measures on the tunnel's seismic response. The outcomes of these simulations serve as the foundation for constructing fragility curves, enabling comparative assessment across varying conditions. To achieve this, a total of 96 fully nonlinear dynamic simulations were conducted using FLAC 2D (Itasca, 2011).

In this study, seismic vulnerability is evaluated through analytically derived fragility functions, which represent the probabilistic likelihood of damage to initially undamaged tunnel structures under seismic loading. These assessments are based on the assumption that damage accumulation is independent of previous seismic events. The primary damage metric adopted is the ratio of the actual bending moment (M) to the design moment capacity (MRd) of the tunnel lining cross-section. This parameter is systematically used to compile the seismic damage database.

The simulation matrix encompasses three tunnel embedment depths (100 m, 200 m, and 400 m), two distinct seismic intensity levels, and two sets of rock material properties, as summarized in Table 10.

doi:10.6342/NTU202503897

Table 10 Total cases of FLAC 2D simulations

Input motion	Depth	Shear wave velocity (m/s)	Scaling PGA	Return period of design earthquake
Chi-Chi Nahanni	100m 200m 400m	417 1000	0.05g 0.1g 0.2g 0.4g 0.6g 0.8g	475 years 2500 years

4.1 Numerical Model Parameters

To investigate the influence of burial depth on tunnel seismic response, three numerical models were constructed, representing tunnel embedment depths of 100 m, 200 m, and 400 m, respectively. The mechanical parameters of the surrounding rock mass used in the analysis are summarized in Table 7. Figure 4.1 provides a simplified schematic of the boundary conditions applied to the models: free-field boundaries were implemented along the lateral sides, while a quiet boundary condition was applied at the base to minimize wave reflection effects.

Table 11 presents the geometric dimensions associated with each model, and includes the damping parameters corresponding to each burial depth.

It should be emphasized that the numerical simulations in this study exclusively evaluate the additional deformation and velocity increments induced by seismic loading.

doi:10.6342/NTU202503897

The pre-existing stress and deformation conditions resulting from tunnel excavation and initial support installation are not accounted for in the models.

Table 11 Model parameters

Model Size			Sig3 model parameters of hysteretic damping			Rayleigh damping	
Depth	Depth	Width	a^*	b^*	x_0^*	f_{min}^*	ξ_{min}^*
100m	200m	200m	1.00	-0.4877	-0.873	0.01059	2.809
200m	400m	200m	1.00	-0.4819	-0.7113	0.01059	1.405
400m	600m	400m	1.00	-0.4819	-0.7113	0.01059	0.936

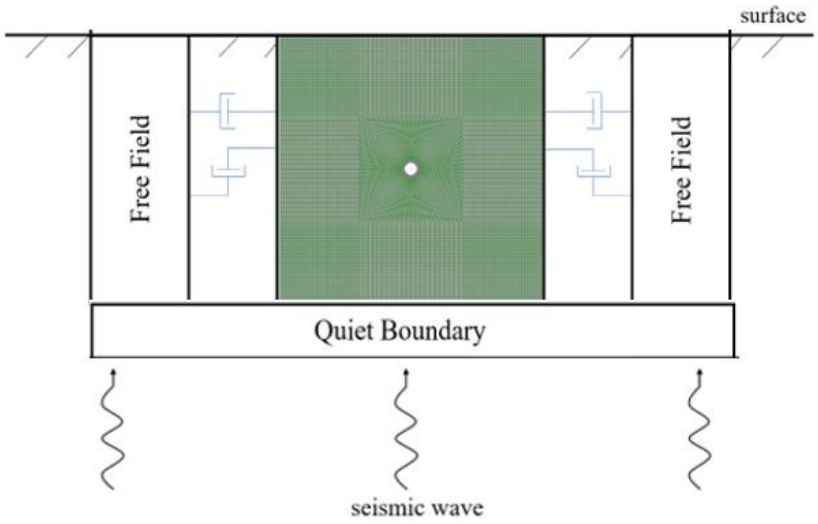

Figure 4.1 Schematic illustration of the boundary condition setup in the numerical model.

doi:10.6342/NTU202503897

4.1.1 Establishment and Derivation of the Allowable Bending Moment

In this study, to ensure that the tunnel lining structure possesses sufficient flexural strength and safety margin, the maximum allowable bending moment of the lining is set to 220 kN·m/m. The assumption that the M_{RD} is the same at any depth. This value is derived based on the fundamental mechanics relationship between bending moment and normal stress:

$$M_{RD} = \sigma_{allow} * Z = \frac{f'_c}{n} * \frac{I}{c} \quad (4.1)$$

Where the parameters are defined as follows:

- f'_c: Concrete compressive strength, taken as **26 MPa**
- n: Safety factor, set to **2.0**
- I: Moment of inertia of the section, assumed as **0.0025** m^4/m:
- c=t/2c: Distance from the neutral axis to the extreme fiber, with lining thickness t=0.3 m, hence c=0.15
- Z=I/c=0.01667 m^3/m: Section modulus

Substituting into the equation:

$$M_{RD} = 220kN * m / m \quad (4.2)$$

doi:10.6342/NTU202503897

4.2 Development of Fragility Curves Using Moment Demand-to-Capacity Ratio

This chapter presents the results of the seismic fragility analysis based on 96 sets of fully nonlinear dynamic simulations performed using the FLAC 2D program. These simulations were designed to systematically explore the influence of multiple parameters on the seismic vulnerability of mountain tunnels. The primary variables considered include overburden depth (100 m, 200 m, and 400 m), material stiffness (represented by two distinct shear modulus reduction curves), and two different seismic intensity measures (PGA and PGV), each evaluated under two return period levels (475 and 2500 years).

For each of the 96 cases, the peak bending moment induced in the tunnel lining was extracted and normalized by its corresponding moment capacity to compute the Damage Index. These indices were then categorized into different damage states, to construct empirical fragility data sets. Using a lognormal cumulative distribution framework, regression analysis was carried out to derive median intensity measures and total standard deviations for each damage state.

The results are organized into fragility curves, each representing the conditional probability of exceeding a specific damage state given a particular intensity measure. Subsections within this chapter compare fragility behavior under different modeling conditions. Furthermore, this study evaluates the sensitivity of fragility curve outcomes to the choice of intensity measure. While PGA remains a conventional choice and PGV and PGD were also investigated.

doi:10.6342/NTU202503897

Regression lines derived from the simulation data are superimposed on the empirical fragility points for each scenario, and their goodness-of-fit is discussed. Through this detailed parametric analysis, this chapter aims to identify the dominant factors influencing tunnel seismic fragility and to provide a basis for performance-based design and seismic resilience assessment of underground structures in mountainous terrain.

The IM values in Section 4.2.1 to 4.2.5 are taken from the bottom of the model, while the IM value in Section 4.2.6 is taken from a point 10 meters away from the center of the tunnel.

4.2.1 The influence of overburden depth

This section investigates how tunnel overburden depth influences seismic fragility under a rock stiffness condition represented by a shear wave velocity of 417 m/s, using peak ground acceleration (PGA) as the seismic intensity measure. Fragility curves were developed for three burial depths: 100 m, 200 m, and 400 m. The input ground motions were scaled across multiple PGA levels, and the resulting damage indices were used to construct fragility curves through lognormal regression. The analysis highlights how increasing overburden depth affects the probability of reaching each damage state. Table 12 summarizes the median PGA values and the corresponding β values for each damage state (Minor and Moderate) at different overburden depths. It is important to note that for all cases analyzed in this study, none of the simulations reached the Extensive damage state. This is likely due to the high stiffness of the rock mass and the resulting low bending moments, which limit the extent of structural damage under the given loading scenarios. Therefore, Extensive damage state results are excluded from the table. Figure 4.2 presents the results of linear regression in natural logarithmic form

Figure 4.3 illustrates the fragility curves for burial depths of 100 m, 200 m, and

doi:10.6342/NTU202503897

400 m, respectively, under a rock condition of $V_s = 417\ m/s$. At 100 m depth, the tunnel exhibits only minor damage, with no exceedance of moderate or extensive damage thresholds within the analyzed PGA range. At 200 m depth, fragility increases significantly, and even low-intensity shaking may cause minor damage. Notably, at 400 m depth, the model predicts minor damage even at near-zero PGA, suggesting that the high overburden stress alone contributes to stress concentrations in the lining. Despite this, no models across all depths exhibit extensive damage, highlighting the strength of the lining design under the selected material and geometric assumptions.

Table 12 Parameters of the fragility curves for different depths

Depth	**Damage state**	**Outcropping bedrock PGA (g)**		
		IM_{DS_i}	β_{D}	β_{tot,DS_i}
100m	Minor	1.4	0.203	0.54
	Moderate	25	0.203	0.54
200m	Minor	0.0065	0.138	0.519
	Moderate	2.502	0.138	0.519
400m	Minor	0	0.047	0.502
	Moderate	3.8127	0.047	0.502

doi:10.6342/NTU202503897

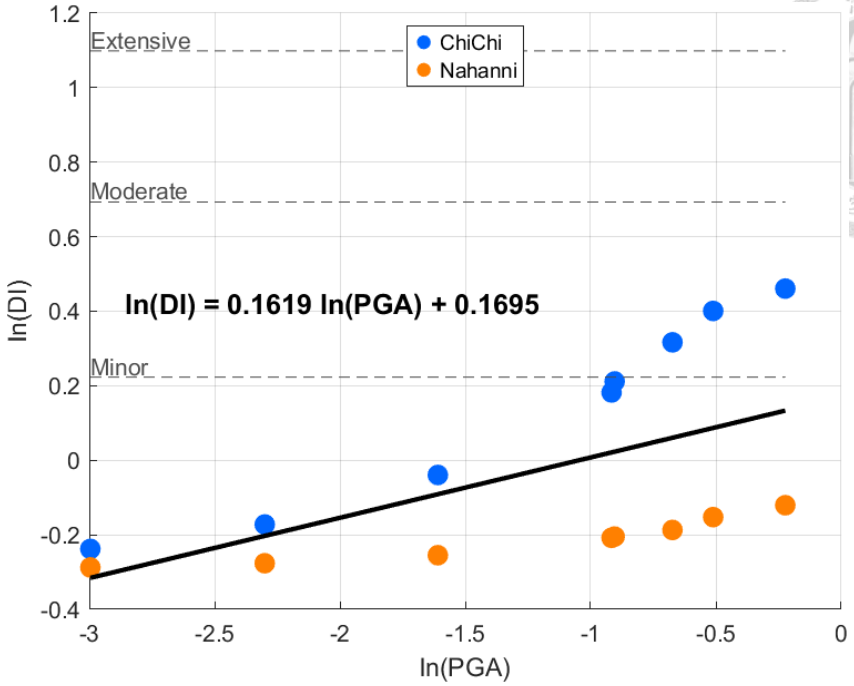

(a) Depth=100m, shear wave velocity=417m/s

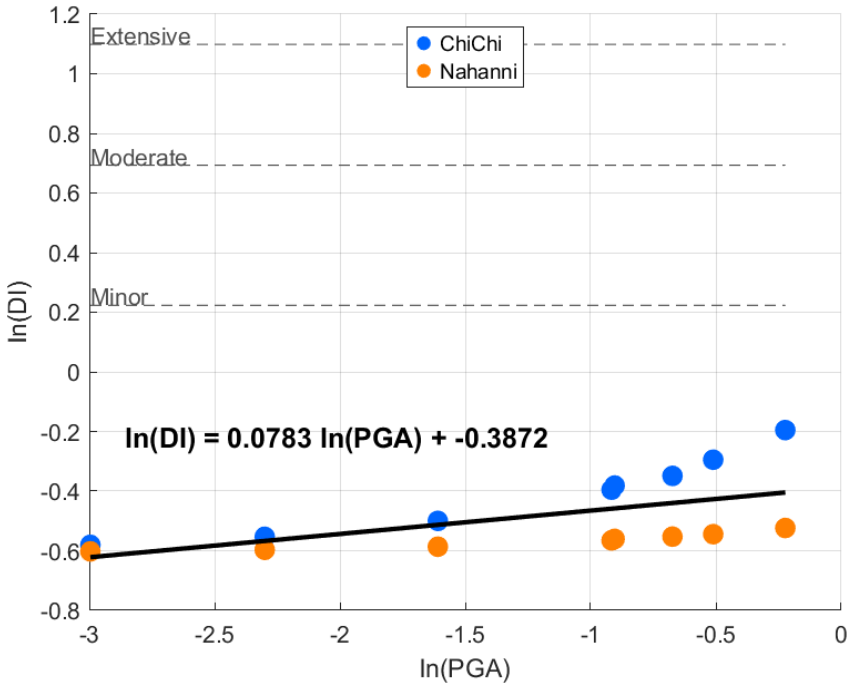

(b) Depth=200m, shear wave velocity=417m/s

doi:10.6342/NTU202503897

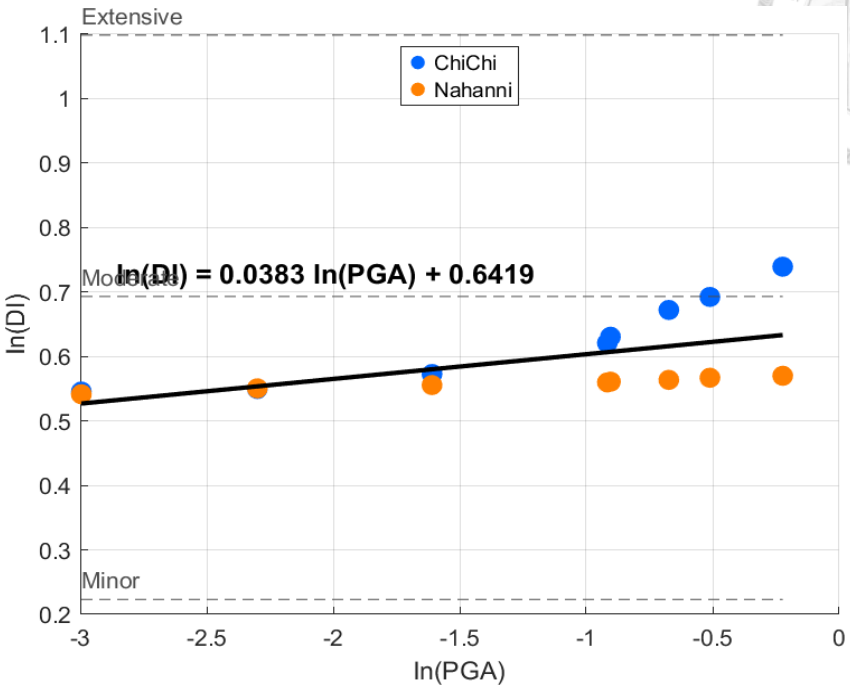

(c) Depth=400m, shear wave velocity=417m/s

Figure 4.2 Linear regression at different depths with PGA

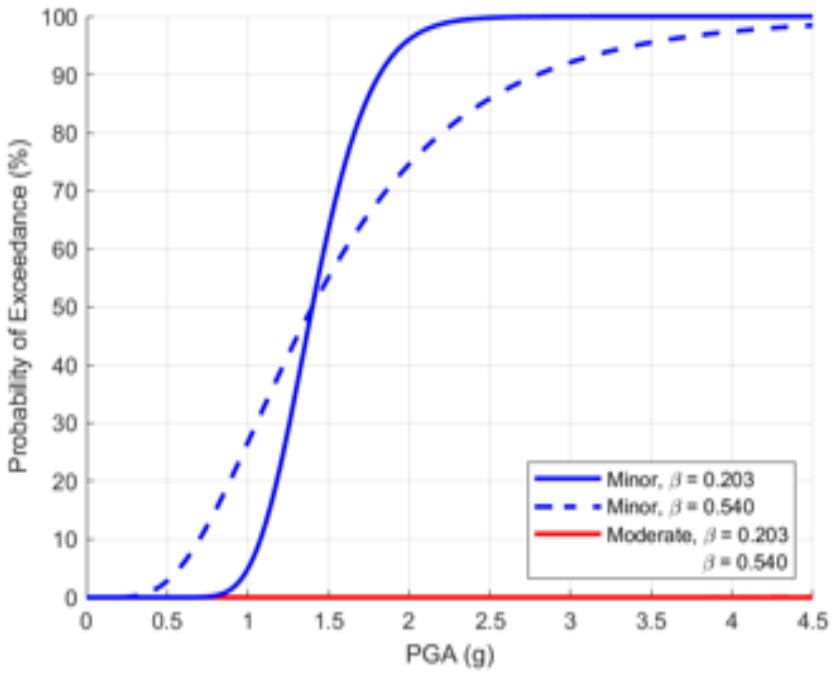

(a) Depth=100m, shear wave velocity=417m/s

doi:10.6342/NTU202503897

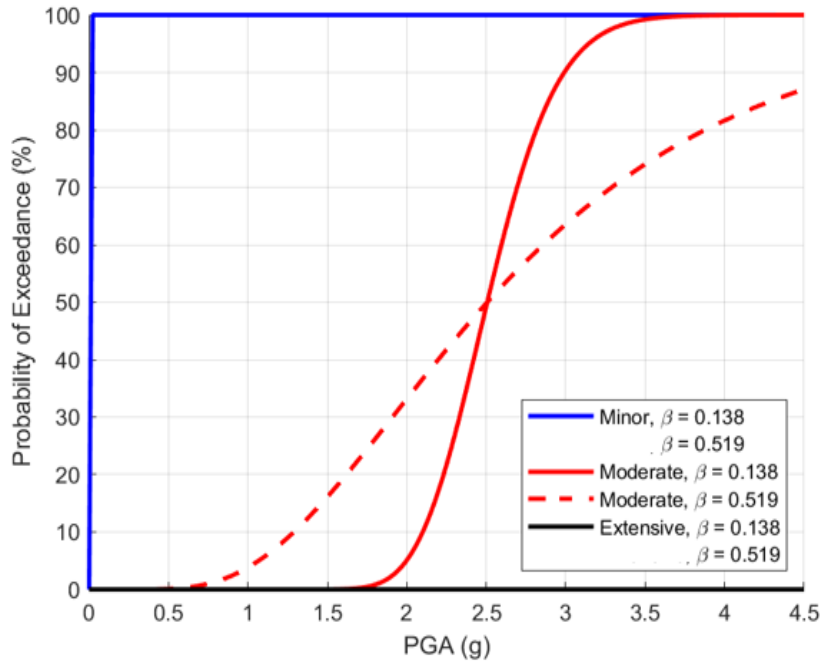

(b) Depth=200m, shear wave velocity=417m/s

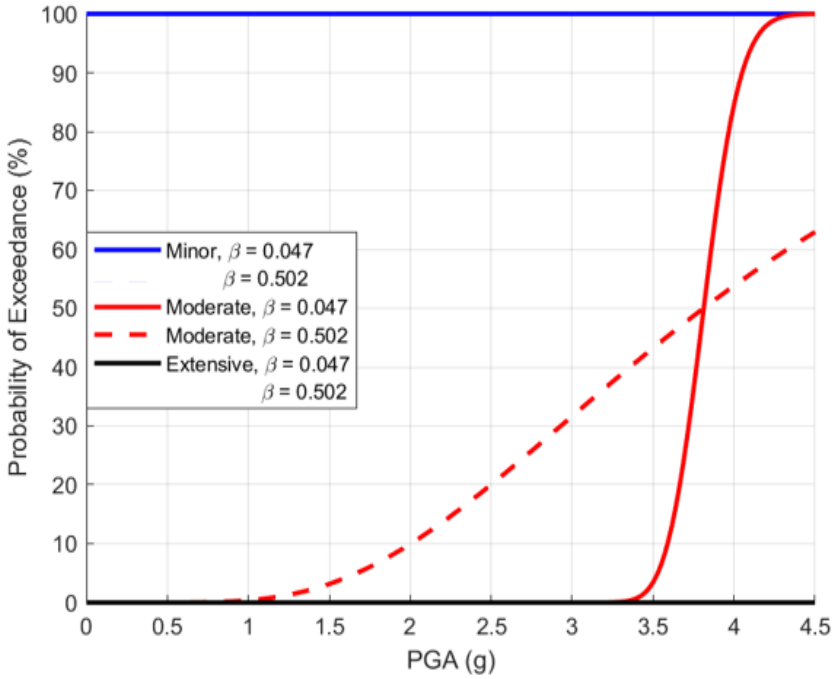

(c) Depth=400m, shear wave velocity=417m/s

Figure 4.3 fragility curves at different depths

doi:10.6342/NTU202503897

4.2.2 Influence of Shear Wave Velocity of rock

This section compares the effect of rock shear wave velocity on tunnel seismic response and fragility. Two representative values were analyzed: 417 m/s (representing softer rock) and 1000 m/s (representing much stiffer and stronger rock).Figure 4.4.represents regression Lines of Damage Index for Different Tunnel Depths under High Shear Wave Velocity (V_s = 1000 m/s) Figure 4.5 illustrates the fragility curves for tunnel depths of 100 m, 200 m, and 400 m under a rock condition characterized by a shear wave velocity of 1000 m/s.

The simulation results show that, for all burial depths (100 m, 200 m, and 400 m), tunnels embedded in rock with a shear wave velocity of 1000 m/s experience significantly smaller bending moments compared to those in the 417 m/s scenarios. The high stiffness and strength of the 1000 m/s rock mass efficiently attenuate seismic energy and restrict tunnel lining deformation, resulting in minimal seismic demand on the structure.

Accordingly, the fragility curves derived for the 1000 m/s cases are essentially flat, indicating that the probability of damage is negligible across the entire range of considered ground motion intensities. In contrast, for 417 m/s rock, the tunnels demonstrate a higher likelihood of reaching minor or moderate damage states, especially at shallower depths and higher PGA levels.

These findings underscore the critical influence of rock stiffness on tunnel vulnerability: tunnels in extremely competent rock are inherently resilient to seismic shaking under the examined far-field earthquake scenarios. This has important engineering implications for both seismic design and risk assessment of deep rock tunnels.

doi:10.6342/NTU202503897

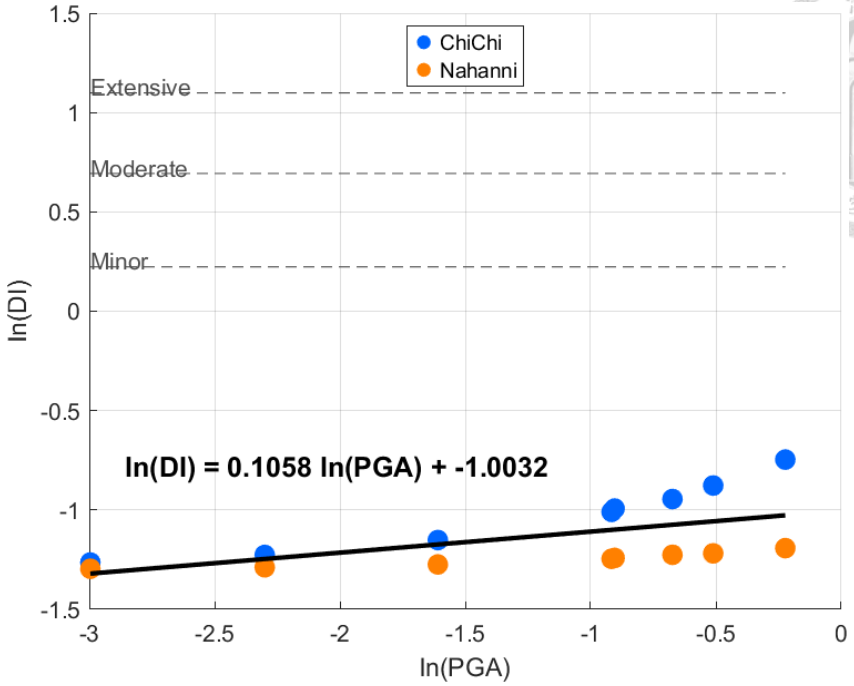

(a) Depth=100m, shear wave velocity=1000m/s

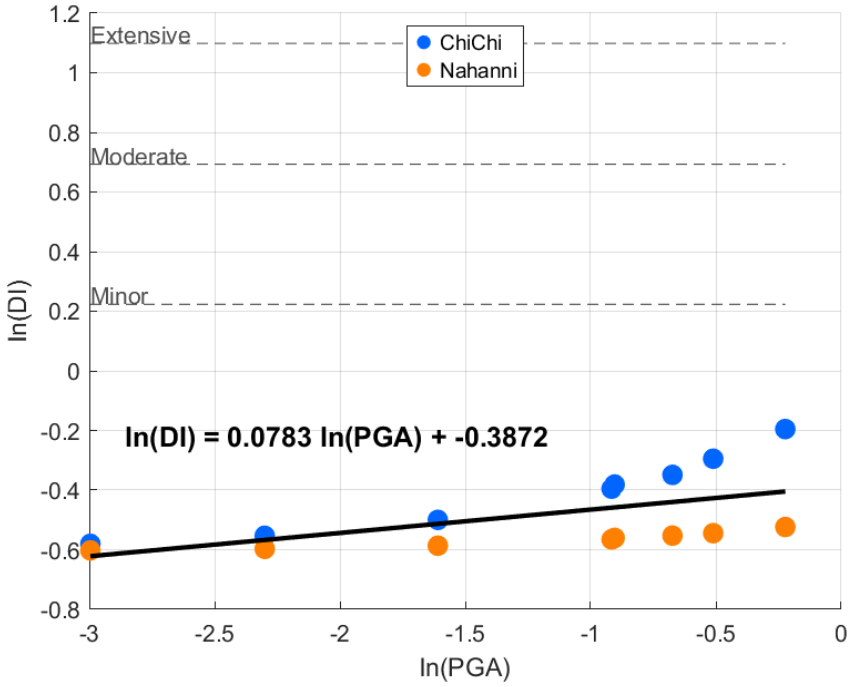

(b) Depth=200m, shear wave velocity=1000m/s

doi:10.6342/NTU202503897

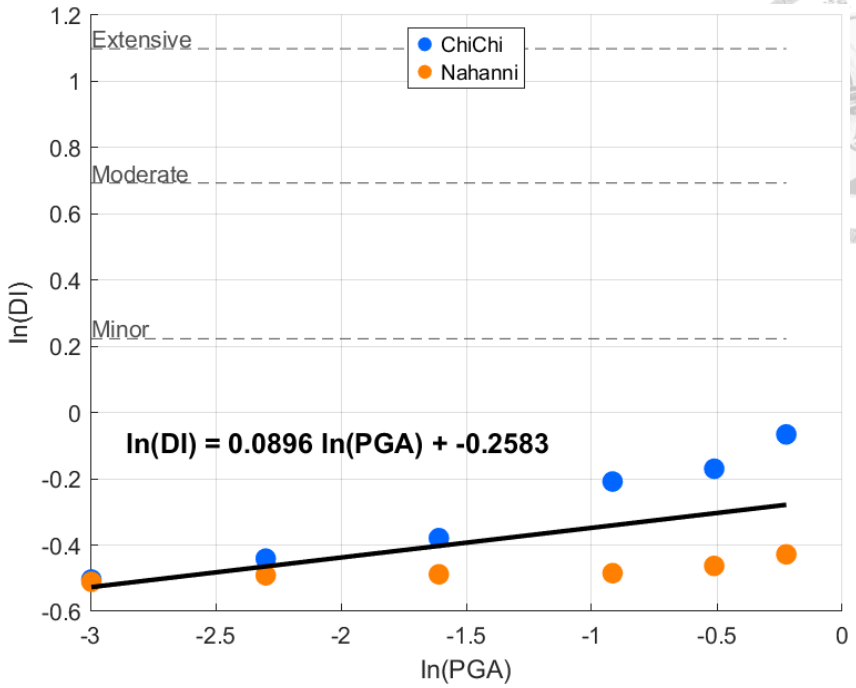

(c) Depth=400m, shear wave velocity=1000m/s

Figure 4.4 Linear regression (shear wave velocity=1000m/s)

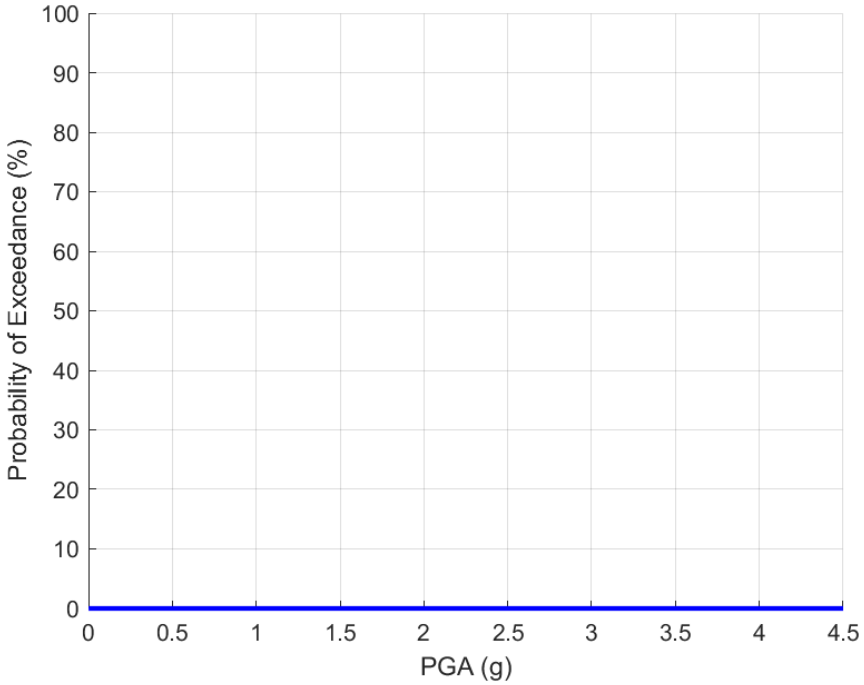

Figure 4.5 Depth-dependent Fragility Curves under Rock with V_s = 1000 m/s (No Damage Observed)

doi:10.6342/NTU202503897

4.2.3 Influence of Different Input Ground Motions

This section examines the influence of different seismic input motions on tunnel fragility, focusing on the comparison between the ChiChi earthquake (Taiwan) and the Nahanni earthquake (Canada), both applied to a rock mass with a shear wave velocity of 417 m/s. Table 13 and Table 14 summarize the regression parameters—specifically the beta values (β) and median intensity measures —for the ChiChi and Nahanni earthquakes, respectively. Figure 4.6 and Figure 4.7 present the regression plots of ln(DI) versus ln(PGA) for the ChiChi and Nahanni earthquakes under different burial depths. Figure 4.8 and Figure 4.9 represent the fragility curves under Chi-Chi and Nahanni earthquake ground motions, respectively.

The results reveal that, at all analyzed depths, the regression slope for the ChiChi earthquake is consistently greater than that of the Nahanni earthquake. Correspondingly, the fragility curves generated for the ChiChi earthquake indicate significantly higher probabilities of damage for the same PGA, when compared to those derived from the Nahanni input motion. This demonstrates that the long-period, high-energy characteristics of the ChiChi earthquake tend to induce more substantial structural demands and higher damage risks in tunnel linings than the short-period, lower-energy characteristics of the Nahanni earthquake.

These findings suggest that the spectral content and duration of seismic input motion have a pronounced effect on tunnel vulnerability, with long-period earthquakes posing a greater risk of inducing damage to deep-buried or stiff tunnel structures. It underscores the importance of considering earthquake frequency characteristics and source mechanisms when developing fragility curves for critical underground infrastructure.

doi:10.6342/NTU202503897

Table 13 Parameters of the fragility curves for ChiChi earthquake

Depth	**Damage state**	**Outcropping bedrock PGA (g)**		
		IM_{DS_i}	β_{D}	β_{tot,DS_i}
100m	Minor	0.3847	0.056	0.503
	Moderate	2.2486	0.056	0.503
	Extensive	10.3134	0.056	0.503
200m	Minor	0.018	0.038	0.501
	Moderate	0.4021	0.038	0.501
	Extensive	5.8685	0.038	0.501
400m	Minor	0.0007	0.029	0.501
	Moderate	0.7448	0.029	0.501
	Extensive	280	0.029	0.501

Table 14 Parameters of the fragility curves for Nahanni earthquake

Depth	**Damage state**	**Outcropping bedrock PGA (g)**		
		IM_{DS_i}	β_{D}	β_{tot,DS_i}
100m	Minor	503	0.019	0.5
200m	Minor	0	0.005	0.5
400m	Minor	0	0.001	0.5

doi:10.6342/NTU202503897

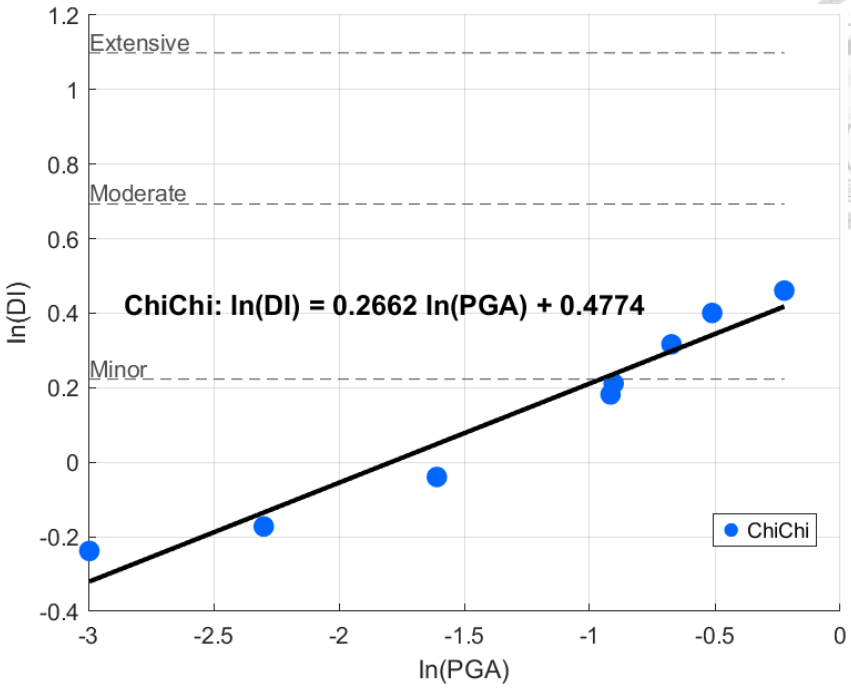

(a) Depth=100m, shear wave velocity=417m/s

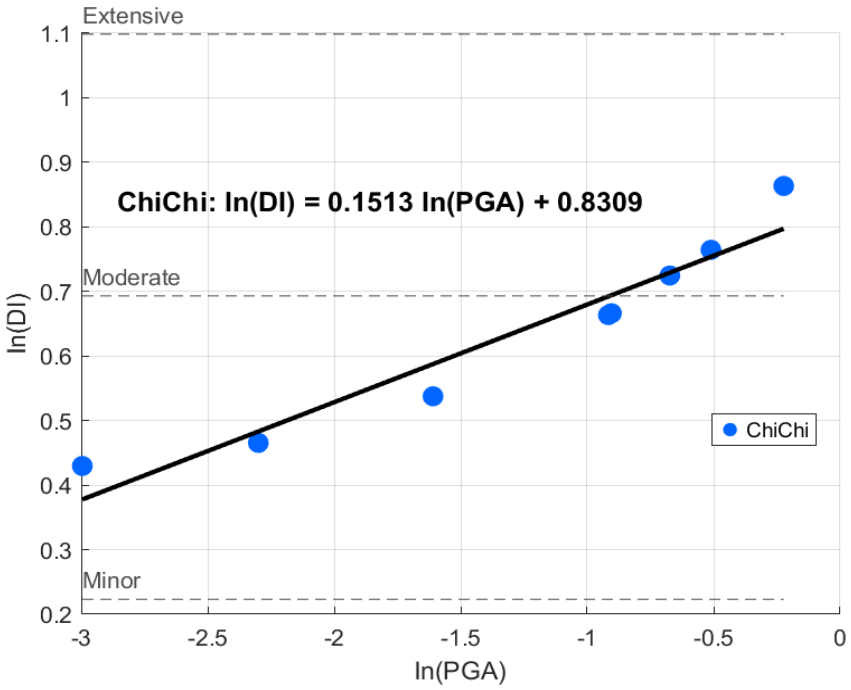

(b) Depth=200m, shear wave velocity=417m/s

doi:10.6342/NTU202503897

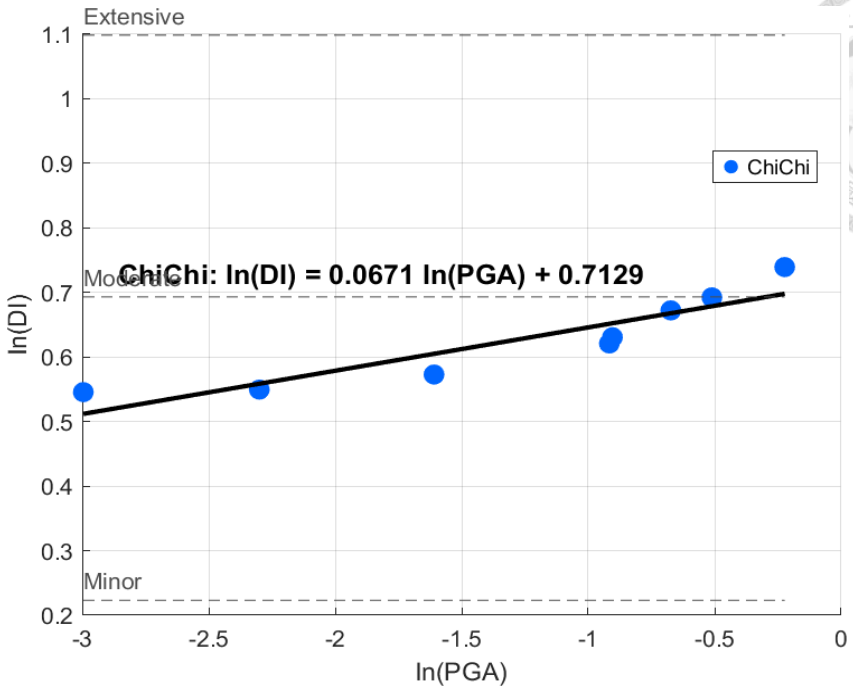

(c) Depth=400m, shear wave velocity=417m/s

Figure 4.6 Linear regression at different depths for ChiChi earthquake

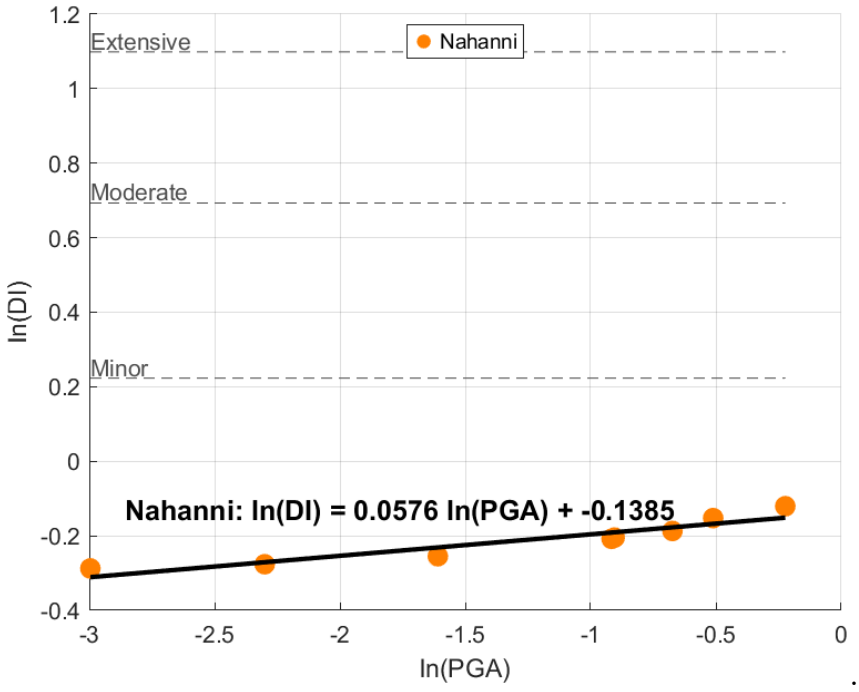

(a) Depth=100m, shear wave velocity=417m/s

doi:10.6342/NTU202503897

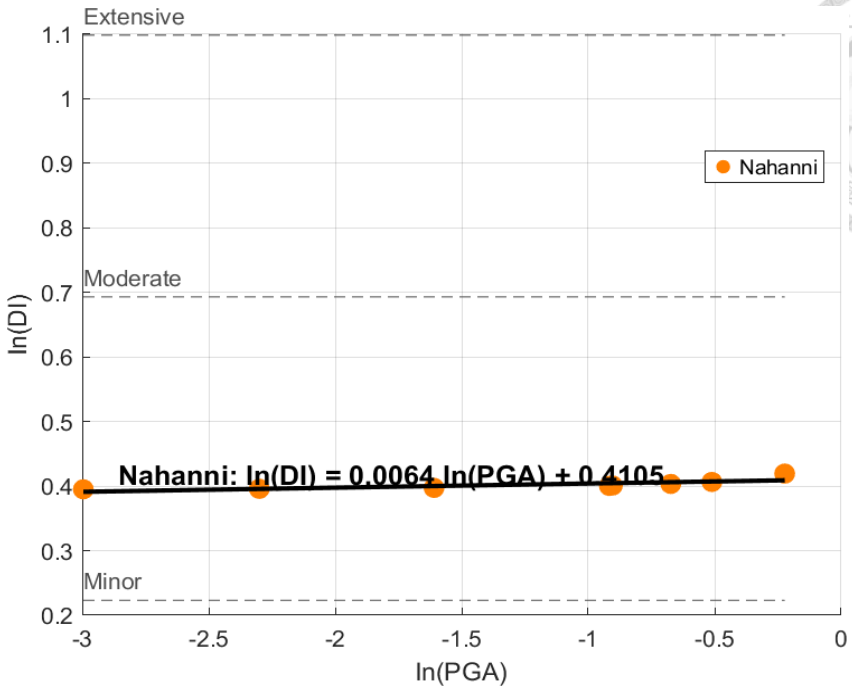

(b) Depth=200m, shear wave velocity=417m/s

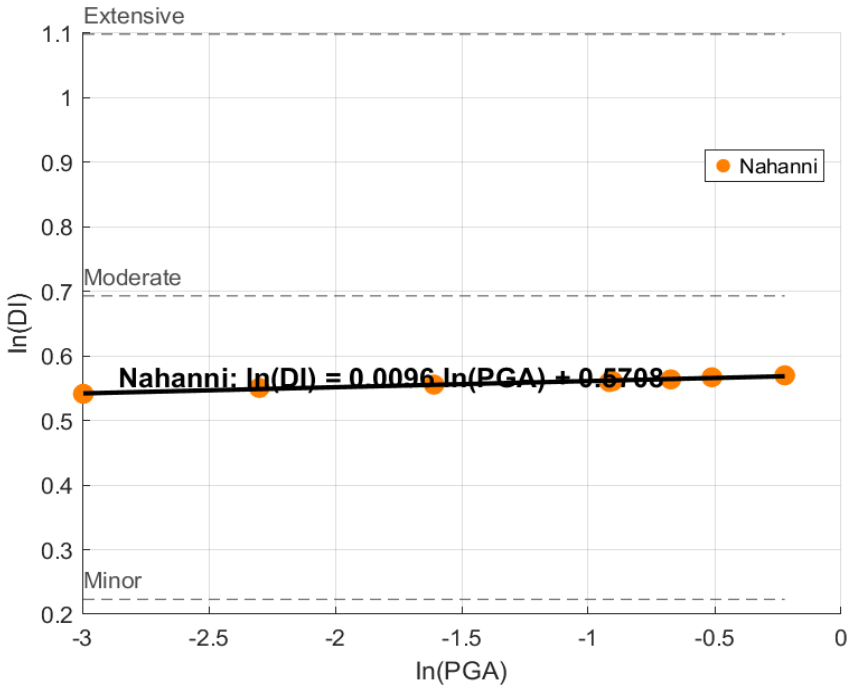

(c) Depth=400m, shear wave velocity=417m/s

Figure 4.7 Linear regression at different depths for Nahanni earthquake

doi:10.6342/NTU202503897

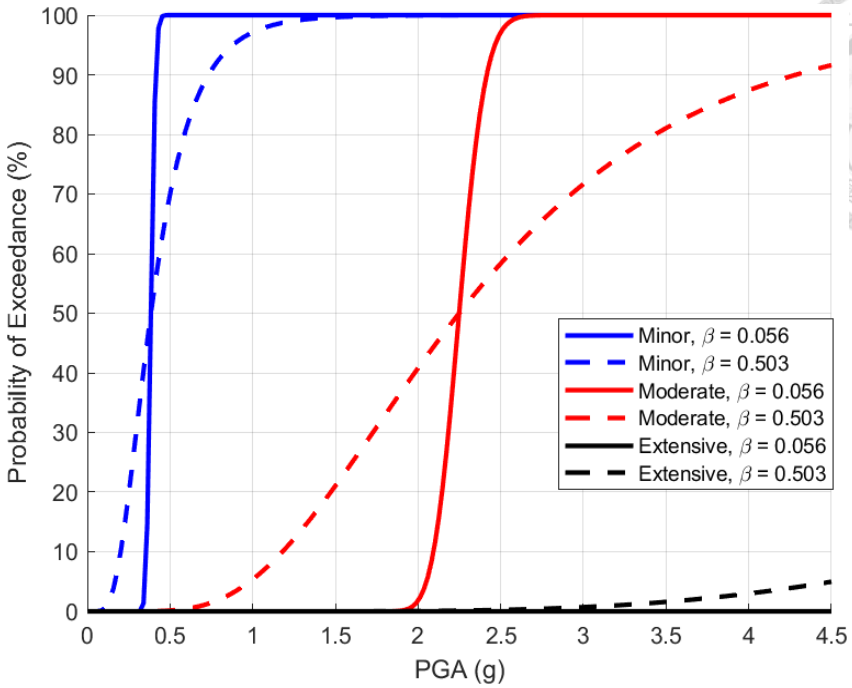

(a) Depth=100m

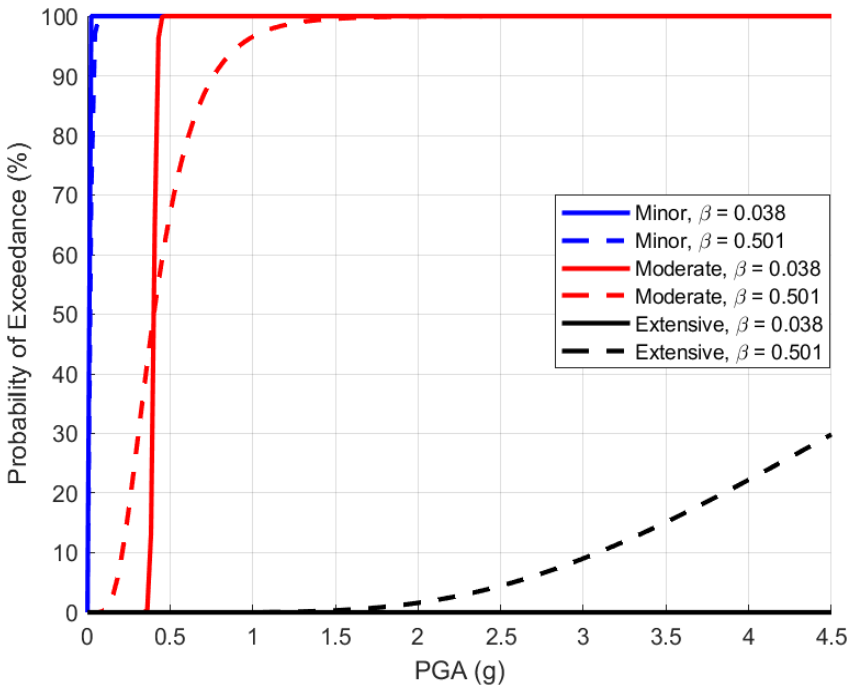

(b) Depth=200m

doi:10.6342/NTU202503897

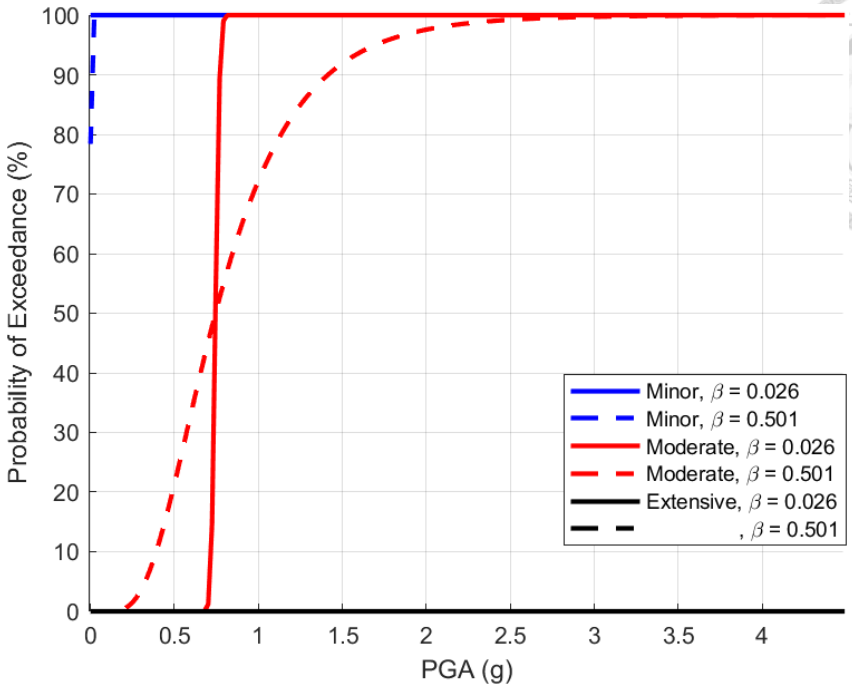

(c) Depth=400m

Figure 4.8 Fragility curves for ChiChi earthquake

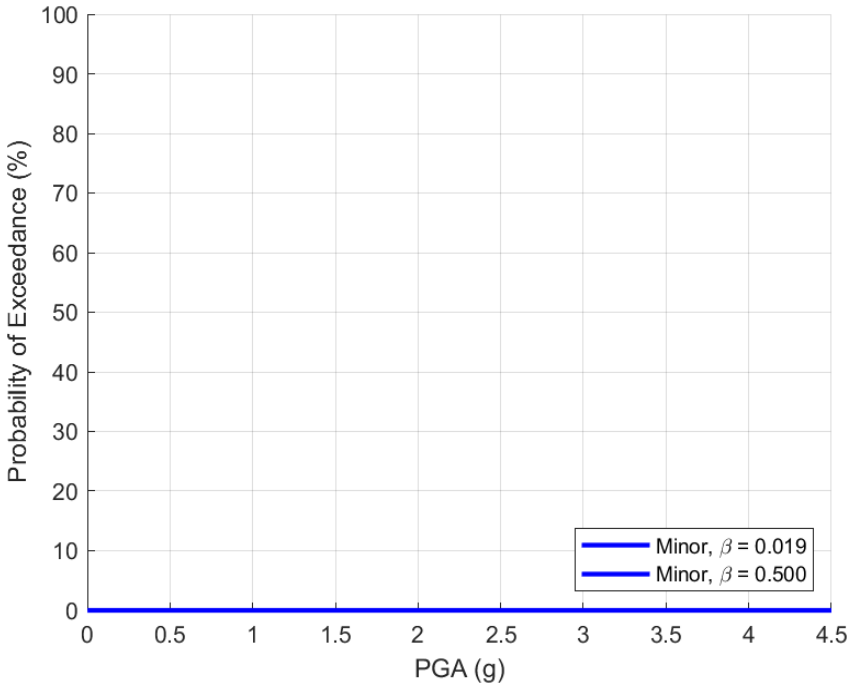

(a) Depth=100m

doi:10.6342/NTU202503897

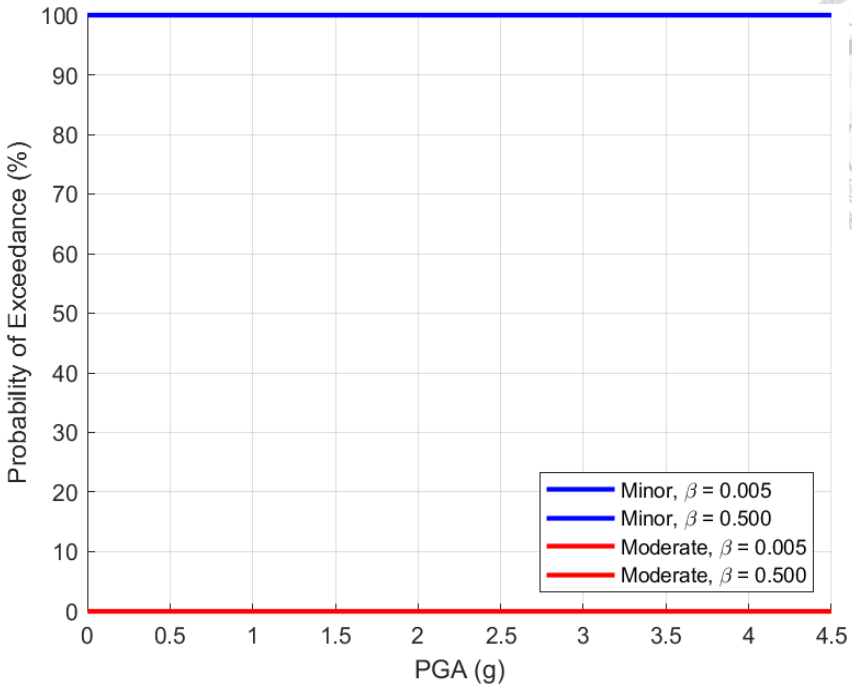

(b) Depth=200m

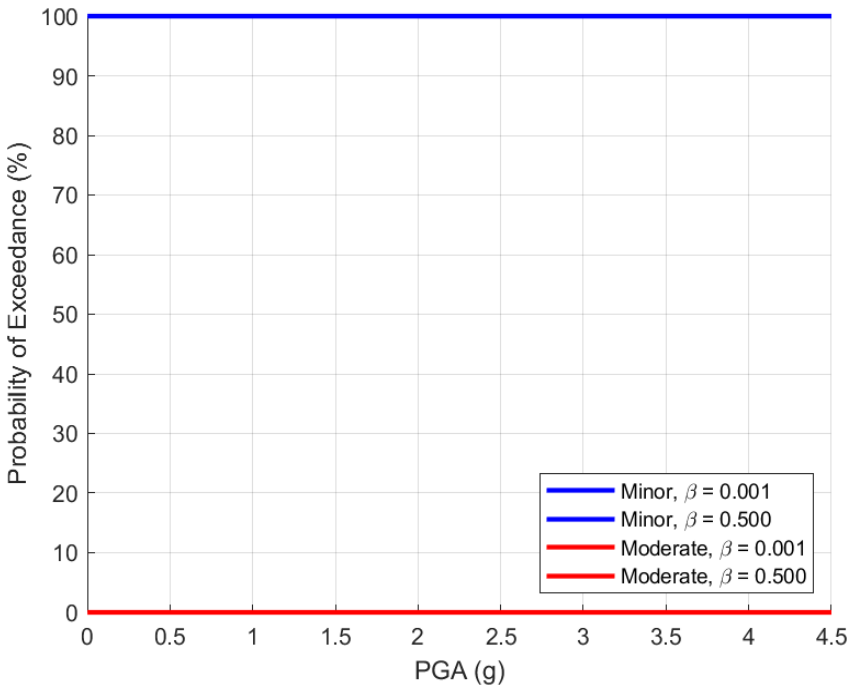

(c) Depth=400m

Figure 4.9 Fragility curves for Nahanni earthquake

doi:10.6342/NTU202503897

4.2.4 Influence of return period design earthquakes

This section compares the effect of incorporating return period design earthquakes (with return periods of 475 and 2500 years) on fragility curve regression, using rock properties corresponding to a shear wave velocity of 417 m/s. The analysis was conducted under tunnel depths of 100 m,200 m and 400m.Table 15 shows the parameters of the probability curves after the inclusion of return period design earthquakes. Figure 4.10 presents the situation of a single regression, and Figure 4.11 compares the fragility curves at different depths.

Looking at the β values, the 100 m case shows a slight increase in β, indicating increased data scatter due to the inclusion of more diverse events. In contrast, at greater depths (200 m and 400 m), the β values decrease, suggesting that adding design earthquakes helps to stabilize the regression and reduce dispersion, as the expanded dataset provides a more consistent trend.

For the 100 m and 200 m depth cases, the inclusion of return period design earthquakes leads to a higher probability of minor damage (i.e., the fragility curve shifts upward for the minor damage state). This indicates that, when considering a broader range of design-level ground motions, the likelihood of incurring slight damage increases—likely because the added low-to-moderate intensity events result in more frequent but less severe responses.

In contrast, for the moderate damage state at both 100 m and 200 m, the probability of exceedance decreases when design earthquakes are included. This is most likely due to the flatter regression line and increased β value (i.e., greater data scatter), which together dilute the predicted risk of moderate damage at the same PGA level.

At 400 m depth, however, the effect reverses for the moderate damage state:

doi:10.6342/NTU202503897

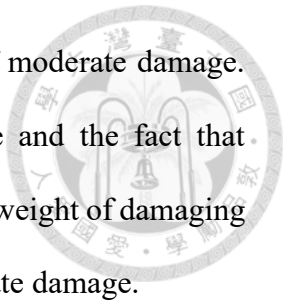

including design-level earthquakes results in a higher probability of moderate damage. This may be attributed to the relatively high overburden pressure and the fact that additional data points at higher intensity levels increase the statistical weight of damaging scenarios, leading to an upward shift of the fragility curve for moderate damage.

These findings demonstrate that the influence of return period design earthquakes on fragility curve predictions is not uniform, but rather depends on both the depth of burial and the damage state considered. The composition of the input dataset and the range of seismic intensities included can significantly affect the assessment of seismic vulnerability for tunnel structures.

doi:10.6342/NTU202503897

Table 15 Parameters of the fragility curves for different depths considering the return period of design earthquakes

Depth	**Damage state**	**Outcropping bedrock PGA (g)**		
		IM_{DS_i}	β_{D}	β_{tot,DS_i}
100m	Minor	1.3931	0.204	0.54
	Moderate	25.3954	0.204	0.54
200m	Minor	0.0065	0.137	0.519
	Moderate	2.51	0.137	0.519
400m	Minor	0	0.041	0.502
	Moderate	1.7527	0.041	0.502

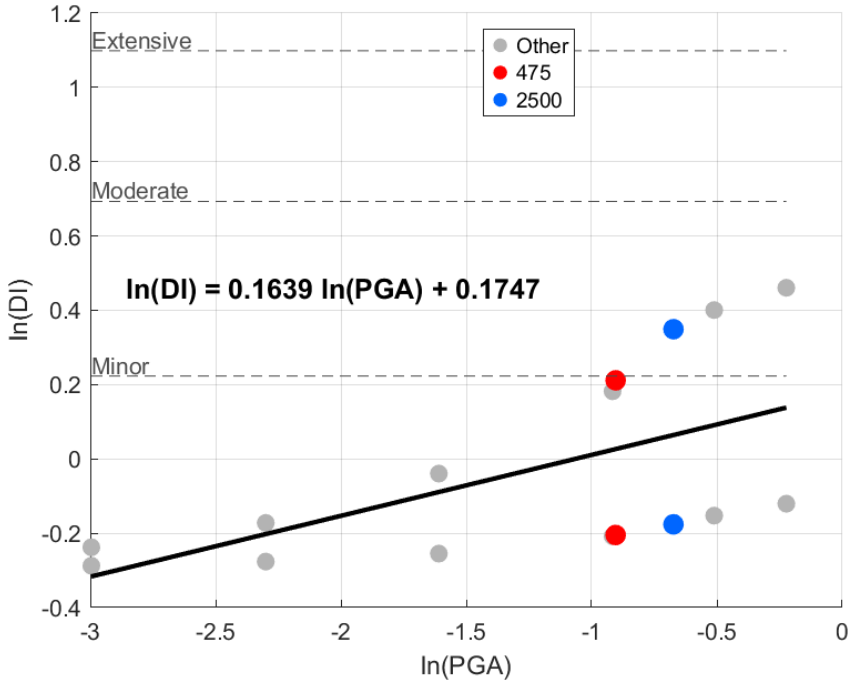

(a) Depth=100m, shear wave velocity=417m/s

doi:10.6342/NTU202503897

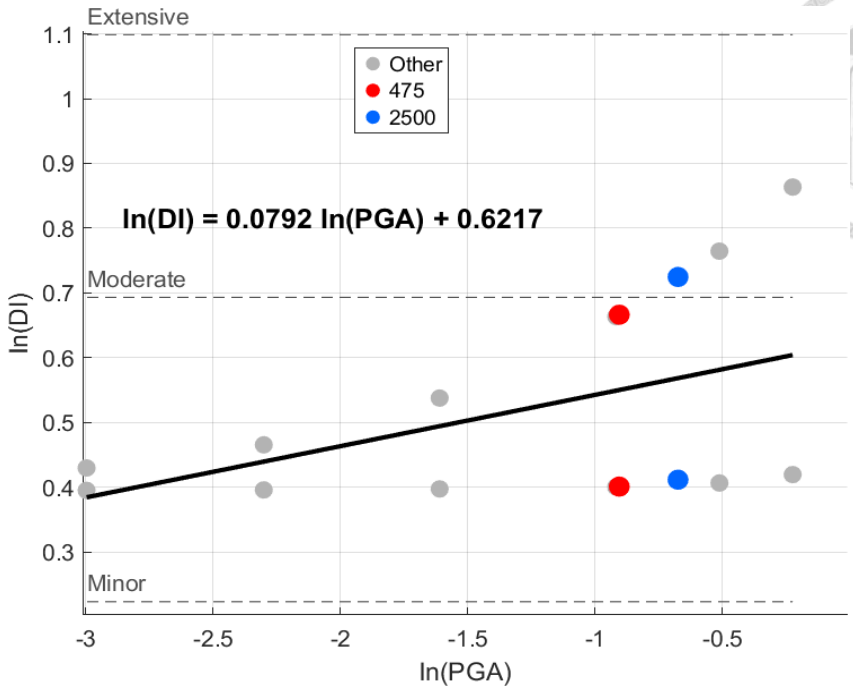

(b) Depth=200m, shear wave velocity=417m/s

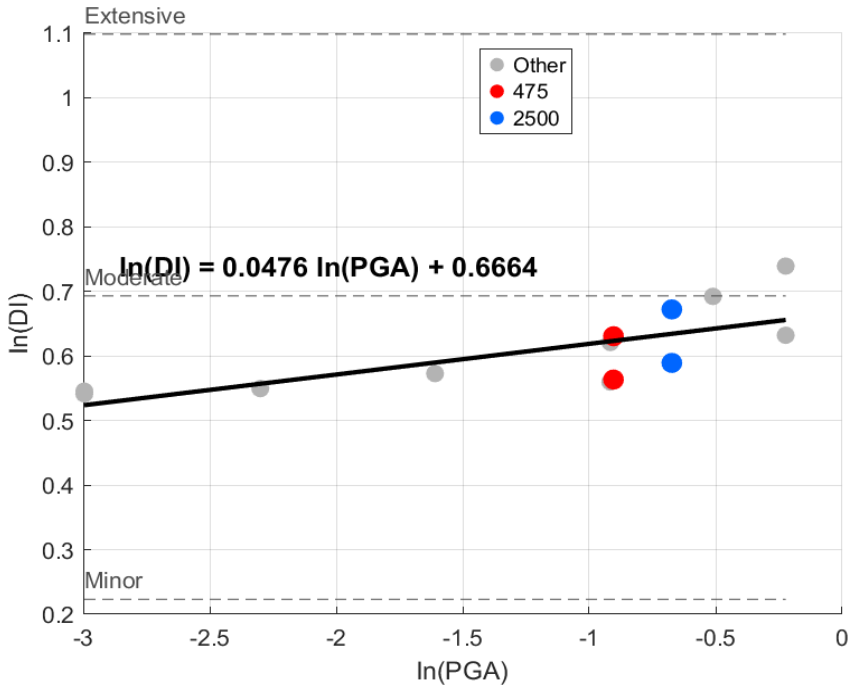

(c) Depth=400m, shear wave velocity=417m/s

Figure 4.10 Linear regression at different depths with 475 and 2500-year design earthquakes

doi:10.6342/NTU202503897

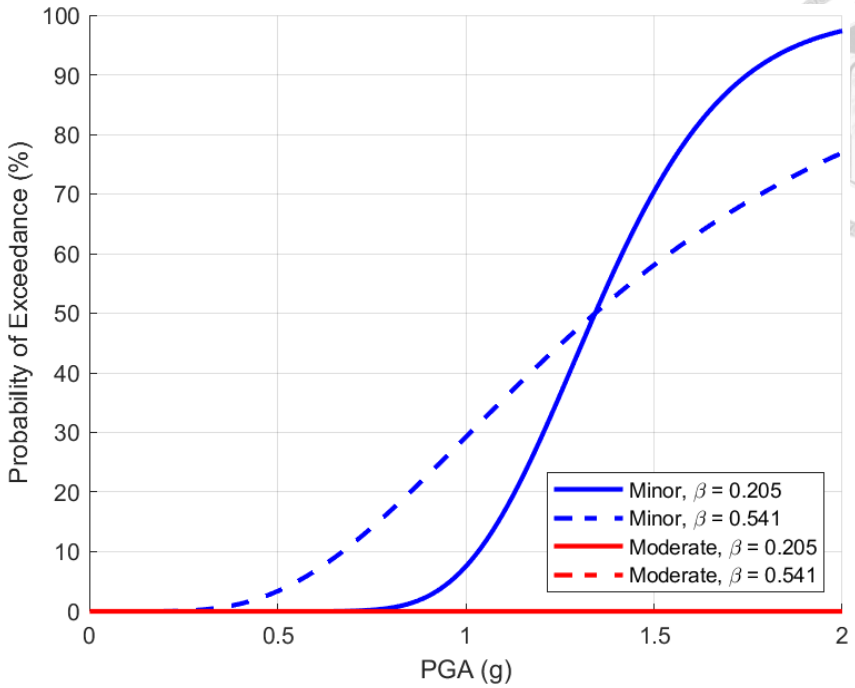

(a) Depth=100m, shear wave velocity=417m/s

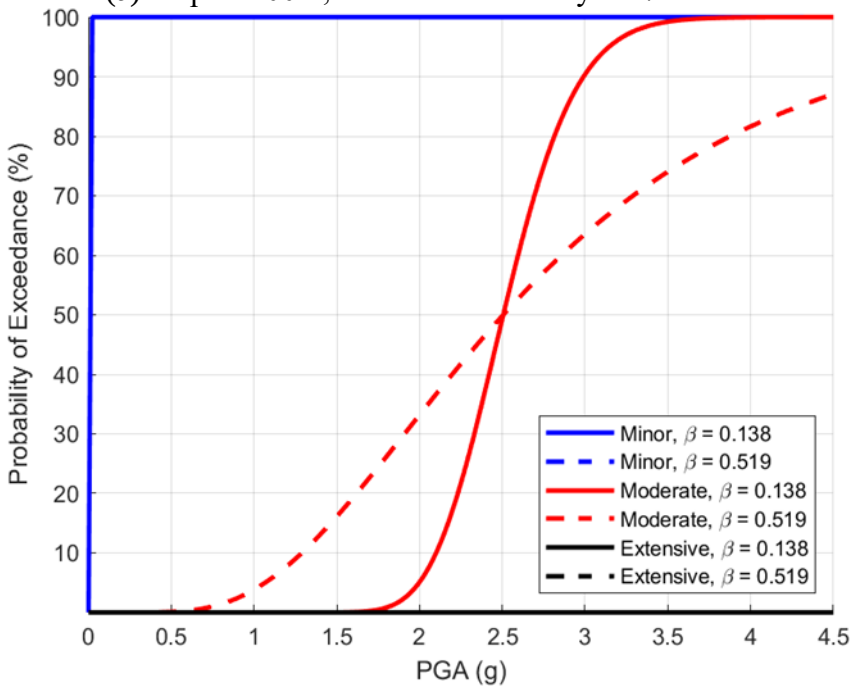

(b) Depth=200m, shear wave velocity=417m/s

doi:10.6342/NTU202503897

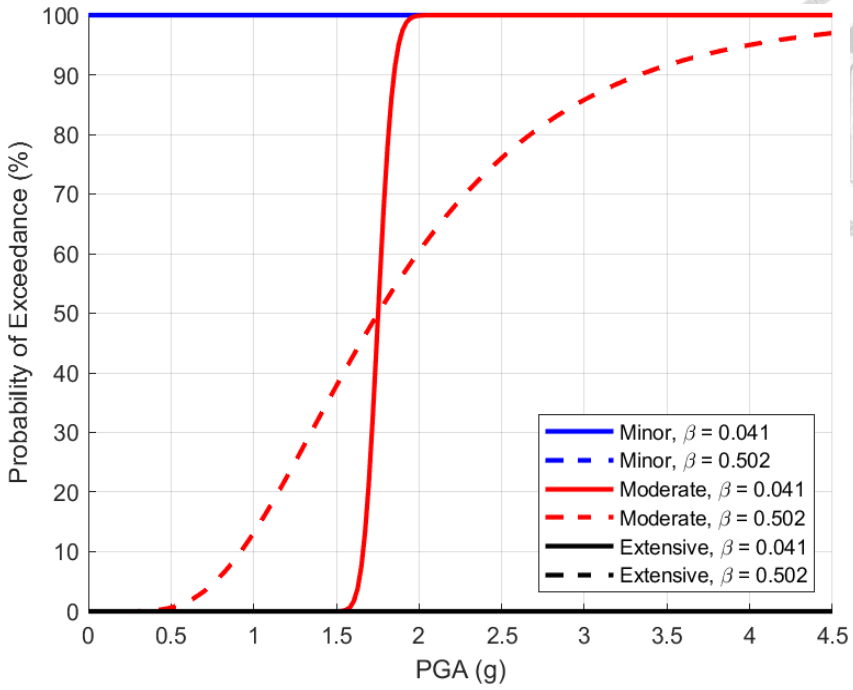

(c) Depth=400m, shear wave velocity=417m/s

Figure 4.11 Comparison of fragility curves at different depths with 475 and 2500-year design earthquakes

4.2.5 Influence of Intensity Measures: PGA vs PGV

Based on the above results, it is found that for different depths, the regression line slopes are identical regardless of whether PGA or PGV is used as the intensity measure. Table 16 is the Parameters of the fragility curves with PGV. Figure 4.12 and Figure 4.13 represent the regression line and the corresponding fragility curves derived using PGV as the intensity measure, respectively. Consequently, since the calculated β values (standard deviations of the residuals from the regression, i.e., the lognormal standard deviation of the PSDM) are also the same, the curvature of the fragility curves remains identical. The only difference observed is in the median threshold (μ), which is affected by the different regression intercepts for PGA and PGV. In other words, the choice between PGA and PGV as the intensity measure in this case does not affect the dispersion or the overall

doi:10.6342/NTU202503897

shape of the fragility curve but shifts the curve horizontally due to the different median values.

Table 16 Parameters of the fragility curves with PGV

Depth	**Damage state**	**Outcropping bedrock PGV (m/s)**		
		IM_{DS_i}	β_{D}	β_{tot,DS_i}
100m	Minor	2.9551	0.204	0.540
	Moderate	52.7722	0.204	0.540
200m	Minor	0.0132	0.138	0.519
	Moderate	4.7908	0.138	0.519
400m	Minor	0	0.047	0.502
	Moderate	2.1302	0.047	0.502

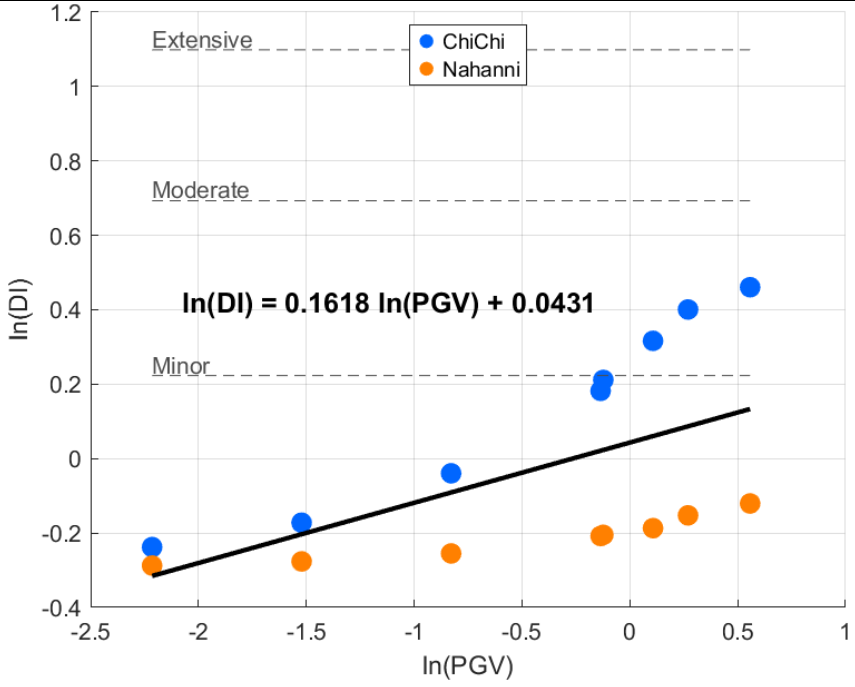

(a) Depth=100m, shear wave velocity=417m/s

doi:10.6342/NTU202503897

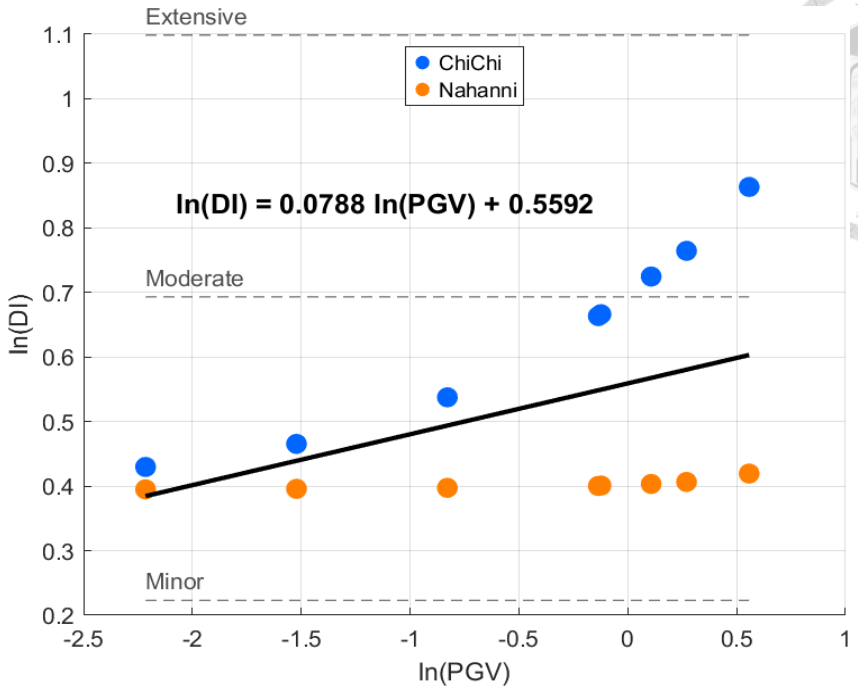

(a) Depth=200m, shear wave velocity=417m/s

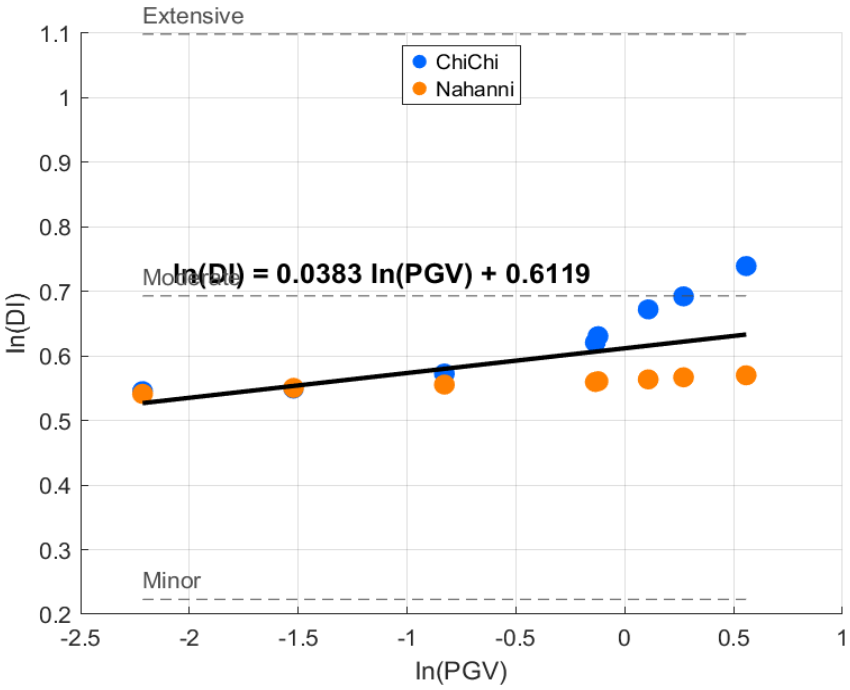

(b) Depth=400m, shear wave velocity=417m/s

Figure 4.12 Linear regression at different depths with PGV

doi:10.6342/NTU202503897

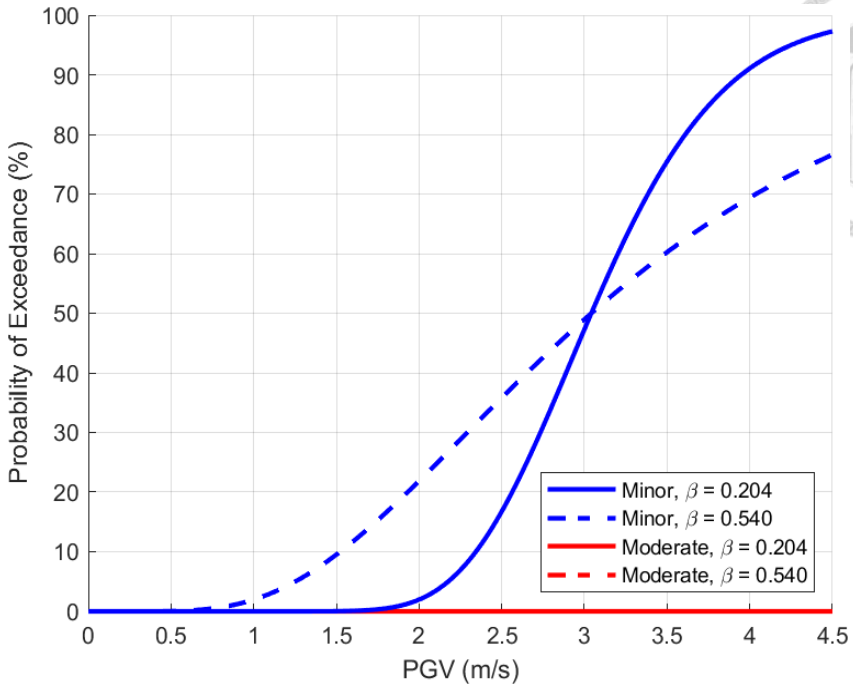

(a) Depth=100m

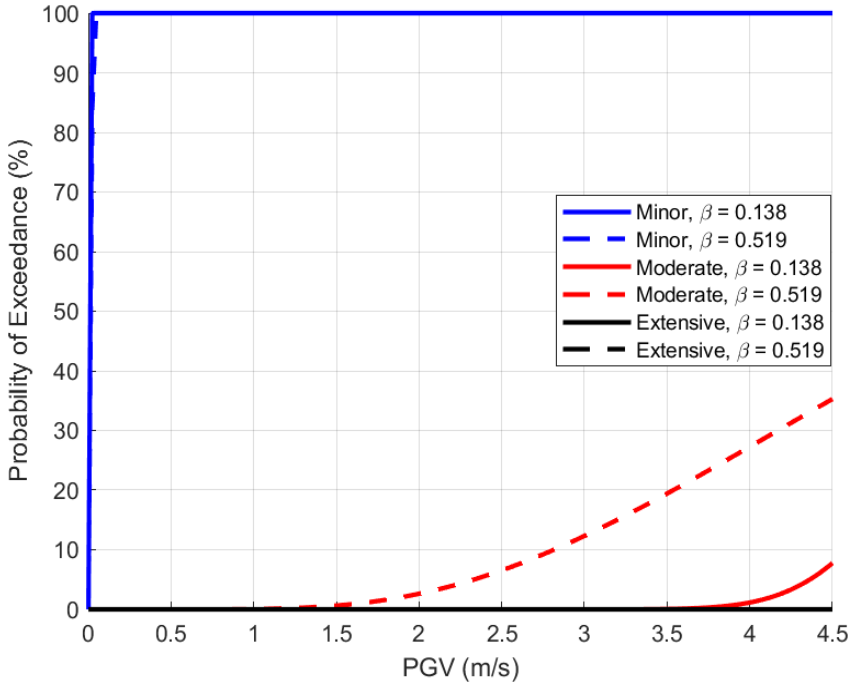

(b) Depth=200m

doi:10.6342/NTU202503897

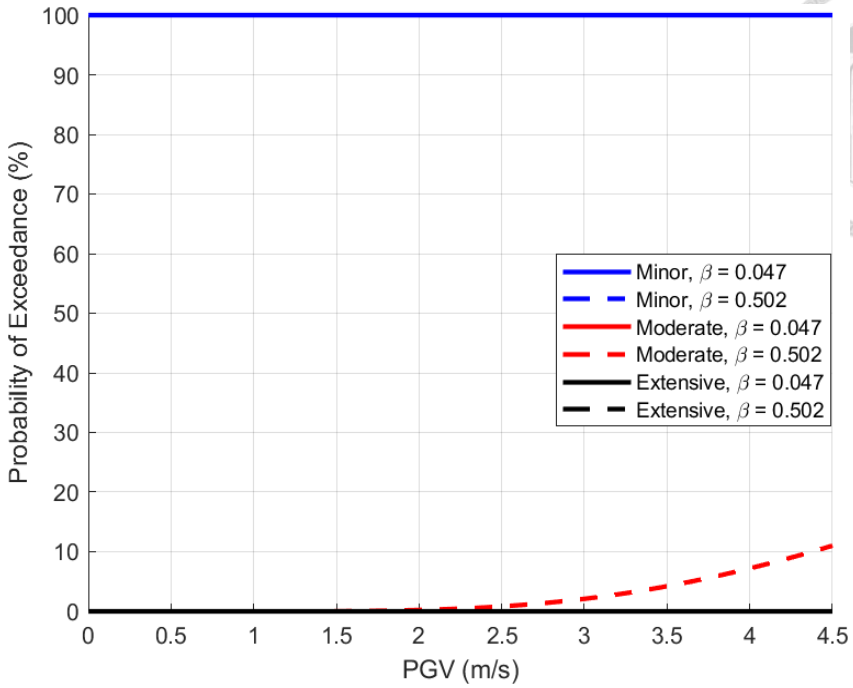

(c) Depth=400m

Figure 4.13 fragility curves at different depths with PGV

4.2.6 Influence of Intensity Measures: PGA vs PGD

Subsequently, the Peak Ground Acceleration (PGA) and Peak Ground Displacement (PGD) were extracted from the vicinity of the tunnel crown and employed for comparative analysis of fragility curves. The analysis was conducted using a numerical model assuming a rock mass with a shear wave velocity of 417 m/s and an overburden depth of 100 m. The results show that the β value derived from PGD is consistently smaller than that obtained from PGA, indicating that the fragility curves based on PGD exhibit less uncertainty. This suggests that PGD provides a more accurate intensity measure (IM), and is therefore a more suitable indicator for seismic fragility assessment in this context. Figure 4.14 and Figure 4.15 represent the regression line and the corresponding fragility curves derived using PGA and PGD as the intensity measures, respectively.

doi:10.6342/NTU202503897

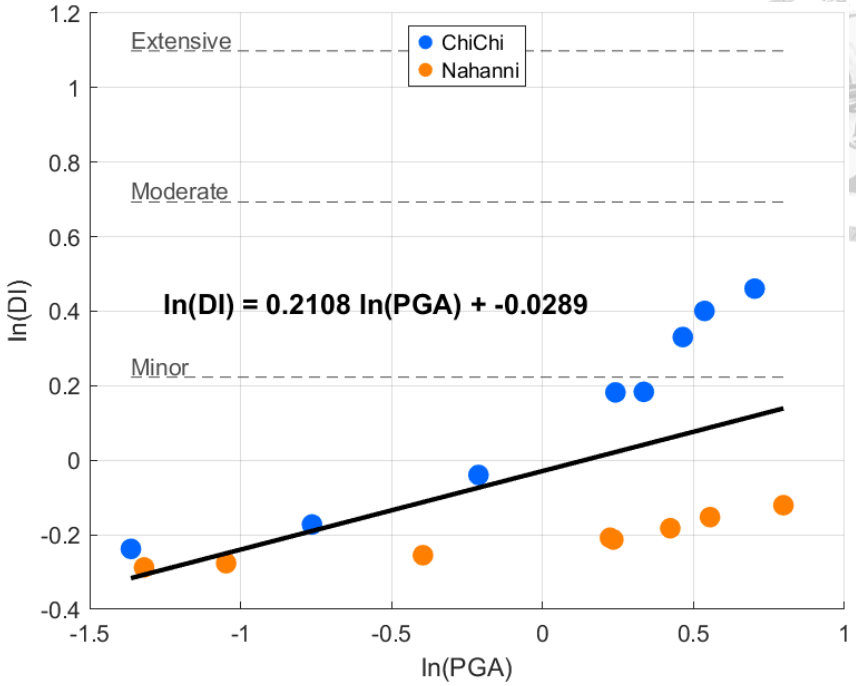

(a) PGA

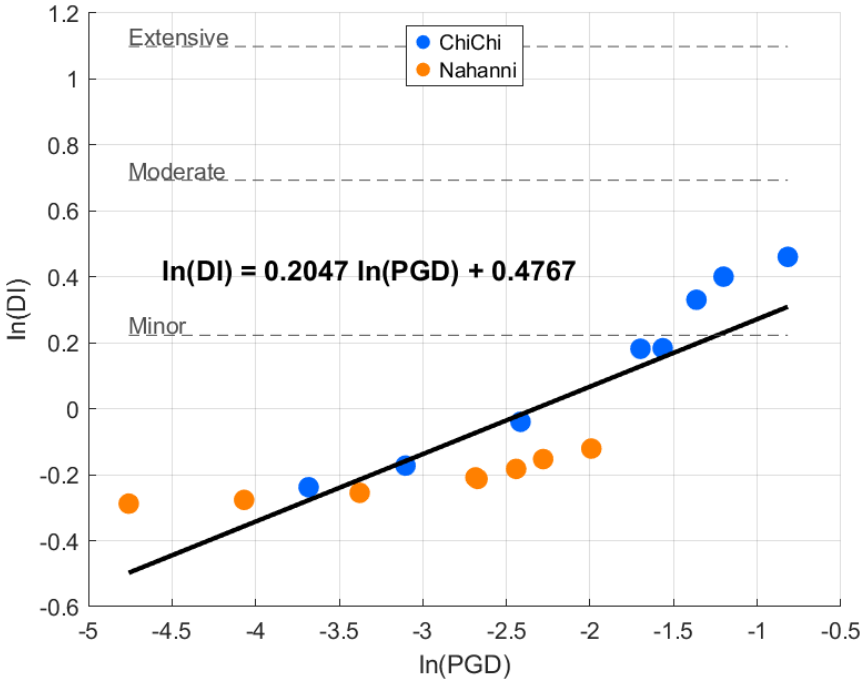

(b) PGD

Figure 4.14 Linear regressions with PGA and PGD

doi:10.6342/NTU202503897

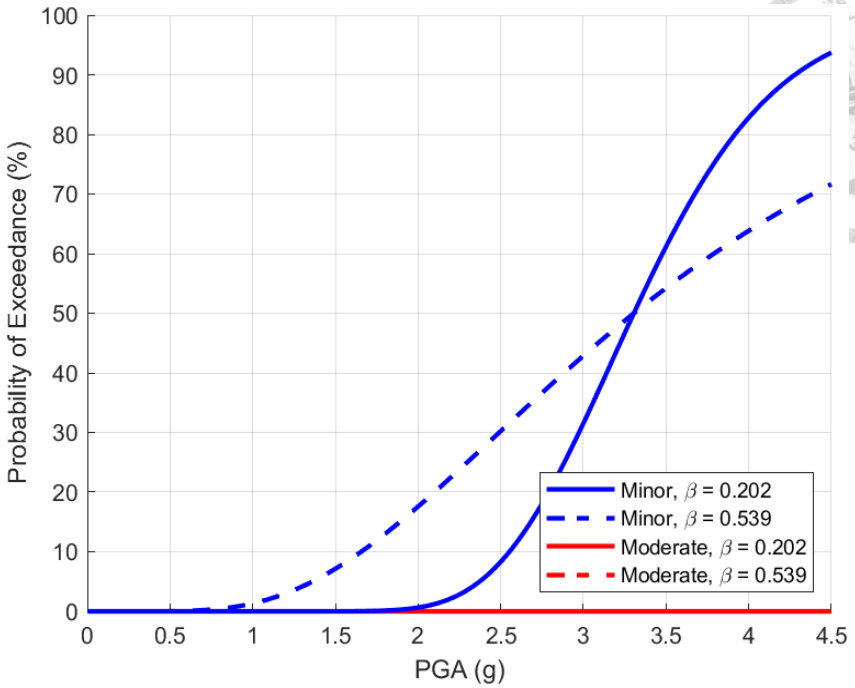

(a) PGA

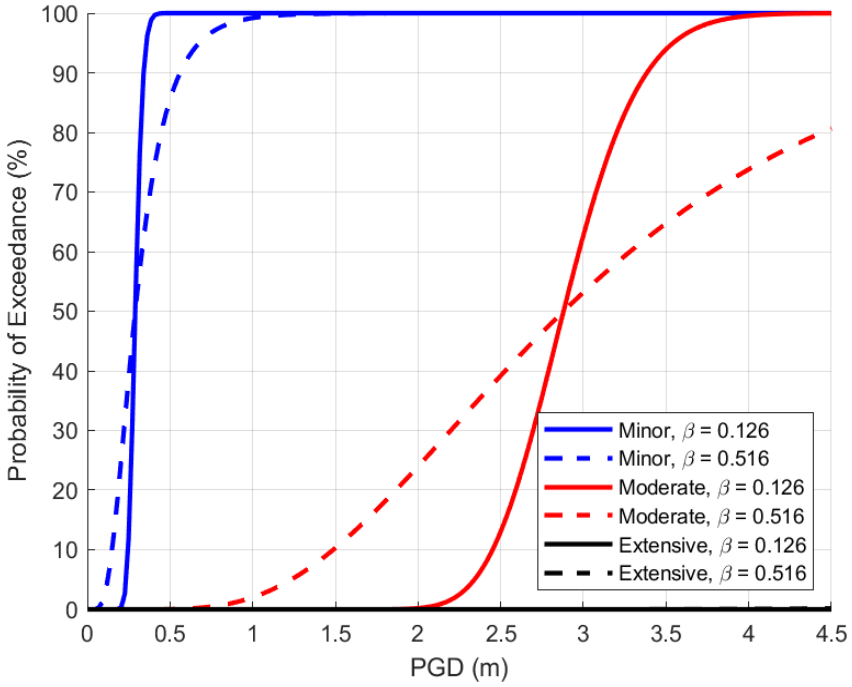

(b) PGD

Figure 4.15 Fragility curves with PGA and PGD

doi:10.6342/NTU202503897

Chapter 5 Conclusion and Recommendations

5.1 Conclusion

This research utilized a systematic numerical approach based on fully nonlinear dynamic analyses in FLAC 2D to investigate the seismic fragility of mountain tunnels. The main findings from the simulations, comprising the analysis cases, can be summarized as follows:

1. Effect of Overburden Depth

The seismic vulnerability of tunnels is significantly influenced by overburden depth. At shallow depths (100 m), tunnels exhibited lower damage probabilities under minor earthquakes but increased vulnerability at higher seismic intensities. Conversely, at greater depths (400 m), minor damage could occur even without seismic excitation due to higher static overburden stress, whereas moderate and extensive damage states remained improbable within the tested seismic intensity range. These findings highlight that tunnels buried at different depths require tailored seismic design approaches.

2. Influence of Rock Stiffness

Comparing the tunnel response in rock with shear wave velocities of 417 m/s (softer rock) and 1000 m/s (stiffer rock), the simulations demonstrated that higher stiffness effectively reduces bending moment demands on tunnel linings. Consequently, tunnels in stiff rock conditions (1000 m/s) did not reach any damage thresholds, indicating a substantial reduction in seismic vulnerability. This emphasizes the importance of accurately assessing rock stiffness in seismic design for tunnels.

3. Impact of Seismic Input Characteristics

Comparing two distinctly different earthquake scenarios—the Chi-Chi earthquake

doi:10.6342/NTU202503897

(long-period, high-energy event) and the Nahanni earthquake (short-period, low-energy event)—revealed that the long-period Chi-Chi earthquake consistently produced higher probabilities of tunnel damage. The results underscore the necessity to account for the frequency content and duration of ground motions in fragility analyses for underground structures.

4. Effects of Return Period Design Earthquakes

Incorporating return period design earthquakes (475-year and 2500-year events) into the analyses influenced the resulting fragility curves in a complex, depth-dependent manner. At shallow depths (100 m and 200 m), using events with larger return period increased the minor damage probability but reduced the probability of moderate damage due to increased data dispersion and decreased regression slope. At greater depth (400 m), however, the return period design earthquakes contributed to increased moderate damage probabilities. This demonstrates the complexity introduced by including a wider spectrum of seismic intensity levels, suggesting careful consideration in selecting appropriate return periods for tunnel fragility analyses.

5. Comparison of Intensity Measures (IMs)

PGA and PGV were compared as intensity measures. While the regression slopes and dispersions were largely similar between the two IMs, the median threshold values differed, horizontally shifting the fragility curves. Thus, the choice of intensity measure primarily affects the position of the curve instead of the shape, emphasizing the necessity to select IMs aligned with the specific structural and geotechnical characteristics of the site.

The analysis reveals that the β value obtained from PGD is consistently lower than that from PGA, implying that PGD-based fragility curves are subject to less variability.

doi:10.6342/NTU202503897

In other words, PGD serves as a more reliable and precise intensity measure (IM) for evaluating seismic fragility in this scenario.

6. Influence of β Values

This study found that fragility curves generated using a total dispersion value (β_{tot,DS_i}) incorporating uncertainties from structural capacity (β_C), demand uncertainty (β_D) and damage state thresholds (β_{DSi}) exhibited greater curvature compared to those generated solely based on demand uncertainty (β_D). Future research is recommended to investigate the appropriate choice of β parameters thoroughly and their effects on fragility curve accuracy and reliability.

5.2 Recommendations

Based on the findings and limitations of this study, several recommendations for further research are proposed:

1. **Three-dimensional Modeling**

While the 2D simulations provided valuable insights into seismic fragility, three-dimensional dynamic analyses considering more realistic geological variations, tunnel geometry, and site-specific boundary conditions are recommended to further validate and enhance fragility assessments.

2. **Near-Fault and Pulse-Like Ground Motions**

Future research should include near-fault and pulse-type seismic events, as these motions possess different frequency contents and pulse characteristics, potentially leading to distinct damage mechanisms in tunnels, especially in stiff rock environments.

3. **Extensive Parametric Analysis**

Expanding the range of parameters, such as different lining types, nonlinear

doi:10.6342/NTU202503897

material models for rock and concrete, and various tunnel geometries, can further generalize the developed fragility curves for broader applicability.

4. **Empirical Data Integration**

Integrating empirical damage data from historical earthquakes and existing tunnel performance databases would enhance model calibration and validation, resulting in more reliable fragility estimates for practical engineering use.

doi:10.6342/NTU202503897

Reference

1. American Lifelines Alliance (2001). Seismic fragility formulations for water systems, part 1-Guidelines, *ASCE-FEMA, Reston, VA.*

2. American Society of Civil Engineers (2013). Minimum design loads for buildings and other structures (ASCE 7-10). *American Society of Civil Engineers, Reston, VA.*

3. Applied Technology Council (1985). Earthquake Damage Evaluation Data for California (ATC-13). *Applied Technology Council, Redwood City, CA.*

4. Andreotti, G., & Calvi, G.M. (2022). Damage model for underground tunnels to evaluate vulnerability and seismic risk. *In: Proceedings of the 12th National Conference in Earthquake Engineering, Earthquake Engineering Research Institute, Salt Lake City, UT.*

5. Anbazhagan, P., Neaz Sheikh, M., Bajaj, K., Mariya Dayana, P. J., Madhura, H., & Reddy, G. R. (2017). *Empirical models for the prediction of ground motion duration for intraplate earthquakes. Journal of Seismology*, 21, 1001-1021.

6. Argyroudis, S., Tsinidis, G., Gatti, F., Pitilakis, K. (2017). Effects of SSI and lining corrosion on the seismic vulnerability of shallow circular tunnels. *Soil Dynamics and Earthquake Engineering*, 98, 244-256.

7. Argyroudis, S., Tsinidis, G., Gatti, F., Pitilakis, K. (2014). Seismic fragility curves of shallow tunnels considering SSI and aging effects. *2nd Eastern European Tunnelling Conference*, Athens, Greece.

8. Argyroudis, S.A., Pitilakis, K.D. (2012). Seismic fragility curves of shallow tunnels in alluvial deposits. *Soil Dynamics and Earthquake Engineering*, 35, 1-12.

9. Bertero, V.V. (1977). Strength and deformation capacities of buildings under extreme

doi:10.6342/NTU202503897

environments. *In: Structural Engineering and Structural Mechanics, Pister KS (ed.). Prentice-Hall: Englewood Cliffs,* NJ, 211–215.

10. Billah, A., Alam, M. (2014). Seismic Fragility Assessment of Highway Bridges: A State-of-the-Art Review. *Structure and Infrastructure Engineering*, 1-29.

11. Corigliano, M., Lai, C.G., Barla, G. (2007). Seismic Vulnerability of Rock Tunnels Using Fragility Curves. *11th ISRM Congress, Lisbon, Portugal.*

12. Dowding, C.H., Rozen, A. (1978). Damage to rock tunnels from earthquake shaking. *Journal of the Geotechnical Engineering Division*, 104(2), 175-191.

13. Federal Emergency Management Agency (2022). HAZUS Earthquake Model Technical Manuals. *Federal Emergency Management Agency, Washington, DC.*

14. Federal Emergency Management Agency. (2000). Recommended seismic evaluation and upgrade criteria for existing welded steel moment-frame buildings. *Report No. FEMA-351, SAC Joint Venture, Federal Emergency Management Agency, Washington, DC.*

15. Fragiadakis, M., Christodoulou, S.E. (2014). Seismic reliability assessment of urban water networks. *Earthquake Engineering and Structural Dynamics*, 43(3), 357-374.

16. Huang, G., Qiu, W., & Zhang, J. (2017). Modelling seismic fragility of a rock mountain tunnel based on support vector machine. *Soil Dynamics and Earthquake Engineering*,*102*, 160-171.

17. Huang, T. H., Ho, T. Y., Chang, C. T., Yao, X. L., Chang, Q. D., & Lee, H. C. (1999). Quick investigation and assessment on tunnel structures after earthquake, and the relevant reinforced methods. *Report for the Public Construction Commission, Taipei, Taiwan.*

18. Hu, X., Zhou, Z., Chen, H., Ren, Y. (2020). Seismic Fragility Analysis of Tunnels with Different Buried Depths in a Soft Soil. *Sustainability*, 12(3).

doi:10.6342/NTU202503897

19. Huang, Z. (2022). Resilience Evaluation of Shallow Circular Tunnels Subjected to Earthquakes *Using Fragility Functions. Applied Sciences*, 12(9).

20. Huang, Z., Argyroudis, S., Zhang, D., Pitilakis, K., Huang, H., Zhang, D. (2022). Time-Dependent Fragility Functions for Circular Tunnels in Soft Soils. *ASCE-ASME Journal of Risk and Uncertainty in Engineering Systems, Part A: Civil Engineering* 8(3).

21. Huang, Z., Zhang, D., Pitilakis, K., Tsinidis, G., Huang, H., Zhang, D., Argyroudis, S. (2022). Resilience assessment of tunnels: Framework and application for tunnels in alluvial deposits exposed to seismic hazard. *Soil Dynamics and Earthquake Engineering*, 162.

22. Itasca. 2011. FLAC Version 7.0 –Manual on line, Minneapolis, Itasca Counsulting Group inc.

23. Kennedy, R.P., Ravindra, M.K. (1984). Seismic fragilities for nuclear power plant risk studies. *Nuclear Engineering and Design*, 79(1), 47-68.

24. Kuhlemeyer, R. L., & Lysmer, J. (1973). Finite element method accuracy for wave propagation problems. *Journal of the Soil Mechanics and Foundations Division*, 99(5), 421-427.

25. Kuesel, T.R., (1969). Earthquake Design Criteria for Subways. J. Struct. Div., *ASCE* ST6, 1213-1231.

26. Lysmer, J., & Kuhlemeyer, R. L. (1969). Finite dynamic model for infinite media. *Journal of the engineering mechanics division*, 95(4), 859-877.

27. Le, T., Huh, J., Park, J.H. (2014). Earthquake Fragility Assessment of the Underground Tunnel Using an Efficient SSI Analysis Approach. *Journal of Applied Mathematics and Physics*, 2, 1073-1078.

28. Moayedifar, A., Nejati, H.R., Goshtasbi, K., Khosrotash, M. (2019). Seismic

doi:10.6342/NTU202503897

fragility and risk assessment of an unsupported tunnel using incremental dynamic analysis (IDA). *Earthquake and Structures*, 16(6), 705-714.

29. Mow, C.C., Mente, L.J. (1963). Dynamic stress and displacement discontinuities due to plane harmonic shear wave, Transactions of the ASME, 598-603.

30. Newmark, N.M., (1968). Problems in wave propagation in soil and rock. *Proceedings of the International Symposium on Wave Propagation and Dynamic Properties of Earth Materials*.

31. Owen, G. N., & Scholl, R. E. (1981). Earthquake engineering of large underground structures.

32. Osmi, S.K.C., Ahmad, S.M. (2016). Seismic fragility curves for shallow circular tunnels under different soil conditions. *International Journal of Civil and Environmental Engineering*, 10, 1351-1357.

33. Osmi, S.K.C., Ahmad, S.M., Adnan, A. (2015). Seismic fragility analysis of underground tunnel buried in rock. In: *Proceedings of the 50th International Conference on Earthquake Engineering and Seismology, Kiel, Germany.*

34. Park, K. H., Tantayopin, K., Tontavanich, B., & Owatsiriwong, A. (2009). Analytical solution for seismic-induced ovaling of circular tunnel lining under no-slip interface conditions: A revisit. *Tunnelling and Underground Space Technology*, 24(2), 231-235.

35. Pao, Y. H. (1962). Dynamical stress concentration in an elastic plate. *Journal of Applied Mechanics*, 29, 299-305.

36. Qiu, W., Huang, G., Zhou, H., Xu, W. (2018). Seismic Vulnerability Analysis of Rock Mountain Tunnel. *International Journal of Geomechanics*, 18(3).

37. Railway Technical Research Institute (2001). Design Code for Tunnels in Urban Areas (in Japanese). *Railway Technical Research Institute, Japan.*

doi:10.6342/NTU202503897

38. Sun, B., Zhang, S., Deng, M., Wang, C. (2020). Inelastic dynamic response and fragility analysis of arched hydraulic tunnels under as-recorded far-fault and near-fault ground motions. *Soil Dynamics and Earthquake Engineering*, 132.

39. St John, C. M., & Zahrah, T. F. (1987). Aseismic design of underground structures. *Tunnelling and underground space technology*, 2(2), 165-197.

40. Sarkar, R., Pareek, K. (2021). Influence of stratification and assessment of fragility curves for mountain tunnels. In: *Proceedings of the Institution of Civil Engineers-Geotechnical Engineering*, 174(3), 279-290.

41. Stefanidou, S.P., Kappos, A.J. (2017). Methodology for the development of bridge-specific fragility curves. *Earthquake Engineering and Structural Dynamics*, 46, 73-93.

42. Tsinidis, G., de Silva, F., Anastasopoulos, I., Bilotta, E., Bobet, A., Hashash, Y. M., He, C., Kampas, G., Knappett, J., & Madabhushi, G. (2020). Seismic behaviour of tunnels: From experiments to analysis. *Tunnelling and underground space technology*, 99, 103334

43. Vamvatsikos, D., Cornell, C.A. (2002). Incremental dynamic analysis. *Earthquake Engineering and Structural Dynamics*, 31(3), 491-514.

44. Wang, J. (1993). Seismic Design of Tunnels: *A Simple State-of-the-art Design Approach. Monograph 7,Parsons, Brinckerhoff, Quade and Douglas, Inc.*

45. Wang, W. L., Wang, T. T., Su, J. J., Lin, C. H., Seng, C. R., & Huang, T. H. (2001). Assessment of damage in mountain tunnels due to the Taiwan Chi-Chi Earthquake. *Tunnelling and underground space technology*, 16(3), 133-150.

46. Yucemen, M.S. (2013). Probabilistic assessment of earthquake insurance rates for buildings. In: *Handbook of seismic risk analysis and management of civil infrastructure systems. Woodhead Publishing*, 787-815.

47. Zi, H., Ding, Z., Ji, X., Liu, Z., Shi, C. (2021). Effect of voids on the seismic

doi:10.6342/NTU202503897

vulnerability of mountain tunnels. *Soil Dynamics and Earthquake Engineering*, 148.

48. 蘇仁偉(2021)。岩石隧道受震反應：現地監測資料解析與三維數值模擬，*國立臺灣大學土木工程學系學位論文*。

49. 葉勇凱、周德光(2018)。土木 404-100 設計例之耐震評估與易損性曲線。*國家地震工程研究中心*，台北，編號：NCREE-18-016，。

50. 朝倉俊弘、志波由紀夫、松岡茂、大矢敏雄、野城一榮(2008)，山岳 トンネルの地震被害 とその メカニズム，*土 木 学 会 論 文 集*，20-36。

51. 陳正勳、王泰典、黃燦輝(2011)，山嶺隧道受震損害類型與原因之案例研究，第 30 卷，第 1 期，P45-57，*岩石力學與工程學報*。

doi:10.6342/NTU202503897